UNIVERSITA' DEGLI STUDI DI PARMA

Dottorato di ricerca in Biologia Vegetale

Ciclo XXVII

Revising the Roles of Phytochelatin Synthases and their Evolutionary History in Different Plant Species

Coordinatore:

Chiar.mo Prof. Marcello Tomaselli

Tutor:

Chiar.mo Prof. Luigi Sanità di Toppi

Co-Tutors:

Chiar.mo Prof. Olena K. Vatamaniuk

Chiar.mo Prof. Flavia Guzzo

Dottoranda:

Maria De Benedictis

2015

CONTENTS

LIST OF PUBLICATIONS

Some results of the following thesis were already published in:

- Petraglia A., De Benedictis M.*****, Degola F., Pastore G., Calcagno M., Ruotolo R., Mengoni A., Sanità di Toppi L. (2014). The capability to synthesize phytochelatins and the presence of constitutive and functional phytochelatin synthases are ancestral (plesiomorphic) characters for basal land plants. Journal of Experimental Botany 65: 1153-1163.

- Degola F., De Benedictis M.*****, Petraglia A., Massimi A., Fattorini L., Sorbo S., Basile A., Sanità di Toppi L. (2014). A Cd/Fe/Zn-responsive phytochelatin synthase is constitutively present in the ancient liverwort *Lunularia cruciata* (L.) Dumort. Plant Cell Physiology 55: 1884-1891.

(***** co-first name)

Other two papers will be submitted.

INTRODUCTION

Heavy Metals and Their Toxicity

Heavy metals are transition elements with densities higher than 5 g cm^{-3}. Metalloids (*e.g.* arsenic, antimony, *etc.*) are elements with intermediate properties between the ones of metals and non-metals. It is important to point out that heavy metals can be divided into two groups: essential and non-essential. Essential heavy metals (*e.g.* copper [Cu], zinc [Zn], iron [Fe], manganese [Mn], *etc*,) serve as micronutrients because they are required at low concentrations for the life cycle of plants, but these essential elements might be toxic when accumulate in excess. Non-essential heavy metals and metalloids (*e.g.* cadmium [Cd], lead [Pb], mercury [Hg], arsenic [As], *etc*.) are potentially highly toxic even at low concentration and interfere with physiological processes with severe consequences for plant life cycle. The basis of heavy metal toxicity lies in their high affinity for thiol groups and, thus, heavy metals can crosslink S-containing essential proteins, replace essential elements from their cellular binding sites and trigger formation of reactive oxygen species (ROS) (Stadtman, 1990).

Heavy Metal Detoxification

To combat heavy metal toxicity, plants have acquired genetic and biochemical mechanisms aimed at maintaining the concentration of essential metals within a homeostatic, physiological range and, at the same time, at detoxifying non-essential metals that enter the cell by using the same transporters for essential metals (Palmer and Guerinot, 2009; Verbruggen et al., 2009). For example, Zinc-related Iron-related Protein (ZIP) transporters that are localized in root cell plasma membrane regulate the uptake not only of a number of essential metals such as Fe, Zn and Mn, but also of Cd (Guerinot, 2000). Free cytosolic Cd is soon sequestered or directed into the vacuole by P_{1B}-ATPases (HMA) (Hussain et al., 2004) and cation exchanger (CAX) (Koren'Kov et al., 2007) transporters localized in tonoplast. Among the major mechanisms of heavy metal detoxification, it has to be mentioned their chelation by thiol-rich peptides, phytochelatins (PCs), and the subsequent sequestration of PC-heavy metal complexes into the vacuole through specific ATP-binding cassette (ABC) transporters, *i.e.* ABCC1/2 (Cobbett, 2000; Mendoza-Cozatl et al., 2011).

Phytochelatin Synthase (PCS)

PCs have a general structure (γ-glutamic acid-cysteine)$_n$-glycine (n=2-11), [(γ-Glu-Cys) $_n$-Gly] (**Figure 1**) and are synthesized posttranslationally by the action of phytochelatin synthases (PCS, γ-glutamylcysteine dipeptidyl transpeptidase [EC 2.3.2.15]) (Rauser, 1990; Zenk, 1996; Grill et al., 1989; Clemens et al., 1999; Ha et al., 1999; Vatamaniuk et al., 1999; 2000; 2004; Romanyuk et al., 2006). PCSs are found in a number of very different organisms, prokaryotes and eukaryotes (Tsuji et al., 2004; Cobbett and Goldsbrough, 2002). First identified in the fission yeast *Schizosaccharomyces pombe* (Kondo et al., 1984), and then in plants (Grill et al., 1985), in some algae, and invertebrates (Cobbett, 1999; Cobbett and Goldsbrough, 2002). PCS was found also in the genome of the nematode *Caenorhabditis elegans* (*CePCS*) that encodes a polypeptide bearing 30 % identity (45 % similarity) to *PCS1* of *Arabidopsis thaliana* (Vatamaniuk et al., 2001; Clemens et al., 2001).

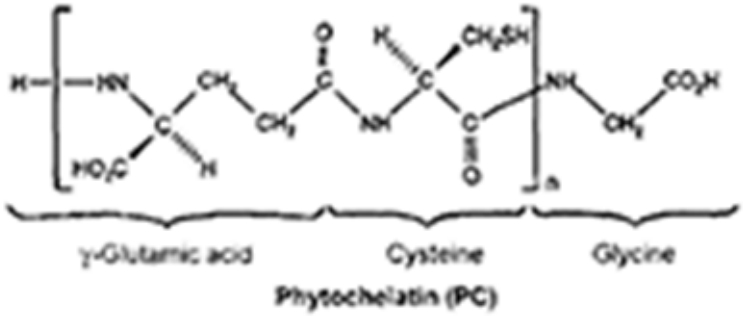

Figure 1: A structure of a canonical phytochelatin, n=2-11. (The picture was taken from Zenk, 1996).

Based on detailed studies of PCS from *A. thaliana* (AtPCS1), PCSs catalyze a desglycylation reaction of glutathione (γ-Glu-Cys-Gly) (GSH) and related thiol-peptides, by the net transfer of a γ-Glu-Cys unit from one GSH to another one, or to a previously synthesized PC molecule (Grill et al., 1989; Clemens et al., 1999; Ha et al., 1999; Vatamaniuk et al., 1999; Vatamaniuk et al., 2000), in order to mediate a peptide chain extension in the N-to-C direction (Vatamaniuk et al., 2004). PCs are synthesized within a few minutes after Cd exposure and their induction is independent on *de novo* protein synthesis. According to some authors (Vatamaniuk et al., 2000; Cobbett, 2000; Rea et al., 2004), the cytosolic enzyme PCS is expressed constitutively, that is independently from any metal exposure.

AtPCS1 is composed of two domains: a conserved N-terminal domain and a variable C-terminal domain. The N-terminal domain is responsible for the catalytic activity, conferred by the so called "catalytic triad", that is the amino acids Cys, His and Asp in specific and highly conserved positions of the N-terminal domain. If one of these amino acids is deleted or substituted, the enzyme

fails to keep its activity (Ruotolo et al., 2004; Rea et al., 2004). The C-terminal domain is considered a "metal-sensing domain", whose multiple Cys residues bind metals and bring them into contact with the catalytic site within the N-domain; last but not least, the C-terminal domain appears to be involved in the enzyme protection against high temperature, oxidative stress, and confers overall better response to a broader metal(loid) range (Ruotolo et al., 2004; Romaniuk et al., 2006). For its distinctive catalytic triad and its ability to catalyse a transpeptidation reaction, the PCS belongs to the clan CA of the papain-like cysteine proteases (Rea et al., 2004; Vivares et al., 2005; Romanyuk et al., 2006; Rea, 2012).

In all of the prokaryotic PCS identified so far (*e.g.* the alr0975 protein from *Nostoc* sp. PCC 7120 [*NsPCS*]), the length of the enzyme is almost half of the size of the eukaryotic ones, consisting, respectively, in 220-237 amino acid residues instead the 421-506 residues. *NsPCS* has been found to catalyze the first step in PC synthesis with only a weak net PC_2 synthesis, with no different concentration of this peptide either in the presence or in the absence of metal ions (Tsuji et al., 2004; Harada et al., 2004; Tsuji et al., 2005).

The importance of PCS for the achievement of heavy metal detoxification was demonstrated by *A. thaliana cad1* mutants, which are Cd-hypersensitive and are PC-deficient (Howden et al., 1995a). In these mutant alleles, *AtPCS1* has mutations that interfere with the catalytic activity of the enzyme (Ha et al., 1999). Likewise, the PCS-deficient mutants of fission yeast *S. pombe* and the nematode worm *C. elegans* are hypersensitive to heavy metals (Ha et al., 1999; Vatamaniuk et al., 2001). Furthermore, heterologous expression of *AtPCS1* in *Saccharomyces cerevisiae*, which lacks PCS homologues, accumulates PCs with a consequent rise of metal tolerance (Vatamaniuk et al., 1999). Thus, PC synthesis is essential for heavy metal and metal(loid) detoxification in different organisms.

GSH and metal-$(GS)_n$ complex (n reflects the valency of the heavy metal) serve as co-substrates for PC synthesis, and thus, their availability is fundamental for PCs induction by PCS (Vatamaniuk et al., 2000). Treatment with buthionine sulfoximine (BSO), a specific inhibitor of γ-glutamylcysteine synthetase (EC 6.3.2.2), the first enzyme in GSH biosynthesis, inhibits PC synthesis and the inhibitory effect of BSO could be reversed by the addition of GSH to the growth medium (Clemens et al., 1999). This observation is also confirmed by a genetic study using the *cad2-1* mutant of *A. thaliana*, which is deficient in the first enzyme for GSH biosynthesis, γ-glutamylcysteine synthetase (Cobbett et al., 1998). The *cad2-1* mutant is Cd hypersensitive and shows a decreased level of PCs resulting from a drop in the level of endogenous GSH (Mutoh and Hayashi, 1988; Howden et al., 1995b).

In plants, GSH also plays an important role in biotic and abiotic stress tolerance. The thiol-tripeptide is ubiquitous in all organisms and plays different physiological functions including redox regulation, conjugation of metabolites and detoxification of xenobiotics (Meister, 1995). Adequate levels of GSH are important also for the regulation of the secondary metabolism (Hacham et al., 2014). GSH treatment of *A. thaliana* wild-type plants changes genes expression of different pathways, leading to innate immune response (*syn.*: nonhost resistance), development processes affecting the balance between auxin and cytokinin signalling and, not least, triggers cell wall synthesis (Hacham et al., 2014).

Physiological levels of GSH and *AtPCS1* enzyme help the plants to counteract a number of biotic and abiotic stresses. The best activators of *AtPCS1* enzyme are Cd^{2+} ions, followed by Hg^{2+}, As^{3+}, Cu^{2+}, Zn^{2+}, Pb^{+}, AsO_4^{3--}, *etc.* (Vatamaniuk et al., 2000). However, it has been shown that the presence of a heavy metal might be not required for AtPCS1-mediated catalysis, and association of a thiol group of GSH with another functional group (*e.g.* methyl, ethyl) is sufficient for PC production (detailed below and described in Vatamaniuk et al., 2000; Romanyuk et al., 2006). Furthermore, *AtPCS1* is not transcriptionally upregulated after heavy metal treatment (Vatamaniuk et al., 2000; Cobbett, 2000). In contrast, the transcript abundance of *AtPCS1* increases under Fe deficiency and after the treatment with a mimetic of the pathogen attack, a synthetic 22-amino acid polypeptide that corresponds to a highly conserved region of the eubacterial flagellin (Flg22) (detailed below and described in Colagelo and Guerinot, 2004; Clay et al., 2009). Taking into account the above, it is possible that AtPCS1 plays other, yet unidentified roles in plants.

Heavy Metals could be Not Essential for AtPCS1 Activation

Vatamaniuk et al. (2000) reported that free metal ions are not essential for the catalysis of AtPCS1 enzyme and their role is rather to make GSH an active substrate for the enzyme itself. Although AtPCS1 is able to bind heavy metals directly and to be primarily activated post-translationally, metal binding *per se* appears to be not responsible for any catalytic activation. Instead, the GSH-containing blocked thiol group is necessary for the enzyme activation. AtPCS1 is able to catalyze the transpeptidation reaction starting form S-methyl-, S-ethyl-, S-propyl-, S-butyl-, S-hexylglutathione, with the respective synthesis of S-alkyl-PCs with a time dependence similar to that obtained in metal-containing media (Vatamaniuk et al., 2000). This suggests that the PCS might process other GSH derivates and thus might play other roles (or perhaps functions) in addition to heavy metals detoxification.

GSH is ubiquitous in eukaryotes, it is involved in many cell physiological processes and constitutes more than 90 % of total non-protein sulphur (Meister, 1995; Cobbett, 2000; Beck et al.,

2003). GSH binds different type of molecules, like endogenous metabolites such as auxin, anthocyanins and sterols and is involved in metabolism, transport and storage of them; GSH also starts a detoxification pathway of xenobiotics (Marrs, 1996). GSH conjugates are generated by GSH transferases (GSTs), which are encoded by a small gene family. Like PC-heavy metal complexes, also GS-conjugates are accumulated in the vacuole by means of specific ABC-type transporters (Rea, 2012).

PCS is Involved in the Catabolism of Gluthatione-Conjugates

Vatamaniuk et al. (2000) hypothesis described above are supported by other papers. For example Beck et al. (2003) and Blum et al. (2007) have reported that PCS is involved in the catabolism of glutathione-conjugates, catalysing the first reaction of degradation by the cleavage of glycine from the GS-conjugate, to generate a γ-EC-conjugate, which will be further catabolised.

In detail, Beck et al. (2003), demonstrated that purified AtPCS1 enzyme is able to catabolise different compounds attached to the sulfhydryl group of GSH, like bimane-GS, or uracil, acetamidofluorescein, nitrobenzyl, benzyl, phenylbenzyl-GS, leading to the formation of the corresponding EC derivatives, without production of PCs. Moreover, the desglycination of bimane-GS by AtPCS1 was more than two-fold more efficient than the transpeptidation of γ-EC to another GSH molecule or already synthesized PCs under comparable conditions (Beck et al., 2003). This work highlights a second crucial role of PCS enzyme in the catabolism of GS-conjugate.

Blum et al. (2007) further substantiated these data by showing that protoplasts of *A. thaliana* knockout mutant for *AtPCS1* were not able to convert GS-conjugate into γ-EC-conjugate and the transfection of PC-deficient cell with *AtPCS1* recovered γ-EC-conjugate levels. It is also interesting that *NsPCS* catabolized GSH to γ-EC rather than synthesize PC peptides (Harada et al., 2004; Tsuji et al., 2004).

PCS and Callose Deposition

It has been demostrated that expression of *AtPCS1* is significantly upregulated by Flg22 treatment (Clay et al., 2009). Flg22 also upregulates genes involved in indole glucosinolate biosynthesis and myrosinase enzyme(s) (Clay et al., 2009). In response to pathogen attack and Flg22 treatment, plants deposit into cell walls callose, a β(1,3)-glucan polymer product. Callose deposition in cell walls at the site of pathogen attack represents a defence mechanism against potential pathogens, referred as nonhost resistance or innate immune response (Thordal-Christensen, 2003; Nurnberger and Lipka, 2005).

Clay at al. (2009) showed also that *cad1-3* plants (knockout mutant of AtPCS1 enzyme) do not produce callose in response to Flg22, suggesting that AtPCS1 is involved in callose synthesis. Callose deposition in *A. thaliana* requires secondary metabolites, *i.e.* indole glucosinolates (Clay et al., 2009). In general, glucosinolates are synthesized constitutively in plants, and are found predominantly in the *Brassicaceae* family (Fahey et al., 2001). These compounds are typically divided into three classes: aliphatic glucosinolates, derived primarily from amino acid methionine; indolyl glucosinolates, derived from tryptophan; and aromatic glucosinolates, derived from phenylalanine (for review see Halkier and Gershenzon, 2006). These metabolites are stored in the vacuole, and when tissue is damaged (*e.g.* by herbivory), they are released from the vacuole and hydrolysed by the endogenous enzyme myrosinase (β-thioglucosidase) that is localized in idioblasts. The products of glucosinolate-myrosinase system are biologically active molecules including isothiocyanates, nitriles, thiocyanates, oxazolidine-2-thiones and epithionitriles, with multiple physiological functions including cell signaling, pathogen resistance, *etc.* (Wittstock and Halkier, 2002; Kim et al., 2008; Wittstock and Burow, 2010).

Differently from *A. thaliana* wild-type plants, *cad1-3* mutants are impaired in callose deposition after Flg22 treatments and accumulate a callose precursor, 4-methoxy-indol-3-ylmethylglucosinolate (4-methoxy-I3G). Other mutants such as *pen2-1* or *pen3-1* accumulate the same glucosinolate and show a complete loss of callose deposition after Flg22 treatment. *PEN2* is a putative myrosinase enzyme involved in the Flg22-induced hydrolysis of 4-methoxy-I3G, whereas *PEN3* is an ABC transporter that is involved in IGS breakdown too (Clay et al., 2009; Bednarek et al., 2009). *PEN2*, *PEN3* and *PCS1* interact with each other to mediate hydrolysis of 4-methoxy-I3G with consequent callose deposition (Clay et al., 2009). How PCS1 is involved in callose synthesis and deposition is currently unknown.

PCS is Involved in Camalexin Biosynthesis

Su et al. (2011) reported a correlation amongst *AtPCS1*, the overall secondary metabolism, and the catabolism of GS-conjugates. The above-mentioned authors found an upregulation of *AtPCS1* during camalexin biosynthesis. Camalexin is a major phytoalexin of *A. thaliana*, and is an antimicrobial compound produced by this species after infection or stress (Hammerschmidt, 1999; Glawischnig, 2007). The work of Su et al. (2011) suggests a role of AtPCS1 enzyme in the catabolism of an intermediate of camalexin biosynthesis, the indole-3-acetonitrile (IAN). It is a common precursor also of indole glucosinolates and indole-3-acetic acid biosynthesis (Hansen and Halkier, 2013). In camalexin pathway, the IAN is conjugated to GSH and the complex GS(IAN) is catabolized by AtPCS1 with the corresponding production of γGluCys(IAN) (Su et al., 2011).

In literature a link between glucosinolate and phenylpropanoid pathways (Hemm et al., 2003) is reported. The phenylpropanoid pathway is a starting point for the production of specialized number of metabolites such as lignins, sinapates, and flavonoids including flavonones, flavonols, and anthocyanins. Lignins are complex phenolic polymers that are mainly deposited in the walls of vasal and fiber cells, and are important for the strength and rigidity of the plant cell wall (Vanholme et al., 2010). Following their synthesis in the cytosol, the lignin monomers (monolignols) are exported to the apoplast where they undergo enzymatic oxidative polymerization. The composition of the resulting lignin polymers substantially varies in the ratios of the different monolignol residues between species, tissues and subcellular location, contributing to lignin complexity (Bonawitz and Chapple, 2010). Flavonoids indeed are a class of low molecular weight phenolic compounds widely distributed in the plant kingdom. They are involved in different biological functions and play an important role in the interaction between plants and environment. Flavonoids are implicated in UV irradiation protection, as attractants or feeding deterrents, and in plant stress resistance (Koes et al., 1993; Treutter, 2006).

Since AtPCS1 is involved in the glucosinolate pathway, lost or high expression of the enzyme might face consequences also in the phenylpropanoid pathway. We will deal with this point by studying the possible effects of AtPCS1 on the secondary metabolism of *A. thaliana*, by using a new approach: the metabolomics. This technique allows to identify and quantify all metabolites in a biological sample on the basis of their retention time, m/z and fragmentation spectrum. These data, combined with multivariate statistical analysis, are able to reveal the metabolic outcome of a genetic or environmental perturbation of a metabolic regulatory network.

Presence or Not Presence of PCS in the First Land Plants

The data in literature about the presence of PCS gene(s) and active PCS enzyme(s) in the earliest diverged extant land plants, collectively referred to as bryophytes [liverworts (Hepatophyta, sin. Marchantiophyta), mosses (Bryophyta), and hornworts (Anthocerotophyta) (Vanderpoorten and Goffinet, 2009)], are not clear. For example, the preliminary screening on liverworts carried out by Gekeler et al. (1989) proved the thalloid species *Marchantia polymorpha* to be a weak producer of PCs under Cd stress. By contrast, these results were the contradicted by Bruns et al. (2001), who exposed *M. polymorpha* and *Pellia epiphylla* to Cd up to 10 d, and did not detect any PC synthesis. Likewise, although the presence of PCs in the metal-exposed freshwater moss *Rhynchostegium riparioides* and in the liverwort *Lunularia cruciata* was considered likely (Jackson et al., 1991; Carginale et al., 2004), no unequivocal proof of PC synthesis was ever provided in these species. Differently, the "model" moss *Physcomitrella patens*, at present the only bryophyte with an entirely

sequenced genome (Rensing et al., 2008), lacks the PCS gene (Kopriva et al., 2007). So, if the capability to produce PCs and the constitutive presence of functional PCS(s) enzyme(s) might represent useful conserved traits for all bryophyte lineage is not clear. Recent studies have acquired a large body of evidence to support the hypotheses that: (i) land plants, and particularly bryophytes, have a charophytic ancestry [given in particular by the Charophyta orders Charales, Coleochaetales, and Zygnematales (McCourt et al., 2004; Qiu et al., 2006; Qiu, 2008; Becker and Marin, 2009; Wodniok et al., 2011)], that are able to synthesize PCs; and (ii) hornworts are the sister group of tracheophytes (Qiu et al., 2006; Qiu, 2008; Villarreal et al., 2010; Ligrone et al., 2012). In addition, the earliest and best preserved bryophytic and vascular flora were present in the Early Devonian Rhynie Cherts of NE Scotland (~396 ± 12 Mya) (Rice et al., 1995; Kenrick and Crane, 1997; Pires and Dolan, 2012), where high levels of As, Hg, Zn, *etc.* were found (Rice et al., 1995). All these elements are inductors of PCs.

AIM OF THE STUDY

Other than a well-established role addressed to heavy metal and arsenic (As) detoxification (Grill et al., 1989; Clemens et al., 1999; Ha et al., 1999; Vatamaniuk et al., 1999; 2000; 2004; Romanyuk et al., 2006), the phytochelatin synthase (PCS) enzyme might perhaps play some additional roles/functions in the plant cell. Indeed, based on studies of *Arabidopsis thaliana* PCS1 (AtPCS1), it has been found that the enzyme is generally not upregulated by excess of toxic metals (Vatamaniuk et al., 2000; Cobbett, 2000), but is rather activated by essential metal (*i.e*: iron, Fe) deficiency conditions (Colangelo and Guerinot, 2004). Moreover, according to Vatamaniuk et al., (2000), metal presence is not essential for the net phytochelatin (PC) synthesis, but such synthesis may be also given by the sole blockage of the glutathione (GSH) thiol group (Vatamaniuk et al., 2000). This evidence was substantiated by the finding that AtPCS1 is involved in the catabolism of glutathione-conjugates (Beck et al., 2003; Blum et al., 2007; Su et al., 2011). In fact, when the sulfhydryl group of GSH binds different type of compounds, like uracil, acetamidofluorescein, benzyl, phenylbenzyl-GS, AtPCS1 is able to catalize a desglycylation reaction, resulting in the formation of the corresponding γGlu-Cys-conjugate (Blum et al., 2007).

Furthermore, the transcript abundance of *AtPCS1* increases under Fe deficiency and after treatment with a mimetic signal of a pathogen attack, a synthetic 22-amino acid peptide that corresponds to a highly conserved region of the eubacterial flagellin (Flg22) (detailed below and described in Colagelo and Guerinot, 2004 and Clay et al., 2009).

Moreover, *AtPCS1* knockout mutant plants: i) are not able to produce callose, suggesting a role of PCS for the pathogen-triggered callose deposition (Clay et al., 2009); ii) show a lower level of camalexin than wild-type plants (Su et al., 2011), indicating a role of PCS also for camalexin biosynthesis.

In this context, the goal of my PhD dissertation is to revise roles of the PCS enzyme, its substrate(s), and its potential, perhaps archaic, homeostatic function, by using *A. thaliana* as an experimental model and array of approaches including LC-ESI-MS-based metabolome analyses, gene expression studies, *etc*. These studies are integrated by research aimed at elucidating the evolutionary roles of PCS, as well as the ability to synthesize PCs, both possible important traits perhaps already present in basal plants such as bryophytes, lycophytes, and charophytes, the latter being sister group of land plants.

MATERIALS AND METHODS

Arabidopsis thaliana plants employed in this work were:

- wild-type accession Columbia-0, from Prof. Gian Pietro Di Sansebastiano, University of Salento, Italy;
- *cad1-3 mutant*, previously characterized by Howden et al. (1995a), and transgenic plants ectopically expressing *AtPCS1* from the Cauliflower Mosaic Virus (*CaMV*) *35S* promoter (*AtPCS1-OE*) using the construct *pCAMBIA::35S-PCS1*, previously characterized by Brunetti et al. (2011) from Dr. Maura Cardarelli, National Research Council, IBPM, Rome, Italy;
- *cad2-1* mutant, previously characterized by Howden et al. (1995b), from Prof. Olena K. Vatamaniuk, Cornell University, Ithaca, NY, USA;
- *pen2-1* mutant, previously characterized by Lipka et al. (2005), from Prof. Georg Jander, Boyce Thompson Institute for Plant Research Ithaca, NY, USA;
- *pad4* mutant, previously characterized by Glazebrook et al. (1997), from Prof. Sorina Papescu, Boyce Thompson Institute for Plant Research Ithaca, NY, USA.

Growth Condition for A. thaliana

For metabolomics study, *A. thaliana* wild-type, *cad1-3* and *AtPCS1-OE* plants were grown in Gamborg's B-5 Basal Salt Mixture medium (Sigma-Aldrich, **Table 1**) supplemented with Gamborg's Vitamin solution (Sigma-Aldrich), sucrose (30g/L), pH 5.8 with KOH 0.1 M and 7g/L agar.

Table 1: Composition of Gamborg's B5 medium used for growing different plant lines for metabolomics.

Gamborg's B5 medium (Gamborg, 1968)			
Nutrient	mg/L	Nutrient	mg/L
KNO_3	2500	$CuSO_4*5H_2O$	0.025
$(NH_4)_2SO_4$	134	$Na_2MoO_4*2H_2O$	0.25
$MgSO_4*7H_20$	250	$CoCl_2*6H_2O$	0.025
$CaCl_2*2H_20$	150	$FeSO_4*7H_2O$	27.8
$NaH_2PO_4*H_20$	150	Na_2EDTA	37.3
$MnSO_4*H_2O$	10	KI	0.75
H_3BO_3	3	$ZnSO_4*7H_2O$	2

For analyses of the role of AtPCS1 in Fe homeostasis, plants were grown in half concentrated Murashige and Skoog base medium (Sigma-Aldrich, **Table 2**) supplemented with sucrose (10g/L), pH 5.6 with KOH 0.1 M (from here on ½ MS). To prepare solid medium, ½ MS was also supplemented with 7g/L agar.

Table 2: Composition of ½ MS medium used for growing different plant lines for analyses of AtPCS1 in Fe homeostasis.

½ **Murashige and Skoog Base Medium**			
Nutrient	mg/L	Nutrient	mg/L
NH_4NO_3	825	$MgSO_4$	90.35
H_3BO_3	3.1	$MnSO_4*H_2O$	8.45
$CaCl_2$	166.1	MoO_3*2H_2O	0.125
$CoCl_2*6H_2O$	0.0125	KI	0.415
$CuSO_4*5H_2O$	0.0125	KNO_3	950
Na_2EDTA	18.63	HK_2PO_4	85
$FeSO_4*7H_2O$	13.9	$ZnSO_4*7H_2O$	4.3

To introduce Fe deficiency, ½ MS medium was supplemented with a Fe^{2+} chelator, 200 µM bathophenanthroline disulfonic acid disodium salt hydrate (BPS, Sigm-Aldrich).

Wild-type, *cad1-3*, *AtPCS1-OE* plants were also grown in hydroponic solution described by Arteca and Arteca (2000). Iron was supplied as FeHBED [HBED: N,N'-Di(2-hydroxybenzyl) ethylenediamine-N,N'-diacetic acid monohydrochloride]. The hydroponic solution was changed every week. For Fe deficiency assays, plants were grown hydroponically for 3 weeks and transferred to medium without FeHBED for one week.

Wild-type, *cad1-3*, *AtPCS1-OE*, *pad4* plants were also grown using Metro-Mix soil. In all assays, plants were grown at 22 °C with 60 % relative humidity under 14 hours of daylight, at a photosynthetic photon flux density of 120 µmol photons m^{-2} s^{-1}.

Metabolites Extraction and HPLC-ESI-MS Analysis

Three-week-old *A. thaliana* wild-type, *cad1-3* and *AtPCS1-OE* were grown in solid Gamborg's B5 medium (Gamborg et al., 1968) (control condition) for twenty-one days. On 20th day, medium was overlaid with liquid solution of cadmium, or jasmonic acid or chitosan to reach a final concentration of 36 µM, 100 µM, 200 mg/L, respectively, and plants were grown under these

conditions (plus control) for additional 24 h. Roots and leaves were separated, frozen in liquid nitrogen and ground to a powder using a mortar and pestle. Twenty plants grown in the same Petri dishes were pooled and designated as a sample. For each treatment, 5 biological replicates were used.

Total metabolites were extracted with 4 volumes of cold methanol (W/V), followed by vigorous mixing with "vortex" type mixer and sonication at 40 kHz for 15 min in an ultrasonic bath (Falc Instruments, Bergamo, Italy), on ice. Then the samples were centrifuged at 16000 × *g* for 10 min at 4 °C and the supernatants were filtered through minisart RC4 (0,2 µm) pore filters. The methanol phases were diluted with LC-MS grade water (1/3, V/V) (Sigma Aldrich, St Louis) just before the chromatographic analysis and analysed by reverse phase HPLC-ESI-MS (high performance liquid chromatography plus electro spray ionization mass spectrometry). Fragmentation experiments were performed in both positive and negative ion modes to assist the identification of the molecules, using a Beckman Coulter Gold 127 HPLC system (Beckman Coulter, Fullerton, CA) equipped with a C18 guard column (7.5 × 2.1 mm) and an analytical Alltima RP C18 column (150 × 2.1 mm, particle size 3 µm) (Alltech Associates Inc, Derfield, IL).

The solvents used for HPLC-ESI-MS analysis were: 0.5 % (v/v) formic acid, 5 % (v/v) acetonitrile in water (solvent A), and 100 % acetonitrile (solvent B). A solvent gradient was established from 0 to 10 % B in 5 min, from 10 to 20 % B in 10 min, from 20 to 25 % B in 5 min, and from 25 to 70 % B in 15 min. The injection volume was 5 µL per injection; the flow rate was 200 µL/min. The HPLC system was coupled on-line with a Bruker ion trap mass spectrometer Esquire 6000, equipped with an electrospray ionization (ESI) source. MS data were collected using the Bruker Daltonics Esquire 5.2-Esquire Control 5.2 software, and processed using the Bruker Daltonics Esquire 5.2-Data Analysis 3.2 software (Bruker Daltonik GmbH, Bremen, Germany). The alternate mass spectra were recorded in the range 50–3000 m/z (full scan mode, 13.000 m/z s^{-1}). For the fragmentation pattern analysis, MS/MS and MS3 spectra were recorded in negative and positive mode in the range 50-3000 m/z, with the fragmentation amplitude set at 1 V. Nitrogen was used as the nebulizing gas (50 psi, 350 °C) and drying gas (10 L min^{-1}). Helium was used as the collision gas.

The metabolites were identified through a comparison of m/z, retention time and the fragmentation pattern with the data available in the MassBank public database (http://www.massbank.jp/) and in the literature. Chromatogram data extraction and alignment were carried out using MZmine software (http://mzmine.sourceforge.net). The relative quantitation (*i.e.*, comparison between samples) was based on the area of each of the signals extracted from the chromatograms and expressed as intensity (arbitrary units).

Statistical Analysis of Metabolomics Study

Once all metabolic profiles from wild-type, *cad1-3* and *AtPCS1-OE* plants were obtained, data were processed using the statistical SIMCA-P+12 software (Umetrix AB, Umea, Sweden). Two main methods were used: PCA (Principal Components Analysis), which is a completely unsupervised method to classify samples based on the x variables (the metabolites); Orthogonal Projection to Latent Structure Discriminant Analysis (O2PLSDA) a supervised method the classes, *i.e.* the groups of samples, are defined by the operator.

In both cases the Pareto scaling was used. In detail, this O2PLSDA-S loading plot analysis correlates the metabolites with the operator defined group of samples (classes, in this case wild-type, *cad1-3* mutant and *AtPCS1-OE* plants) and highlight the difference in terms of metabolites accumulation among them. Models were cross validated using a permutation test (200 permutations). The average value of the two technical replicates of each sample was calculated for each metabolite for these analyses.

Callose Staining Methods

Callose staining was performed as described in Clay et al. (2009). Briefly, 10-day-old seedlings of wild-type, *cad1-3*, *AtPCS1-OE*, *pen2-1* were fixed in a solution, containing ethanol and glacial acetic acid (3:1 ratio, respectively) using short-term vacuum infiltration, and then for about 4 h (until cotyledons appeared slightly translucent) on a shaking platform with several changes of fixing solution. Seedlings were re-hydrated in 70 % ethanol for ≥ 2 h and in 50 % ethanol for ≥ 2 h, washed in water twice, and left in water overnight on a shaking platform.

After several washes with de-ionized water, seedlings were made transparent in 10 % NaOH, which was introduced using vacuum infiltration for several minutes. Seedlings were washed-free from NaOH with de-ionized water, incubated for more than 4 h in 150 mM K_2HPO_4 (pH 9.5) solution containing 0.01 % aniline blue and mounted on slides with 50 % glycerol.

Callose-mediated fluorescence was visualized using a DAPI filter set (excitation filter 390 nm; dichroic mirror 420 nm; emission filter 460 nm) of an Axio Imager M2 microscope equipped with the motorized Z-drive (Zeiss). Images were collected with AxioCam MR Camera and processed using the Adobe Photoshop software package, version 12.0.

Bacterial Growth Assay

Pseudomonas syringae DC3000 cells were grown at 30 °C on LB medium containing rifampicin at a concentration of 50 μg mL^{-1}. Prior to infiltration, bacteria were suspended in sterile 10 mM $MgCl_2$ and bacterial cell density (OD_{600}) was measured using a Jenway 6320D

spectrophotometer (Bibby Scientific Limited, Staffordshire, UK). *Pseudomonas syringae* DC3000 was infiltrated at a concentration of 3.10^5 bacterial colony forming units (CFU) per mL onto leaves of 4-week-old wild-type, *cad1-3*, *AtPCS1-OE* and *pad4* plants, all grown in soil. To determine the bacterial propagation on leaves, we measured internal bacterial population at time 0 and 48 h after infiltration. Internal bacterial populations were evaluated from 12 biological replicates and each replicate represented a pool of 3 leaves from the same infiltrated plant. To do so, inoculated leaves were collected by cutting the leaf with a punch (diameter 6 mm) and all samples were transferred to a 96-well plate containing 1 mL of 10 mM $MgCl_2$ buffer and stainless steel beads. Homogenising proceeded in a shaker chamber. The extracts were 5 fold diluted serially (1:10) and were plated on petri dishes with LB medium containing the antibiotic rifampicin. The plates were incubated for 2 days at 30 °C and CFU was counted using the diluted samples. Bacterial populations were evaluated using three independent experiments.

Stretch experiment

Stems of wild-type, *cad1-3*, *AtPCS1-OE* two-month-old plants were sectioned in: the base, the middle and the upper zones. After, the pressure (MPa) required to break them was measured by means of the Intron instrument.

Lignin Staining

Staining of lignin was performed on hand-made sections of stems collected from two-month-old wild-type, *cad1-3*, *AtPCS1-OE* plants, all grown in soil. Sections were stained with 1 % phloroglucinol (w/v) in 12 % HCl for 5 min according to Weng et al. (2010). Lignin was visualized using a light of an Axio Imager M2 microscope equipped with the motorized Z-drive (Zeiss). Images were collected with AxioCam MR Camera and processed using the Adobe Photoshop software package, version 12.0.

RNA Isolation and cDNA Synthesis

Total RNA was isolated from roots of 10-day-old seedlings and 4-week-old mature plants using a Trizol reagent (Invitrogen) according to manufacturer's instructions. Briefly, frozen samples were ground in liquid nitrogen to a powder using a mortar and a pestle and transferred into microcentrifuge tubes before adding 1mL of the Trizol reagent. After incubating samples in Trizol for 5 min at room temperature, 0.2 mL of chloroform was added and samples were mixed by vortexing. Then samples were centrifuged at 12000 × *g* at 4 °C. After that, the aqueous phase was transferred to a fresh microcentrifuge tube and RNA was precipitate by mixing with 0.5 mL of

isopropanol. After, the samples were incubated at room temperature for 10 min and centrifuged for 20 min at 12000 × *g* at 4 °C. Supernatant was decanted and pellet was washed with 1 mL 75 % (v/v) RNase-free ethanol. Samples were then mixed by inverting the tube and centrifuged at 7500 × *g* for 20 min at 4 °C. The ethanol was removed and pellets were dried at room temperature. RNase-free water was added to the RNA pellet and it was resuspended by vortexing. The RNA concentration was then determined using a spectrophotometer.

To obtain the best quality of cDNA, contaminant genomic DNA in total RNA samples was digested with DNase I (Roche Applied Science). In detail, 1 µg of RNA was treated with 2 units of RNase-free DNaseI at 37 °C for 20 min and then incubated at 65 °C for 15 min. Tubes with DNA-free RNA were cooled on ice for 1 min prior to cDNA synthesis. To initiate cDNA synthesis, oligo(dT) primer and the AffinityScript RT/RNase block enzyme mixture were added to DNA-free RNA, as described in the protocol provided with the cDNA synthesis kit. The content of the tube was mixed and the reaction mixture was incubated in the PCR machine (BioRad) using the following temperature regime: 25 °C for 5 min, 42 °C for 30 min, 95 °C for 5 min. The synthesized cDNA was stored at -20 °C before use.

Quantitative Real-Time (qRT)-PCR and Data Analysis

Primer pairs (forward [F] and reverse [R]), specific to the tested genes were designed based on the genes sequence from *A. thaliana* website (http://www.arabidopsis.org/) and are reported in **Table 3**:

Table 3: Primers used for qRT-PCR analyses.

GENE NAME	**5' ⟶ 3'**
ACTIN2-F	GACCTTTAACTCTCCCGCTA
ACTIN2-R	GGAAGAGAGAAACCCTCGTA
PCS1-F	CCCAATTTCGAATCTCACACACCG
PCS1-R	GAGATCGCCGATATAAACTCGCCA
IRT1-F	ACCCGTGCGTCAACAAAGCTAAAG
IRT1-R	TCCCGGAGGCGAAACACTTAATGA
FRO2-F	TGTGGCTCTTCTTCTCTGGTGCTT
FRO2-R	TGCCACAAAGATTCGTCATGTGCG
OPT3-F	CTCTTCATCGTCTTGACCACTC
OPT3-R	ACTTGTTTTCCTTCTCGTGC

qRT-PCR was performed as described in Gayomba et al. (2013). Briefly, 2 µL of 15-fold diluted cDNA was used as a template for quantitative PCR in a total volume of 15 µL containing 300 nM of each PCR primer and the iQ SYBR Green Supermix (BioRad). PCR was performed in the CFX96 Real-Time PCR system (BioRad). The thermal cycling parameters were: denaturation at

95 °C for 3 min, followed by 39 cycles of 95 °C for 10 s, 55 °C for 30 s. Amplicon dissociation curves, *i.e.* melting curves, were recorded after cycle 39 by heating from 60 °C to 95 °C with 0.5 °C increments and an average ramp speed of 3.3 °C s^{-1}. Real-time PCR experiments were conducted using three independent biological samples, each consisting of three technical replicates. Data were normalized to the expression of two reference genes encoding ACTIN-2 (AT3G18780). The fold difference ($2^{-\Delta\Delta Ct}$) was calculated using the CFX Manager Software, version 1.5 (BioRad). Statistical analysis was performed using the Relative Expression Software Tool (REST, Qiagen).

Elemental Analysis

Roots and leaves of hydroponically grown 4-week-old wild-type, *cad1-3*, *AtPCS1-OE* plants were harvested and roots were desorbed of Fe as well as other elements by washing with 10 mM EDTA followed by washing in a solution with 0.3 mM bathophenanthroline disulphonate and 5.7 mM sodium dithionite and then rinsed with deionized water (Jung et al., 2012). Shoots were rinsed with deionized water. Samples were dried at 80 °C for 2 days. Elemental analysis was performed by inductively coupled plasma mass spectroscopy (ICP-MS, Agilent 7500) as described (Lahner et al., 2003; Jung at al., 2012).

Charophyte, Bryophyte and Lycophyte Species

The material employed consisted of non axenic pure monocultures, collected in Italian locations (Apuan Alps, Massaciuccoli Lake, surroundings of Parma, Salerno, Naples Botanical Gardens) in February-October of 2012-2014. In addition, specific monocultures of *Coleochaete scutata* were obtained from the Carolina Biological Supply Company, Burlington, NC, USA, and set up as the other cultures. All material was abundantly rinsed with double-distilled water, carefully checked for the absence of all potential soil/biological contaminants and endosymbiotic organisms (*i.e.* Cyanobacteria, Glomeromycota, *etc.*) under a stereomicroscope (WILD, Heerbrugg, Switzerland) and an Olympus BH2 microscope ×40 (Olympus Italia, Segrate, Italy). All Charophytes and bryophyte species investigated in this work are reported in the simplified phylogenetic tree below:

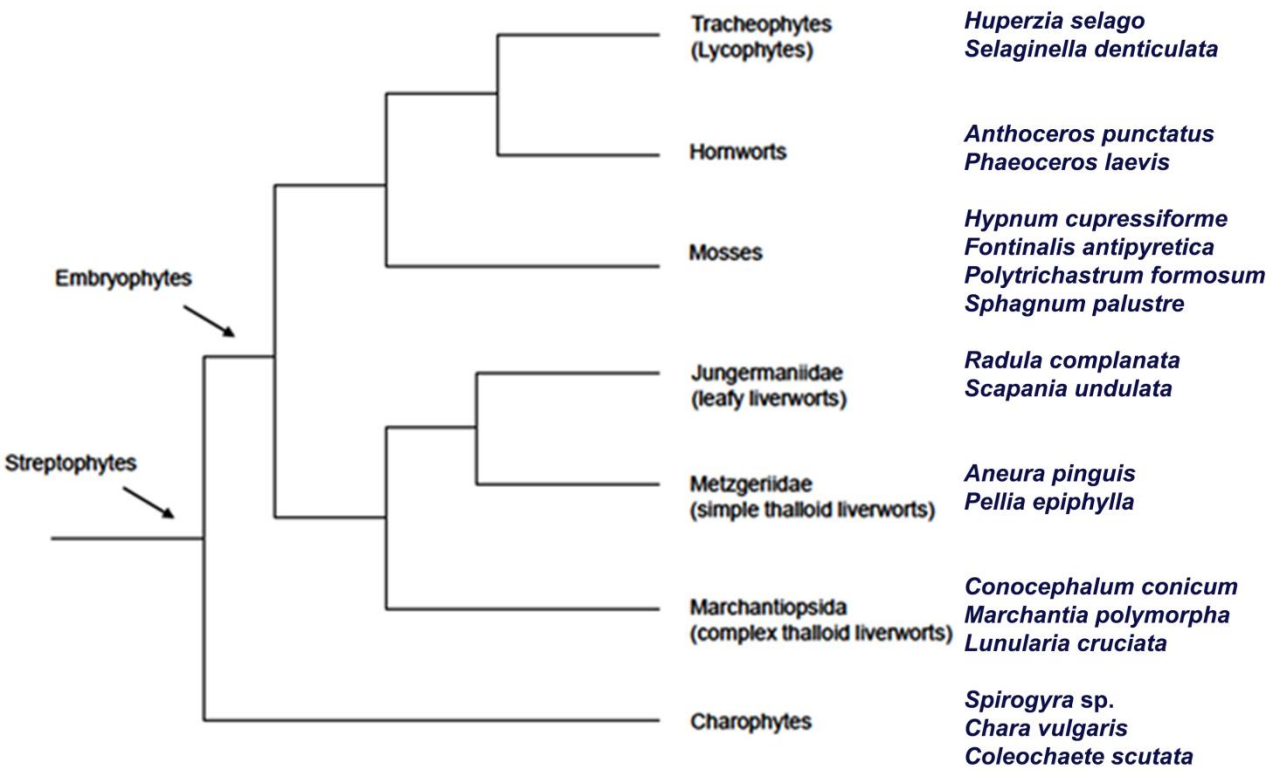

Grown Conditions

After selection and cleaning, all species were transferred into sterilized plant culture vials (Phytacon™), filled with 100 mL of sterile modified Chiaudani–Vighi (Chiaudani and Vighi, 1977) culture medium pH 6.0. Ethylenediaminetetraacetic acid (EDTA) was omitted from original protocol in order to avoid undesirable Cd chelation. The final composition of the medium was as follows:

Table 4: Composition of Chiaudani-Vighi medium used for treating different species of charophytes, bryophytes and lycophytes.

Chiaudani-Vighi medium			
Nutrient	mg/L^{-1}	Nutrient	$\mu g/L^{-1}$
$NaNO_3$	2.55	$FeSO_4$	5.58
$K_2HPO_4*6H_20$	0.10	H_3BO_3	18.55
$MgCl_2*6H_20$	0.57	$MnCl_2$	26.43
$MgSO_4*7H_20$	2.94	$ZnCl_2$	3.28
$CaCl_2*2H_20$	0.44	$CoCl_2$	0,08
$NaHCO_3$	1.50	$CuCl_2$	0,0009
EDTA	0	$Na_2MoO_4*2H_2O$	0,73

Then, all vials were placed in a growth chamber at 20 ± 1 °C, under a photoperiod of 16 h light [photosynthetic photon flux density (PPFD) 60 µmol m^{-2} s^{-1}]/8 h dark. With regard to the

species to be analysed for their thiol-peptide content, half of the samples were treated for 72 h with 36 µM Cd, in the form of $3CdSO_4*8H_2O$, whereas the other half (controls) were given deionized water in an identical volume as for the Cd solution. Moreover, the bryophyte cultures were daily sprayed with Cd at the same concentration as that in the medium (as well as deionized water in controls), because of their well-known capability to absorb elements also from the atmosphere (Tyler, 1990). At the end of the treatments, all plants were carefully rinsed with deionized water, gently blotted dry with filter paper, wrapped in aluminium foil, frozen in liquid nitrogen, and briefly stored at -80 °C for further analyses.

Thiol-Peptide Separation, Detection and Quantification by HPLC

Cd-treated and control cultures [at least 250 mg fresh weight (FW) for each sample] were homogenized for 10 min in a mortar with a filter GF/C (Whatman International Ltd., Maidstone, UK), in 400 µL ice-cold 5 % (w/v) 5-sulphosalicylic acid, containing 6.3 mM diethylenetriaminepentaacetic acid, according to de Knecht et al. (1994).

All samples were taken from mortar and transferred into an eppendorf with 600 µL of H_2O. After, the samples were centrifuged at 10000 × *g* for 10 min at 4 °C and the supernatants fraction were filtered through Minisart RC4 0.45 µm filters (Sartorius, Goettingen, Germany) and immediately assayed by HPLC (Model 200, Perkin-Elmer, Wellesley, MA, USA) with an injection loop of 200 µL.

Thiol-containing peptides (GSH and PCs) were separated by a Supelco Ascentis Express reverse-phase C18 column (Sigma-Aldrich, Milan, Italy). The separation was achieved using a 0-26 % acetonitrile gradient, with a flow rate set at 0.3 mL min^{-1}. The elution solutions contained 0.05 % trifluoroacetic acid. Thiol-peptides were determined using post-column derivatization with 300 µM Ellman's reagent [5,5'dithio(2-nitrobenzoic acid); DTNB] (Sigma-Aldrich) and with a flow rate set at 0.1 mL min^{-1} and detected at 412 nm (PerkinElmer detector mod. 200). The derivatization was done in bath of water at the temperature of 50 °C. The thiol peptides were quantified by calibration curves for standard SH groups and expressed in nmol SH g^{-1} FW. Identification of GSH and individual PCs was based on the comparison of their retention times with standard GSH (Merck, Darmstadt, Germany) and PC samples from *Silene vulgaris*.

Thiol-Peptide Characterization by Mass Spectrometry

The identity of putative GSH and PCs was verified by electrospray ionization mass spectrometry (ESI-MS) and tandem mass spectrometry (MS/MS). Liquid chromatographic elution was carried out on a Supelco Ascentis Express reverse-phase C18 column (Sigma- Aldrich), using a

gradient solvent system [solvent A, aqueous 0.05 % (v/v) trifluoroacetic acid; solvent B, 0.05 % (v/v) trifluoroacetic acid in acetonitrile] as follows: solvent B was set at 2 % for 12 min, raised with a linear gradient to 11 % in 3 min, raised with a linear gradient to 26 % in 16 min, and then raised with a linear gradient to 98 % in 7 min. Solvent B was maintained at 98 % for 6 min before column re-equilibration (10 min). The flow rate was 0.3 mL min^{-1}.

The mobile phase was delivered by an Ultimate 3000 system (ThermoElectron Corporation, San José, CA, USA). The injection volume was 20 µL. An LTQ Orbitrap XL (ThermoElectron Corporation) with a pneumatically assisted ESI interface was used. The system was controlled by Xcalibur software. The sheath gas (nitrogen, 99.999 % purity) was delivered at a flow rate of 50 arbitrary units; sweep and the auxiliary gas (nitrogen, 99.999 % purity) were delivered at a flow rate of 20 arbitrary units. The optimized conditions of the interface were as follows: ESI voltage, 3.5 kV; capillary voltage, 30 V; capillary temperature, 300 °C; and tube lens, 110 V. MS experiments were carried out in the 200-1500 mass-to-charge ratio (m/z) range.

MS/MS experiments were performed in the ion-trap collision cell with a normalized collision energy of 35 arbitrary units and an isolation width of 1 m/z; the product ions were analysed with an Orbitrap analyzer, with the m/z set as a function of GSH and PC molecular mass.

Statistical Analysis

Statistical analyses of the majority of experimental data were performed using Student's t test. Asterisks indicate statistically significant data at * $p < 0.05$; ** $p < 0.01$.

Statistical analyses of PC content in the above species and PCS activity were performed by SPSS Statistics, version 20. Comparisons amongst independent samples were done by the Kruskal–Wallis non-parametric test.

Western Blots

Proteins were extracted from about 150 mg of fresh tissue of *Nostoc* sp., sporophytes of *Phaeoceros laevis*, gametophytes of *P. laevis*, *Conocephalum conicum*, *Scapania undulata*, *Sphagnum palustre*, *Physcomitrella patens*, *Selaginella denticulata* roots by using 300 µL of lysis buffer, containing 50 mM TRIS-HCl pH 7.5, 2 M thiourea, 7 M urea, 2 % (v/v) Triton X-100, 1 % dithiothreitol (DTT), 2 % (w/v) polyvinylpolypyrrolidone (PVPP), 1 mM phenylmethylsulphonyl fluoride (PMSF), and 0.2 % β-mercaptoethanol.

Protein concentration was determined according to Bradford (1976), using bovine serum albumin as a standard. Aliquots of protein extracts (~20 µg of total protein per well) were separated using a 12 % SDS–polyacrylamide gel (Laemmli, 1970), and electrotransferred at 100 V for 60 min

to a nitrocellulose membrane (GE Healthcare Bio-Sciences AB, Uppsala, Sweden), using the Mini Trans-Blot cell apparatus (Bio-Rad Laboratories, CA, USA). Protein loading and transfer efficiency of extracts were verified by Ponceau-S staining.

Western blot analyses were performed with a polyclonal antibody (diluted 1:5000 in blocking buffer and probed for 2 h) raised against *A. thaliana* PCS1. As references for the immunoblotting specificity/detection, were used recombinant *A. thaliana* PCS1 (AtPCS1, 56 kDa) (Ruotolo et al., 2004) and extracts from root samples of in vitro grown *A. thaliana* seedlings. Immunoreactivity was visualized using an anti-rabbit IgG antibody conjugated to horseradish peroxidase (GE Healthcare Bio-Sciences AB) and a chemoluminescence western blotting detection system (Pierce ECL Plus Western blot Substrate; Pierce, Rockford, IL, USA), according to the manufacturer's instructions.

PCS Activity

Lunularia cruciata PCS (*LcPCS*) activity was assayed in 150 mg of fresh gametophytic material, as described in Petraglia et al. (2014) and Wojas et al. (2008), with the sole difference that, for each metal(loid) to be tested, the extraction and reaction buffers contained individually: 100 µM Cd, Fe(II), Pb, Hg, As(III) and 10-100 µM Zn, Cu, Sb(III), in the following forms: 3 $CdSO_4*8H_2O$, $FeSO_4*7H_2O$, $Pb(NO_3)_2$, $HgNO_3$, Na_3AsO_3, $ZnSO_4*7H_2O$, $CuSO_4*5H_2O$and $SbCl_3$. After an incubation time of 90 min at 35 °C with each metal(loid), in the presence of the protease inhibitor cocktail 'complete mini EDTA-free' (Roche Italia, Milan, Italy), and termination of the reaction with 125 µL 20 % trichloroacetic acid, assays of PCS activity were immediately performed by HPLC-ESI-MS. As a reference organism for PCS activity, *A. thaliana* 28-day-old in vitro sterile plants were tested under the same conditions used for *L. cruciata*. *LcPCS* and *AtPCS1* activities were calculated from the integrated PC peak areas, and expressed as pmol PCs mg^{-1} protein min^{-1}, according to calibration curves set up with known concentrations of standard GSH (Merck, Darmstadt, Germany). Total protein content was determined according to Bradford (1976), using bovine serum albumin as standard. The 'fold' of *LcPCS* and *AtPCS1* metal(loid)-induction *vs*. the respective controls, as well as the relative *LcPCS* and *AtPCS1* 'response ratio' (that is, the ratio between the activity of the metal(loid)-affected PCS and the respective control; Coleman et al. 2006) were calculated.

RESULTS

Metabolomics Study

It is recognized that AtPCS1 and other phytochelatin synthases (PCSs) are activated by glutathione (GSH), in which a thiol group is blocked by another functional group including transition metals, hydrocarbons, *etc.*, to produce canonical phytochelatins or other glutathione derivatives (Vatamaniuk et al., 2000; Beck et al., 2003; Blum et al., 2007). We hypothesized that yet unidentified glutathionated compounds might be also used as substrates of PCSs to form metabolites that serve important biological functions. The identification of these substrates and products could shed a light on biological functions of PCSs other than their roles in metal(loid) detoxification. First, to revise the physiological function of PCSs in plants, we used the metabolomic study.

To identify putative substrates and products of PCSs, we compared metabolite profiles of small molecules isolated from leaves and roots of *Arabidopsis thaliana* (wild-type), the *PCS1* mutant (*cad1-3*), and transgenic plants ectopically expressing *AtPCS1* under the control of the Cauliflower Mosaic Virus 35S promoter (CaMV-35S) (*AtPCS1-OE*).

All plant lines were grown for three weeks on solid Gamborg's B5 medium (Gamborg et al., 1968) (control). After that time a subset of plants was treated for 24 h with cadmium, or jasmonic acid, or chitosan by overlaying with liquid solution of each substance to reach the final concentration of 36 µM, 100 µM or 200 mg/L, respectively.

Plants were divided in roots and shoots and after extraction with methanol, the metabolite extracts were examined by LC-ESI-MS (Liquid Chromatography Electrospray Ionization Mass spectrometry). A representative LC-ESI-MS chromatogram of the metabolic profile from shoots of wild-type plants is shown in **Figure 2**. Peaks correspond to metabolites, their isotopes, fragments and adducts.

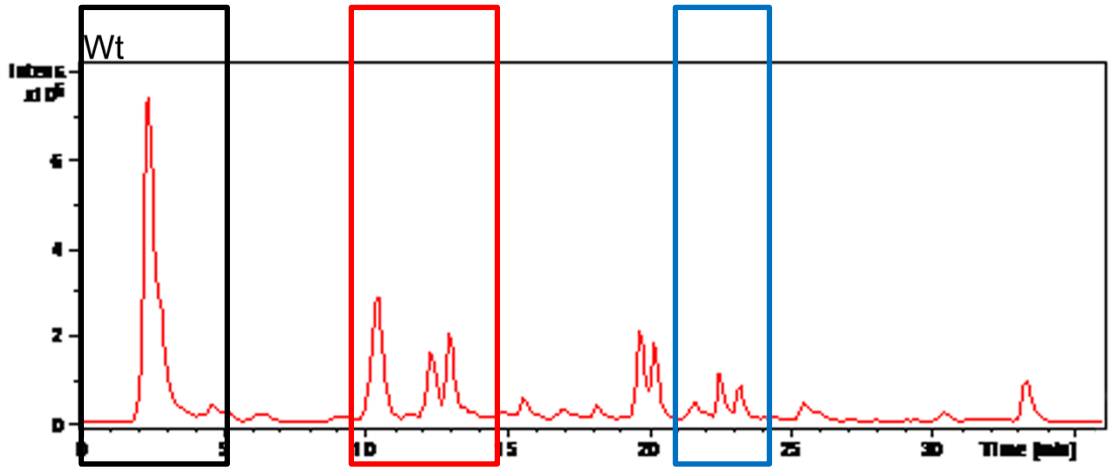

Figure 2: LC-ESI-MS chromatogram of methanolic extracts. The metabolites framed in colored rectangles are: gluthatione (black rectangle), hydroxycinnamic acids (red rectangle), flavonoid glycosides (blue rectangle).

The relevant data were extracted by the raw chromatograms using the M/Z MINE software, and the resulting data matrices were analysed by multivariate statistic methods, especially PCA and O2PLS-DA using the statistical software SIMCA. The product of these analyses are models that can be represented by plots such as those shown in **Figures 2-3**: in the score plots every colored dot corresponds to a sample(*) and every color corresponds to a different plant line, or an experimental set, while in the loading plot each of the black triangle corresponds to a specific metabolite and the red triangles corresponds to the class of sample (*i.e.* different plant line or experimental set). In the loading plot the distances between the metabolites and the class of sample reflects their relationship.

(*)To minimize the biological variability between plants, metabolite extracts from 20 plants grown under identical conditions were pooled and were designated as a sample.

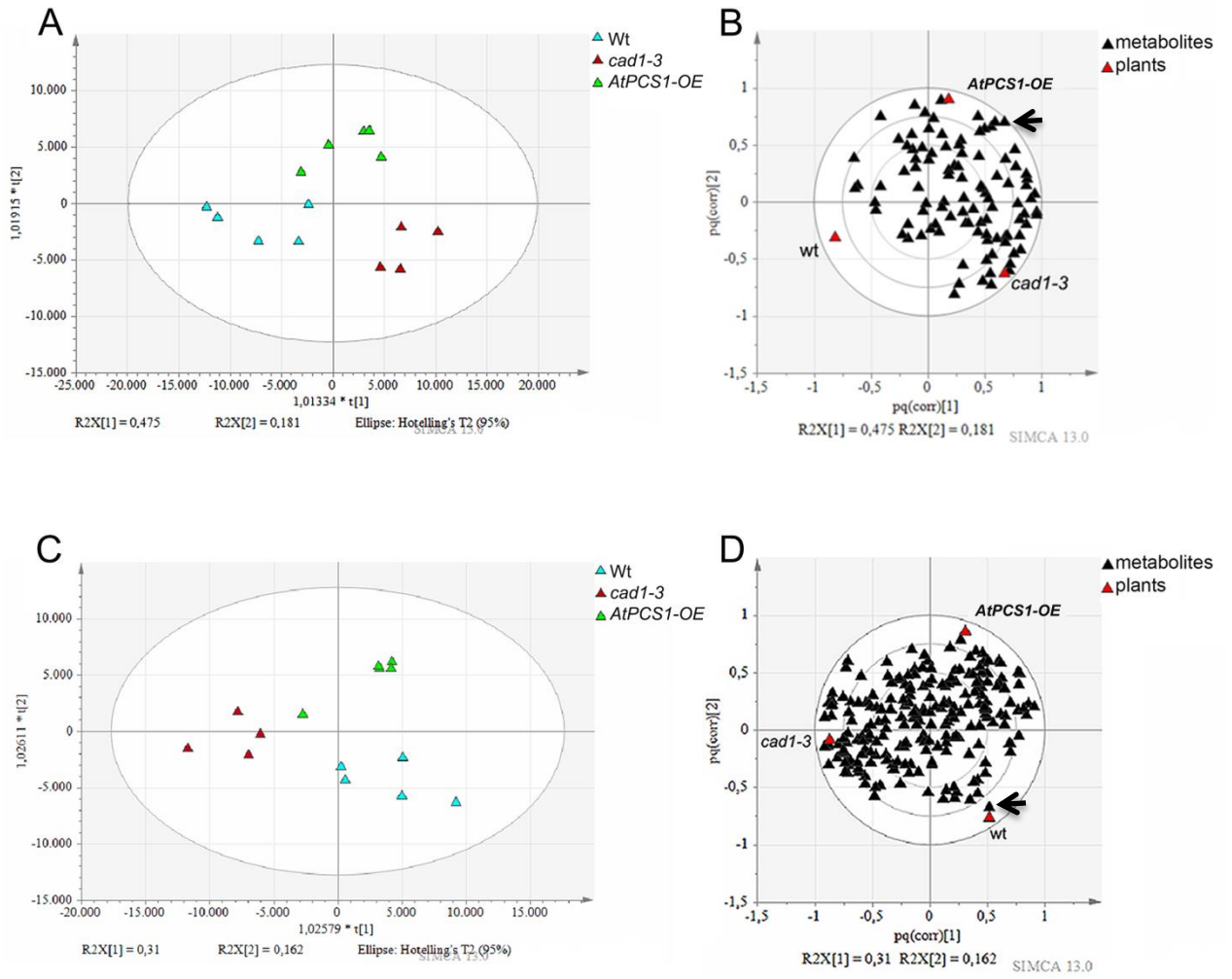

Figure 3: The multivariate statistical analysis of metabolites extracted from leaves and roots of different plants lines, Wt, the *PCS1* mutant (*cad1-3*) and transgenic plants ectopically expressing *AtPCS1* from the *35S* promoter (*AtPCS1-OE*), grown under control condition respectively.

The LC-ESI-MS-detected features were used as X variables. Orthogonal Projection to Latent Structure Discriminant Analysis (OPLS-DA) score scatter plots **(A)** from leaves and **(C)** from roots. **(B)** and **(D)** are the corresponding O2PLS-DA loading plots, the black triangles are the metabolites detected and the red triangles represent the various plants lines. The models are statistically significant with $p \leq 0.000809$ and 0.029477, respectively.

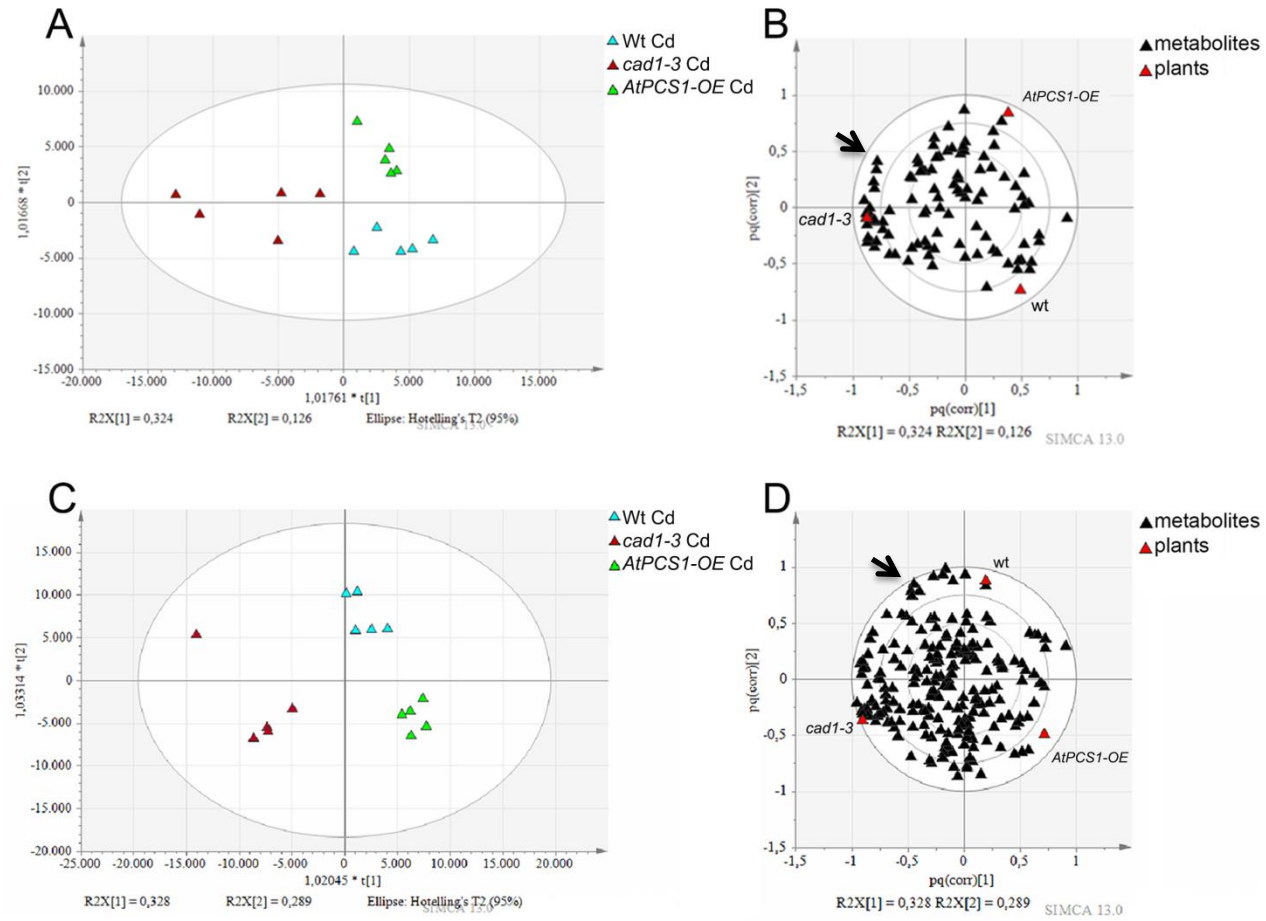

Figure 4: The multivariate statistical analysis of metabolites extracted from leaves and roots of Wt, *cad1-3* and *AtPCS1-OE* plants, all grown under 36 µM $CdCl_2$. The LC-ESI-MS-detected features were used as X variables. OPLS-DA score scatter plots **(A)** from leaves and **(C)** from roots. **(B)** and **(D)** show the metabolites that are present in different concentrations in leaves and roots respectively. Models are statistically significant with $p \leq 0.014$ or $p \leq 0.00006$, respectively.

Models show distinct clusters that are separated among the three plant lines along the first two principal components, both in leaves (**Figures 3A-4A**) and roots (**Figures 3C-4C**) of plants grown under control condition and after Cd treatment, respectively. Both models are statistically significant, cross validated using a test with 200 permutations and ANOVA.

To determine which metabolites are responsible for separating clusters from different groups separately, an O2PLS-DA loading plots discriminant analysis was performed (**Figures 3B,D-4B,D**). This analysis correlates the metabolites with plants. For example, metabolites that are localized in the last ring of the model and near a plant line (indicated by black arrows), are more accumulated in that plant line than the others.

This model highlights a clear difference among the three plants lines also under control conditions and shows the effect of *AtPCS1* on the secondary metabolism of plants. Specifically, we

found that the *AtPCS1* mutant plants had altered level of GSH and metabolites from glucosinolate and phenylpropanoid pathways.

Relationship Between AtPCS1 and GSH Levels

Given that AtPCS1 utilizes GSH in the presence of metals, we expected that roots and shoots of the Cd-grown *cad1-3* mutant would have higher concentration of GSH, while tissues of Cd-grown *AtPCS1-OE* transgenic plants would have less GSH in comparison with wild-type plants. Since the Gamborg's medium contains transition elements some of which (*e.g.* Zn and Cu) could promote PC synthesis, it was also possible that we would detect changes in GSH concentration between plant lines even under control conditions. Consistent with our predictions, leaves of the *cad1-3* mutant contained more GSH (relative level) than leaves of wild-type plants, with a *p* value near the significance ($p \leq 0.06$) even when grown under control conditions (**Figure 5**) and accumulated more than 2-fold of GSH after Cd treatment ($p \leq 0.005$). Surprisingly, we did not find statistically significant differences in GSH accumulation in roots of the *cad1-3* mutant *vs.* wild-type plants ($p \leq 0.5$; **Figure 5**). In contrast, leaves and roots of *AtPCS1-OE* plants contained significantly less GSH in comparison with the corresponding tissues of the wild-type plants, regardless whether plants were grown under control conditions or were treated with Cd.

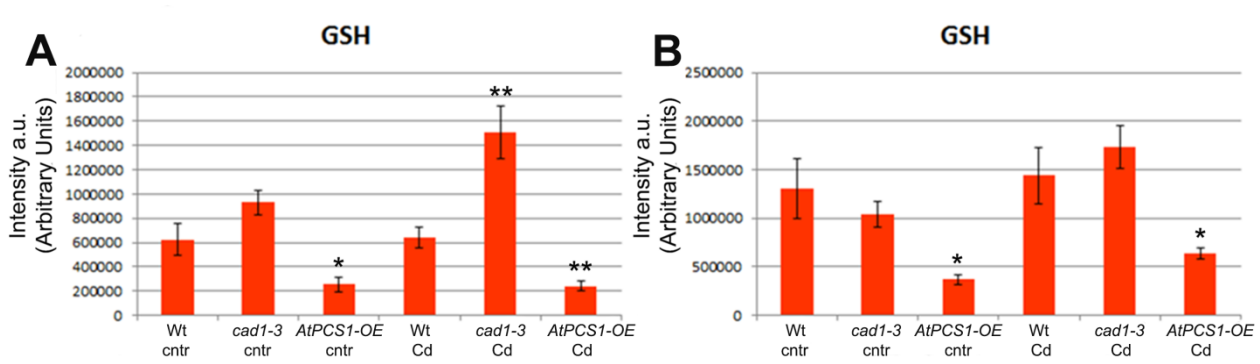

Figure 5: Relative levels of GSH in leaves **(A)** and roots **(B)** of Wt, *cad1-3* and *AtPCS1-OE* plants grown under control condition or after treatment with 36 µM of $CdCl_2$ for 24 hours.

Taken together, our data show that *AtPCS1* is essential for GSH metabolism in *A. thaliana*. This role of *AtPCS1* is most prominent in leaves and is observed even in plants grown under control conditions.

Glucosinolate Pathway

Comparison of metabolite profiles from tissues of wild-type, *cad1-3* and *AtPCS1-OE* plants showed that abundance of the 4-methoxy-indol-3-ylmethylglucosinolate increases in leaves of *cad1-3 vs.* wild-type plants, both grown under control condition and after Cd treatment (**Figure 6**).

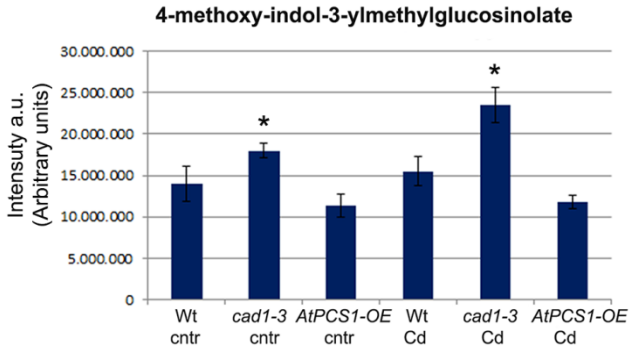

Figure 6: Glucosinolates accumulated differently in leaves of Wt, *cad1-3* mutant and *AtPCS1-OE* plants, all grown with or without 36 µM $CdCl_2$.

In roots of the same plant lines, the concentration of 8-methylthiooctylglucosinolate decreased in *cad1-3* mutant as well as *AtPCS1-OE vs.* wild-type regardless whether plant lines were grown under control condition or in a medium with Cd (**Figure 7**). On the contrary, an increase of 4-methoxy-indol-3-ylmethylglucosinolate in roots of *cad1-3* plants was found only after Cd treatment (**Figure 7**). Indeed, the relative levels of 4-methylsulfinylbutyl, 7-methylsulfinylheptyl glucosinolates was more than 2-fold higher in roots of *cad1-3 vs.* wild-type plants only after Cd treatment; and also higher in roots of *AtPCS1-OE vs*. wild-type under control condition (**Figure 7**).

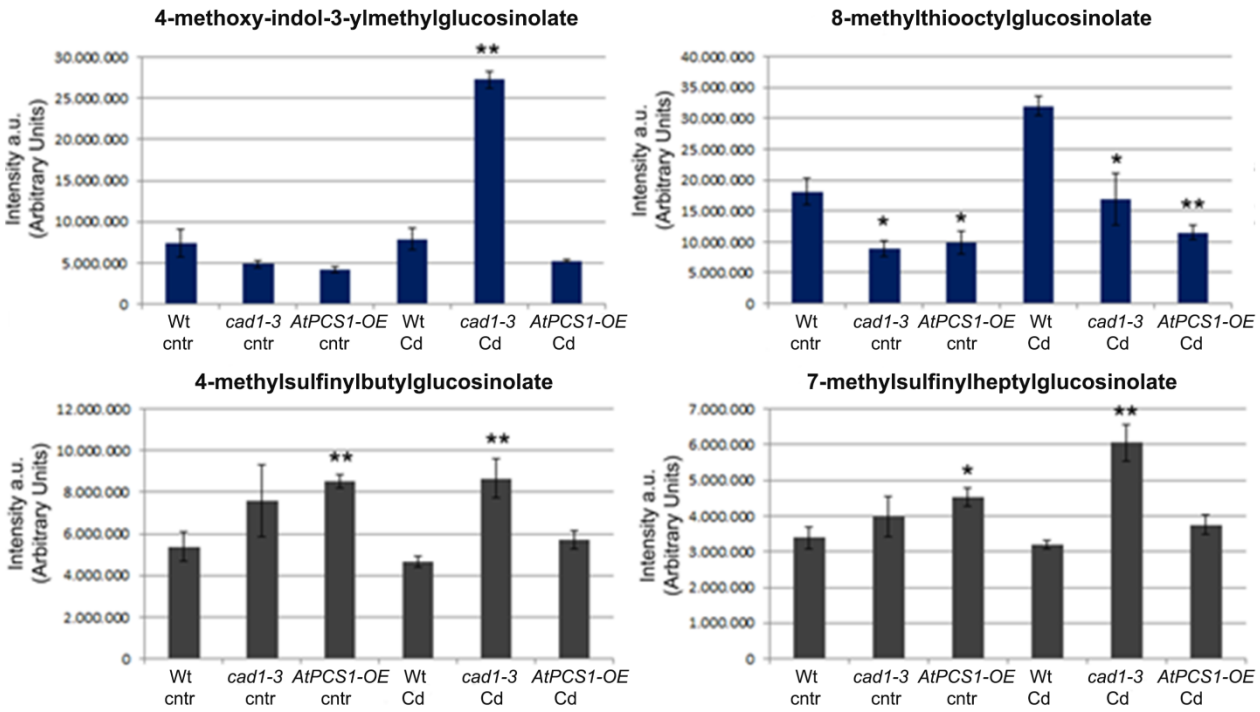

Figure 7: Concentration of glucosinolates in roots of indicated plant lines grown with or without 36 µM $CdCl_2$.

The Role of AtPCS1 in Callose Deposition in Relationship to Pathogen Resistance in A. thaliana.

Our data showing that the concentration of 4-methoxy-indol-3-ylmethylglucosinolate is higher in leaves of the *cad1-3* mutant *vs.* the wild-type both grown under control condition (**Figure 6**) are coherent with the previous work by Clay et al. (2009). The hydrolytic products of 4-methoxy-indol-3-ylmethylglucosinolate are required for synthesis of callose [β(1,3)-glucan polymer] (Clay et al., 2009). Callose is deposited in the plant cell wall and this process is considered to serve as a protection mechanism against the pathogen attack. As a result of the failure to the degradation of 4-methoxy-indol-3-ylmethylglucosinolate, the latter accumulates in leaves of the *cad1-3* mutant and the mutant does not produce callose in response to treatment with the pathogen mimetic signal, a synthetic 22-amino acid polypeptide, flagellin (Flg22) (Clay et al., 2009). We, therefore, argued that the *cad1-3* mutant will be more sensitive to pathogen infection, while transgenic plants overexpressing *AtPCS1* will be more tolerant to pathogen infection. To test this prediction we compared the sensitivity of different plant lines to the hemibiotrophic bacterial pathogen, *Pseudomonas syringae* DC3000 (*PsDC3000*). As we predicted, the *cad1-3* plants were more sensitive than wild-type to *PsDC3000* regardless whether the sensitivity was measured as a number of colonies formed by the pathogen (**Figure 8A**) or as lesions on the leaf surface (**Figure 8B,C**). Surprisingly, however, *AtPCS1-OE* plants were also more sensitive to the pathogen then the wild-

type (**Figure 8**). We used the pathogen-sensitive *pad4* mutant as a control for our condition, and as would be expected, *pad4* plants were more sensitive to pathogen as well (Xing and Chen, 2006).

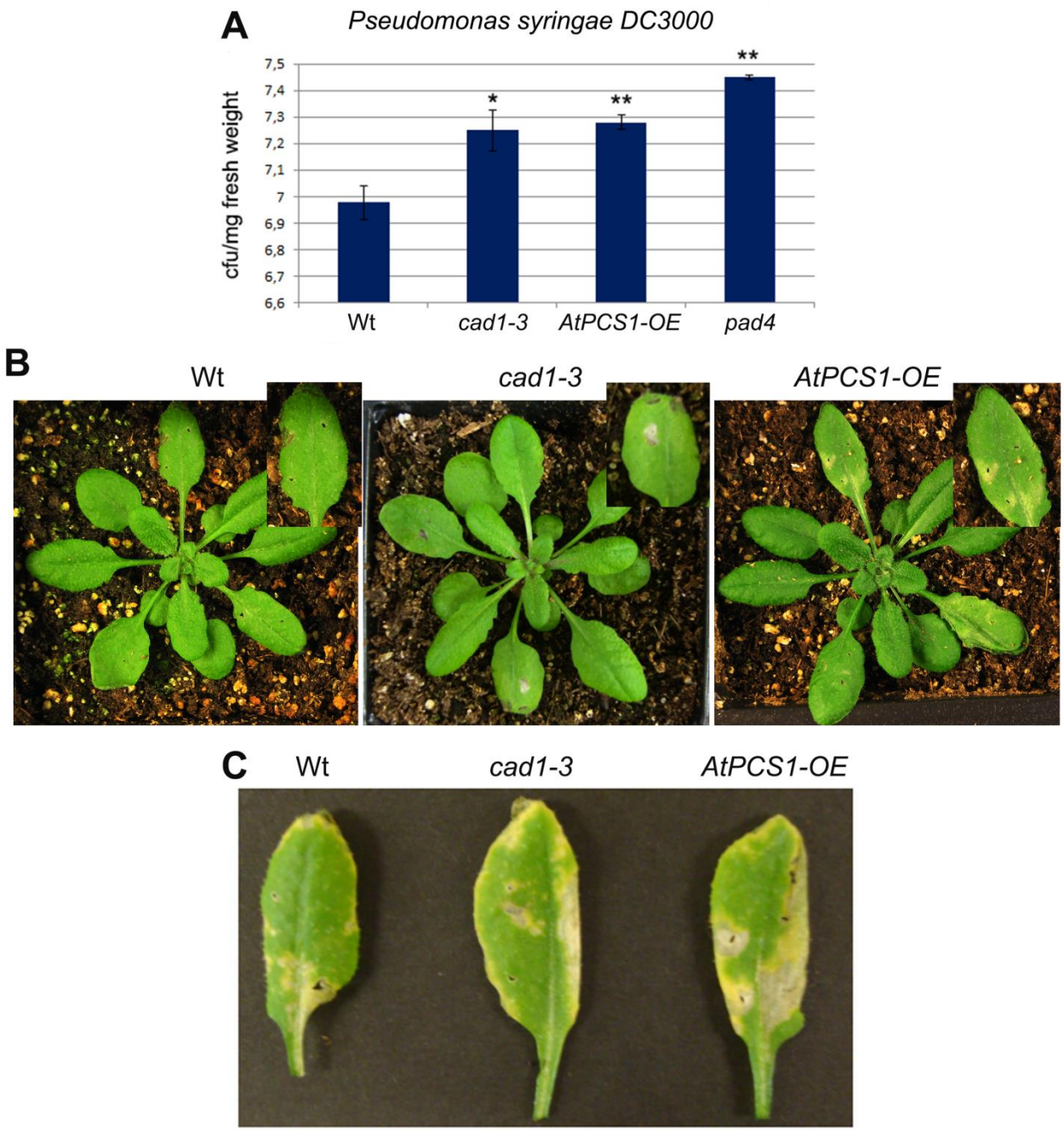

Figure 8: Growth analysis and disease symptoms of *Pseudomonas syringae* DC3000 (*PsDC3000*) in 4-week-old Wt, *cad1-3* and *AtPCS1-OE* plants. **(A)** Bacteria were infiltrated at $3*10^5$ CFU/mL and populations were measured in leaves after two days after inoculation. Error bars indicate S.E. of populations measured from three leaves from each of twelve plants. Asterisks (*) indicate statistically significant values with * $p\leq$ 0.05, ** $p\leq$ 0.01, n = 10; T student test was used for statistical analyses. **(B)** Disease symptoms of Wt, *cad1-3* and *AtPCS1-OE* plants after two days of incubation with *PsDC3000*; **(C)** Development of symptoms on a single representative leaf one week after the infiltration with the bacteria.

The increased susceptibility to the pathogenic bacteria on the infiltrated leaves of *cad1-3* and *AtPCS1-OE* plants was also manifested by increased lesions compared to wild-type plants.

The Role of AtPCS1 in Callose Deposition in Relationship to Cd detoxification in A. thaliana.

Callose synthesis and deposition in the cell wall is activated under exposure of plants to toxic metals, thus suggesting that callose is involved in protection against heavy metal toxicity as well (Ueki et al., 2002 and 2005). However, the direct role of callose in protection against such toxicity has not been experimentally validated until now. Given that the *cad1-3* mutant fails to produce callose in response to Flg22, which results in its increased sensitivity to pathogenic bacteria, we used the *cad1-3* mutant as a tool to determine: 1) whether the *cad1-3* mutant will also fail to produce callose in response to Cd treatment; 2) whether other callose-deficient mutants would be sensitive to Cd as well. To answer these questions, we compared callose formation in wild-type to the *cad1-3* and *AtPCS1-OE* mutants and to the callose-deficient, the *pen2-1* mutant in response to Flg22 (as control for callose formation) and Cd. *PEN2* encodes a putative myrosinase involved in the callose deposition (Bednarek et al., 2009; Clay et al., 2009). The *pen2-1* mutant, as well as the *cad1-3* mutant accumulates 4-methoxy-indol-3-ylmethylglucosinolate due to a lack of myrosinase activity (Clay et al., 2009).

In these experiments, 10-day-old wild-type, *cad1*-3, *AtPCS1-OE* and *pen2-1* plants were grown either under control condition or were treated for 24 h with 1 µM Flg22, or with 25 µM Cd (**Figure 9**).

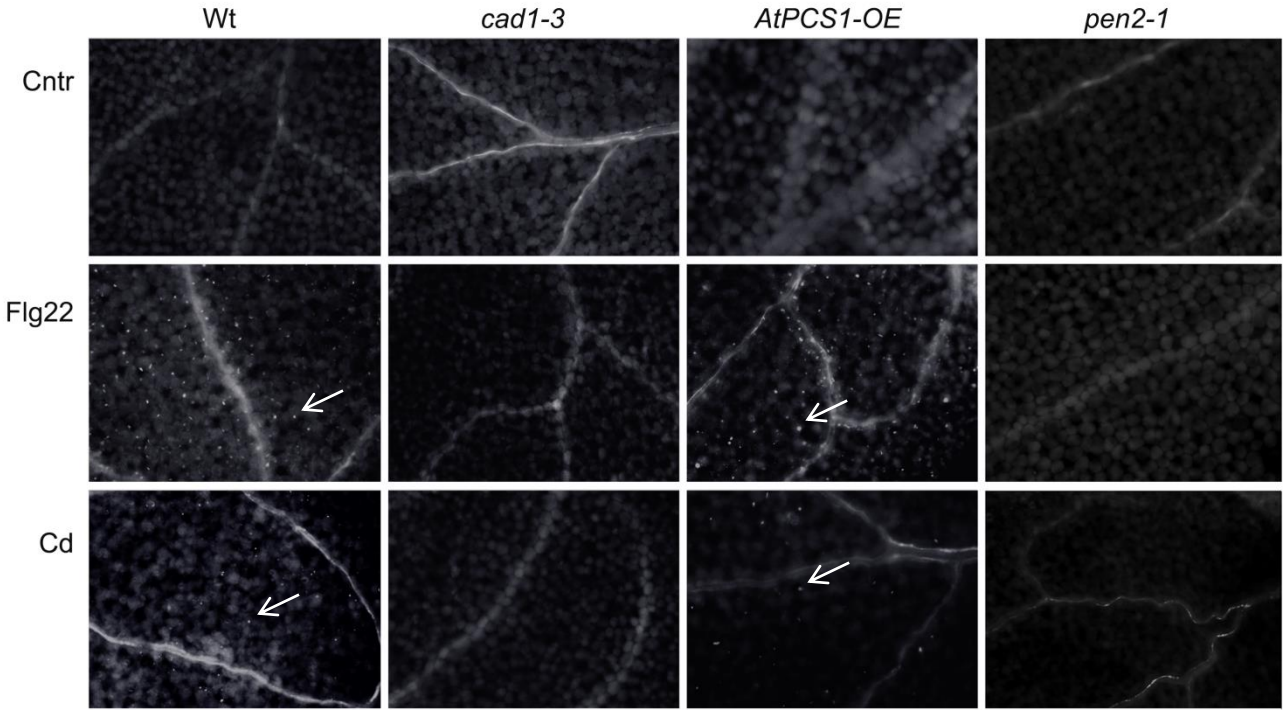

Figure 9: Callose formation in cotyledons of 10-day-old Wt, *cad1-3*, *AtPCS1-OE* and *pen2-1* plants treated for 24 h with water (Cntr), or 1 µM Flg22, or 25 µM $CdCl_2$. The figure shows a representative result of three independent experiments. Callose-mediated fluorescence (white arrows) was visualized using a DAPI filter set of an Axio Imager M2 microscope equipped with the motorized Z-drive (Zeiss). Images were collected with AxioCam MR Camera and processed using the Adobe Photoshop software package, version 12.0.

We found that *cad1-3* and *pen2-1* mutants were not able to produce callose after both treatments. While *AtPCS1-OE* plants produced callose, the level of production was similar to wild-type plants. We also noticed that induction of callose deposition after Cd stress was not as prominent as after Flg22 treatment (**Figure 9**).

To test the role of callose formation in Cd resistance, we compared Cd sensivity of wild-type, *cad1-3* and *pen2-1* plants by comparing root length of seedlings that were germinated and grown in the presence of the indicated concentrations of Cd for 14 days. We did not find differences in root length among different plant lines grown under control conditions (**Figure 10**). As was shown previously (Lee et al., 2003) *cad1-3* plants were sensitive to Cd, regardless of the concentration used for analyses (**Figure 10**). Likewise, roots of the *pen2-1* mutant were more sensitive to Cd than roots of wild-type but less sensitive than roots of the *cad1-3* mutant (**Figure 10**).

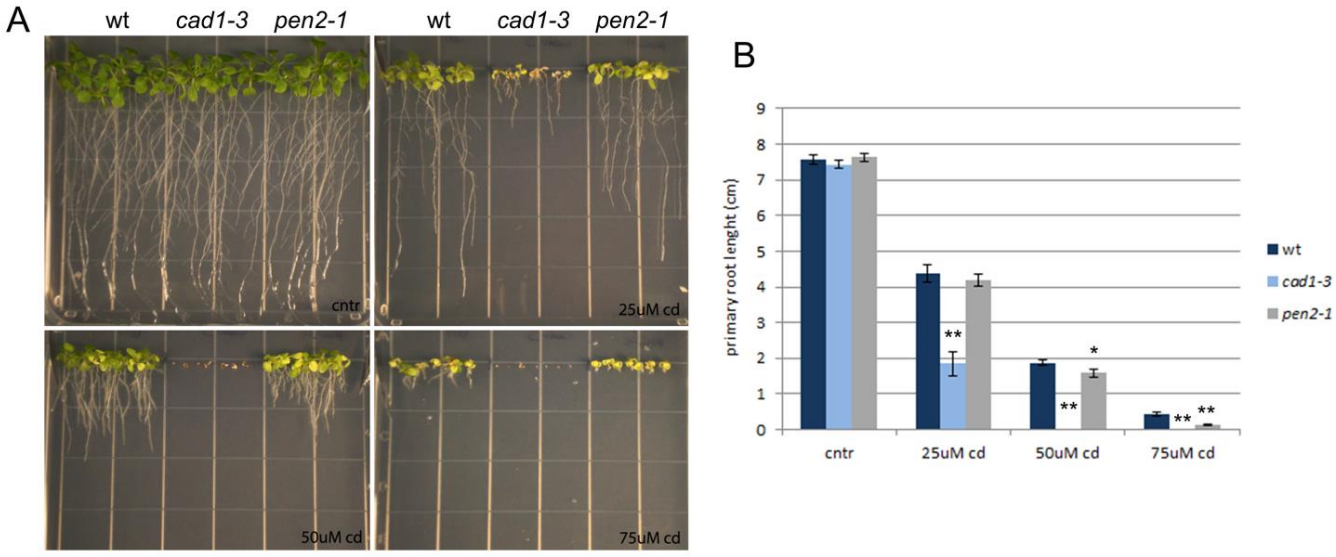

Figure 10: (A) Length of the primary root of two-week-old Wt, *cad1-3*, and *pen2-1* plants treated with 0, 25, 50, and 75 µM of $CdCl_2$. Note the dose-dependent manner of the decrease in length of the primary root in all lines. **(B)** Length of the primary root of two weeks old Wt, *cad1-3*, *pen2-1* plants treated with 0, 25, 50, and 75 µM of $CdCl_2$. Error bars show S.E. Statistically significant differences are indicated with asterisks were * $p \leq 0.05$, ** $p \leq 0.01$. Statistical significance was evaluated using a T-student test (2-tailed distribution).

The increased Cd sensitivity of callose formation-defective mutants provides the first molecular evidence of the role of callose deposition in protecting plants from Cd toxicity.

The Phenylpropanoid Pathway

The literature reports a metabolic link between glucosinolate and phenylpropanoid pathways (Hemm et al., 2003). We also found changes in the phenylpropanoid metabolism in mutant plants *vs*. wild-type, both grown under control condition.

We found that sinapic acid hexoside accumulated at a higher level in leaves of *cad1-3* plants than in wild-type, both grown under control or under Cd treatment. On the contrary, *AtPCS1-OE* plants accumulated lower amounts of it in stress condition (**Figure 11A**). Another component of phenylpropanoid metabolism such as a ferulic acid derivate was accumulated at higher levels in *cad1-3* roots *vs*. wild-type, only after heavy metal treatment (**Figure 11B**).

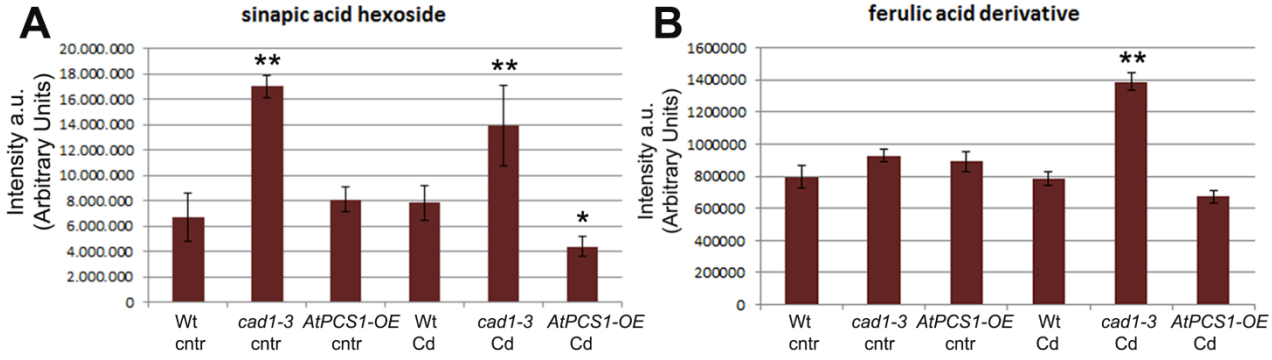

Figure 11: Accumulation of hydroxycinnamic acids in leaves (**A**) and in roots (**B**) of *A. thaliana* depends on expression of *AtPCS1*, under control condition or after treatment with 36 µM of $CdCl_2$ for 24 hours.

Since these metabolites are implicated in lignin biosynthesis, we suggested that cell wall properties would differ among different plant lines used in our analyses. To test this hypothesis we used a so-called "stretch experiment". In this experiment stems of mature plants are subjected to a mechanical stretch and stems stretchability is documented as a force/pressure (in MPa) required for breaking a stem. Difference in stretchability is the first and the simplest indicator of a difference in cell wall composition.

To examine if wild-type, *cad1-3* and *AtPCS1-OE* plants have differences in cell wall composition, we stretched stems of two-month-old plants. We used different stem areas: the base, the middle and the upper zones.

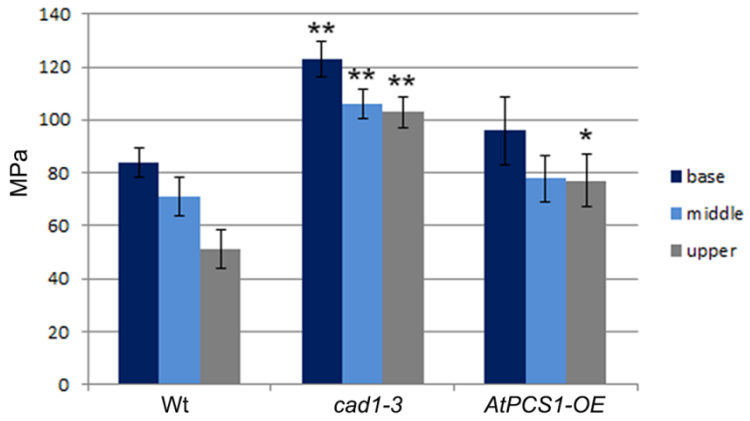

Figure 12: Stems of Wt, *cad1-3*, *AtPCS1-OE* plants were sectioned in basal, middle and upper parts and subjected to a stretch. Pressure (MPa) required by that the Intron instrument to break stems is shown.

We found differences in stretchability of *cad1-3* stems *vs.* wild-type in all zones subjected to analyses (**Figure 12**). We also found difference in stretchability of the upper area of *AtPCS1-OE* plants *vs*. wild-type. To test if differences in cell wall properties of the *cad1-3* and *AtPCS1-OE* plants were due to differences in lignin deposition, we compared lignin accumulation among different plant lines.

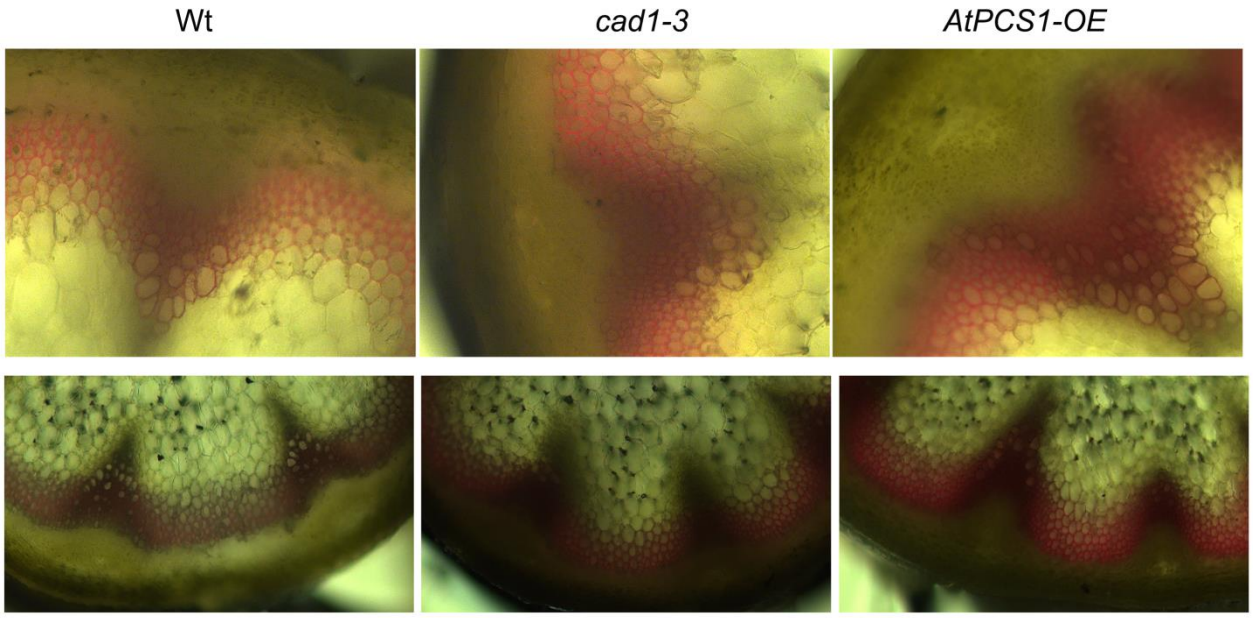

Figure 13: Lignification in the stems of 2-month-old Wt, *cad1-3*, *AtPCS1-OE* plants. Sections from the basal part of the stems were stained for lignin with phloroglucinol-HCl to give a red-violet color.

While we did not find significant differences in staining patterns between lines, the stained area of the *cad1-3* and *AtPCS1-OE* appeared perhaps thicker and the color was more intense as compared to wild-type (**Figure 13**) suggesting that the observed increased stretchability of the stem

of the *cad1-3* mutant (**Figure 12**) might be preliminarily due to increased lignin content. However, more experiments using much more sensitive techniques should be done to obtain conclusive evidence supporting this suggestion. It is also noteworthy that not only the total lignin content might be affected by changes in *AtPCS1* expression but also the composition of lignins. Therefore, future studies will be directed towards analyses of monolignol concentrations in different plant lines.

In addition to precursors of lignin biosynthesis, accumulation of other compounds such as flavonols produced from phenylpropanoid pathway differed between plant lines. For example, we found that *cad1-3* plants accumulate more kaempferol in leaves and quercetin in roots than wild-type, under control conditions as well as after Cd treatment (**Figure 14**).

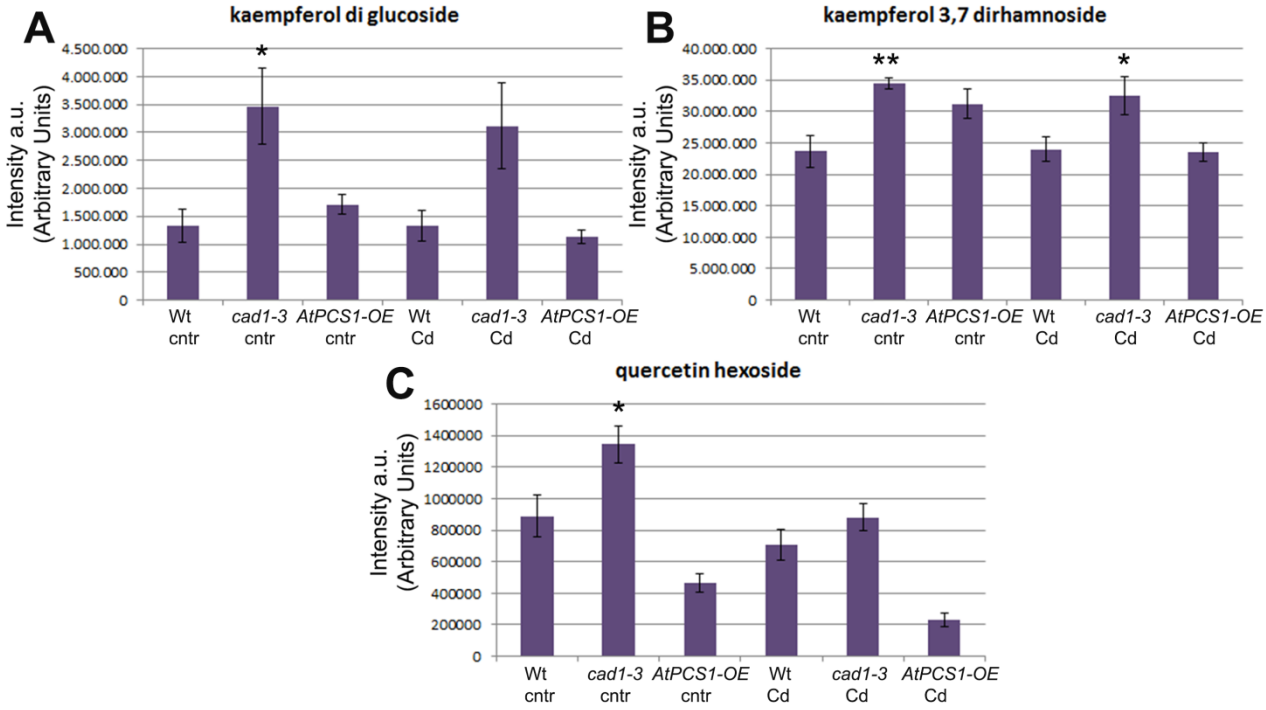

Figure 14: Levels of flavonols accumulate in higher amounts in *cad1-3* plants. kaempferol diglucoside **(A)** and kaempferol 3,7 dirhamnoside **(B)** are more abundant in leaves; quercetin hexoside in roots **(C)**.

Plants flavonols are considered natural regulators of cellular auxin efflux and consequent auxin polar transport (Jacobs and Rubery, 1988; Peer and Murphy, 2007). Kaempferol is an active flavonoid that regulates rootward auxin transport in the *A. thaliana* inflorescence (Yin et al., 2013); in contrast, quercetin inhibits shootward auxin transport and gravitropism (Lewis et al., 2011), and was shown to inhibit indole-3-acetic acid (IAA) transport *in vitro* (Geisler et al., 2005). Furthermore, quercetin and kaempferol were shown to perturb auxin transport in hypocotyls of various plants (Jacobs and Rubery, 1988; Murphy et al., 2000). Based on the above literature data

and our findings (**Figure 14**), future studies will be directed towards about the measure of indolacetic acid among the plant lines.

AtPCS1 and Iron Homeostasis

Iron (Fe) is essential for plant growth and development, but can be toxic when is accumulated in cells in excess (Palmer and Guerinot, 2009). To avoid Fe deficiency while omitting toxicity plants, Fe homeostasis is regulated by the Fe transporter IRT1 and the ferric reductase FRO2. FRO2/IRT1 system constitutes the major pathway for Fe entry into root epidermal cells (Robinson et al., 1999; Eide et al., 1996; Hindt and Guerinot, 2012).

It has been reported that *AtPCS1* expression is upregulated under Fe deficiency condition (Colangelo and Guerinot, 2004). This finding is intriguing because it suggests that *AtPCS1* may play a role in Fe homeostasis even though Fe is a moderate activator of *AtPCS1*-mediated PCs formation (Loscos et al., 2006). By contrast, although Cd is the best activator of *APCS1*-mediated PC production (Vatamaniuk et al., 2000), it does not affect significantly the expression level of *AtPCS1* (Vatamaniuk et al., 2000; Cobbett, 2000). Findings of Loscos et al. (2006) and Colangelo and Guerinot, (2004) prompted us to test the role of *AtPCS1* in Fe homeostasis. On the onset of this work we analysed the level of *APCS1* transcript in roots of *A. thaliana* wild-type plants grown on solid ½ MS plates under control or Fe-limited conditions. Fe limitation was achieved by supplementing ½ MS medium with 200 µM of a specific Fe chelator BPS (bathophenanthrolinedisulfonic acid).

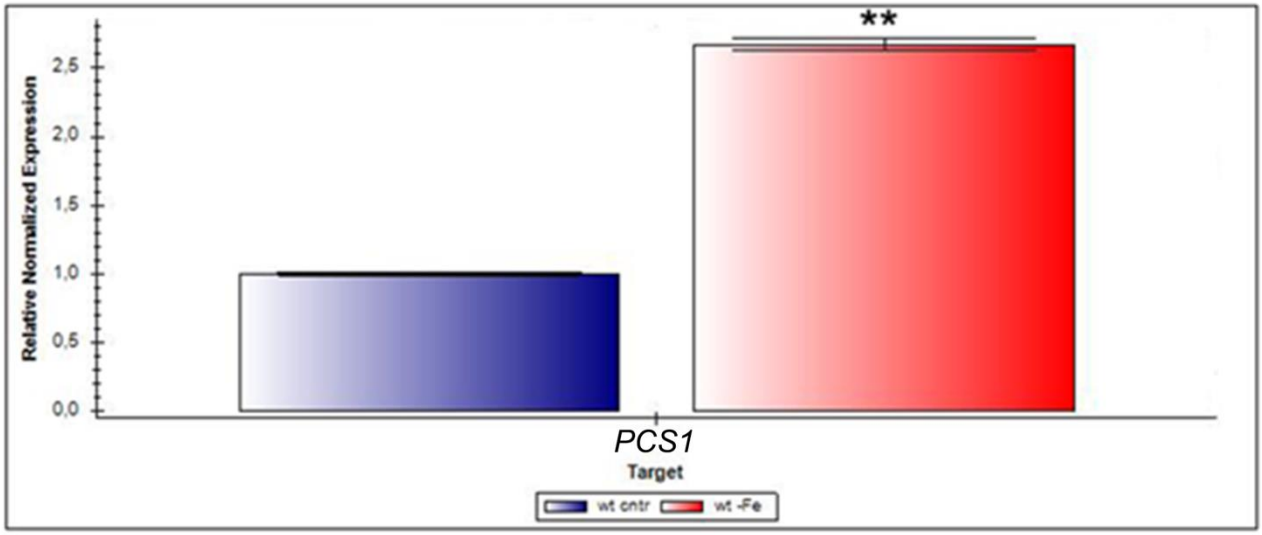

Figure 15: qRT-PCR analysis of *AtPCS1* transcript in roots of *A. thaliana* grown under control condition or in Fe-limited conditions. Error bars indicate S.E.; asterisks (**) indicate statistically significant difference with $p \leq 0.01$ (n=3).

Consistent with Colangelo and Guerinot (2004), we found that the expression of *AtPCS1* increased more than 2-fold in roots of plants grown under Fe-limited *vs.* control conditions (**Figure 15**). To test whether AtPCS1 is involved in Fe homeostasis we compared Fe-deficiency phenotypes of wild-type, the *cad1-3* and *AtPCS1-OE* plants. Among the first common responses of higher plants to low Fe supply is the increased root hair density and elongation (Schmidt, 1999; Schmidt et al., 2000; Lopez-Bucio et al., 2003). We hypothesized that if AtPCS1 is involved in Fe homeostasis, the absence or overexpression of *AtPCS1* might be manifested as altered root hair density.

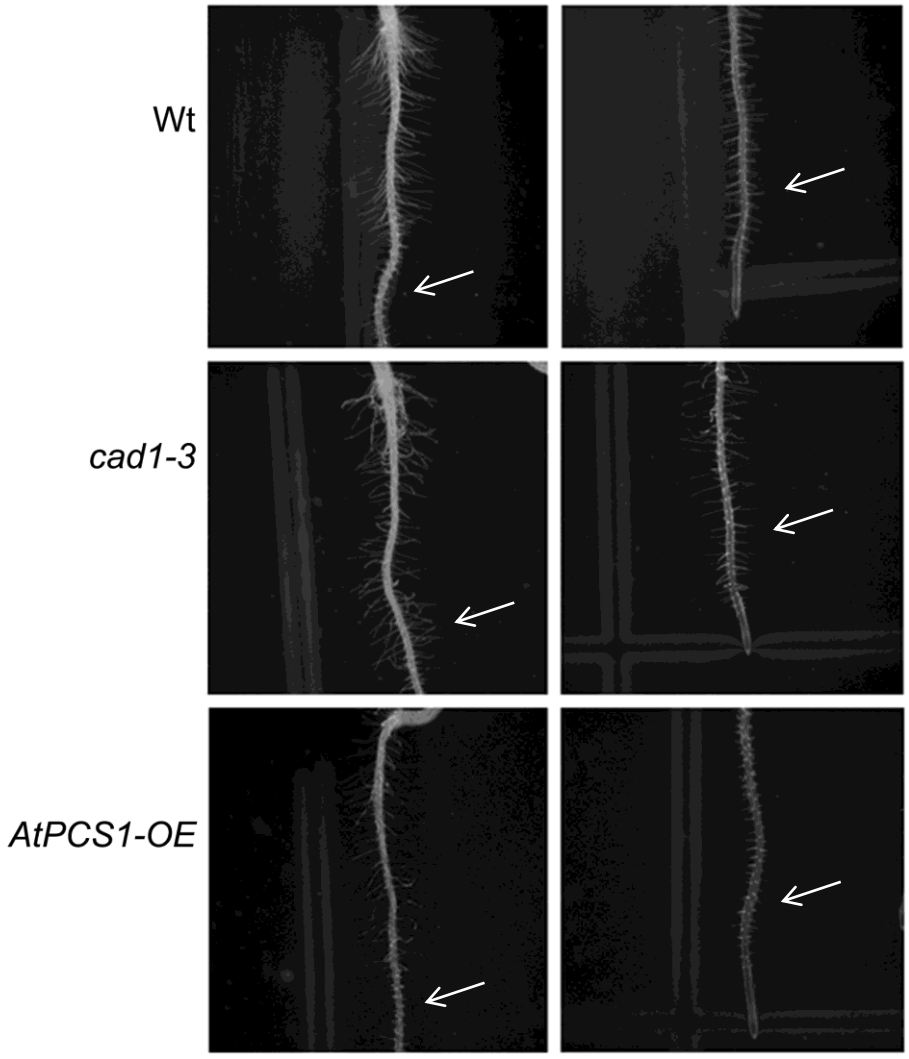

Figure 16: Images of different parts of the root of Wt, *cad1-3* and *AtPCS1-OE* plants. All plant lines were grown for 5 days on solid ½ MS medium. White arrows show increased root hair density.

Within agreement with our predictions, we found that root hair density was significantly higher in the *cad1-3* mutant, and significantly lower in *AtPCS1-OE* compared to the wild-type, all grown under control conditions (**Figure 16**). These findings are consistent with suggestion that although Fe was present in the medium, the *cad1-3* mutant might have experienced Fe deficiency. On the contrary, *AtPCS1-OE* plants may have experienced (sensed) more Fe. This phenotype was

more evident at the distal zone of the primary structure of the roots. These differences were also evident when plants were grown under Fe-limitation (**Figure 17**).

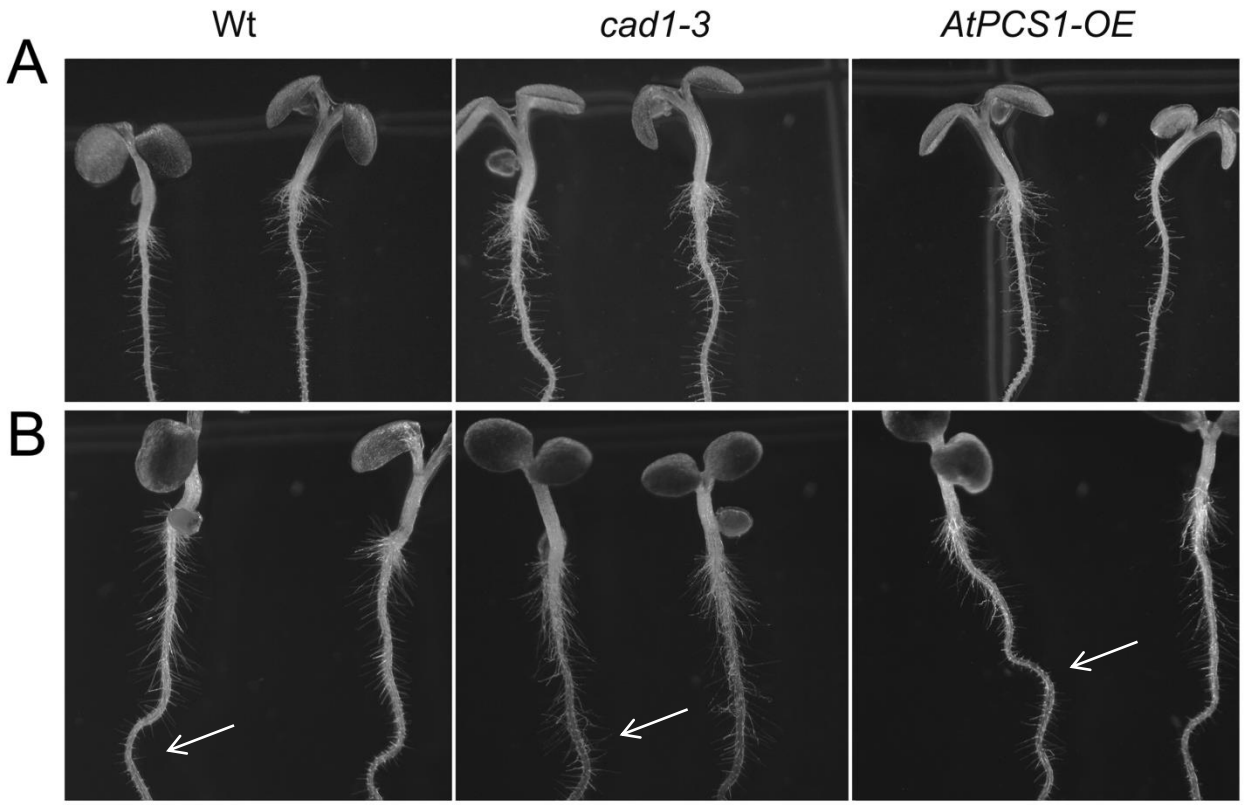

Figure 17: Images of the root of Wt, *cad1-3* and *AtPCS1-OE* plants. Plant lines were grown for 5 days on solid ½ MS medium without **(A)** or with the Fe chelator, bathophenanthroline disulfonate (BPS) **(B)**. White arrows show increased root hair density.

In medium supplemented with 200 µM of a Fe chelator bathophenanthroline disulfonate (BPS), the root hair formation was increased in all plant lines. More root hairs in *cad1-3* plants suggested a Fe deficiency condition and, if this suggestion is correct, then expression of genes encoding Fe transport systems in the root (the Fe transporter IRT1 and ferric reductase, FRO2, must be downregulated) in the mutant grown under standard conditions. To test this hypothesis, we compared the expression of *IRT1* and *FRO2* in roots of *cad1-3* and *AtPCS1-OE* with wild-type, all grown under standard condition (**Figure 18**).

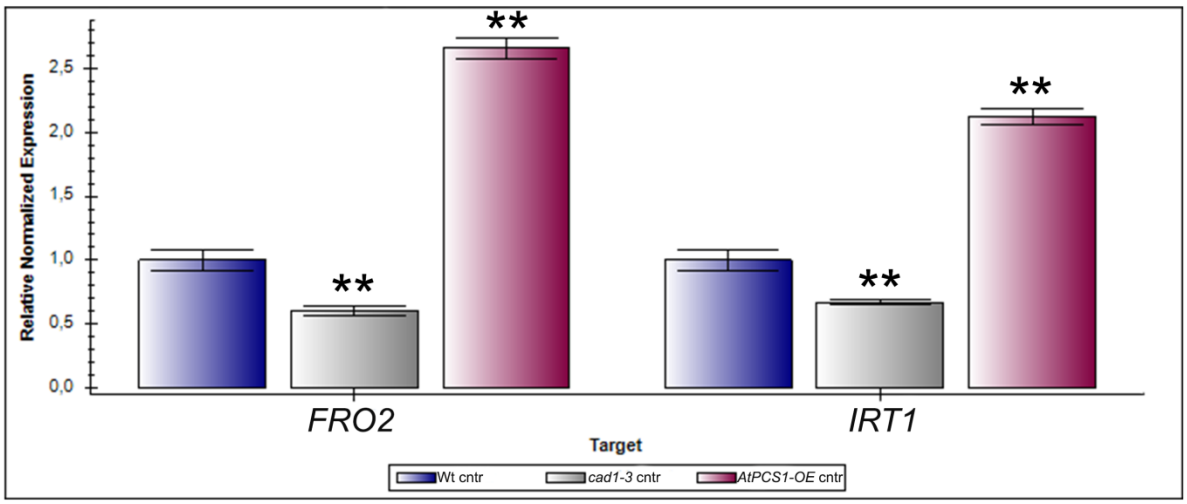

Figure 18: Quantitative real-time (qRT)-PCR analysis of the expression of *IRT1* and *FRO2* in roots of Wt, *cad1-3* and *AtPCS1-OE* plants. All plant lines were grown on ½ MS solid medium for 10 days. Error bars indicate S.E. (n=3); asterisks (**) indicate statistically significant differences with $p \leq 0.01$.

We found that expression of *IRT1* and *FRO2* was downregulated in roots of knockout plants (**Figure 18**). On the contrary, expression of both genes was upregulated in *AtPCS1-OE* plants (**Figure 18**).

We next analysed Fe accumulation in different plant lines. Although we did not find statistically significant differences in Fe accumulation in roots of the *cad1-3* plants *vs.* wild-type (**Figure 19B**), leaf Fe content of *cad1-3* plants was only 15 % of that of the wild-type (**Figure 19A**). In contrast to Fe accumulation in tissues of the *cad1-3* mutant, leaves and roots of *AtPCS1-OE* plants contained 60-fold and 15-fold more Fe respectively, than corresponding tissues of wild-type plants (**Figure 19**).

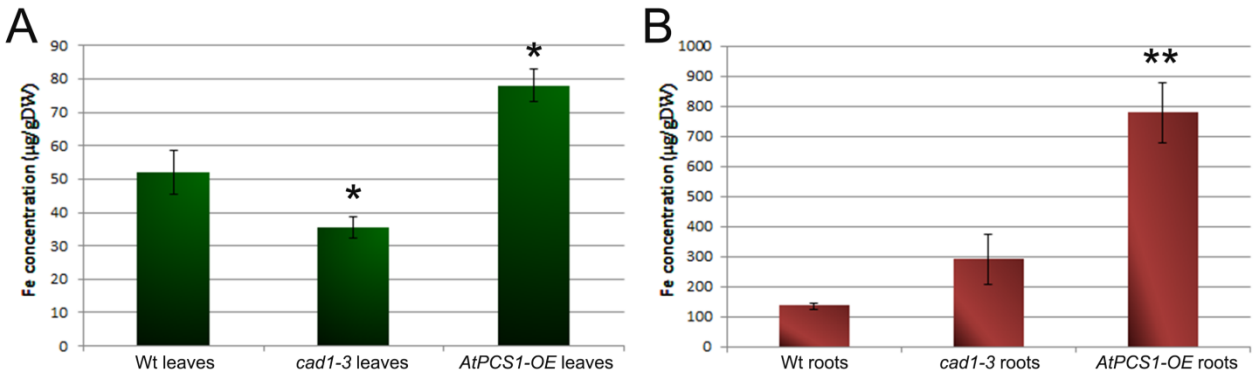

Figure 19: Iron concentration in leaves **(A)** and roots **(B)** of Wt, *cad1-3*, *AtPCS1-OE* plants grown hydroponically for 4 weeks under standard conditions. Shown are mean values ± SE (n=3); asterisks indicate statistically significant differences (* $p \leq 0.05$; ** $p \leq 0.01$).

These data show that Fe accumulation in roots, and particularly in shoots, depends on the level of *AtPCS1* expression. Furthermore, our finding that the *cad1-3* mutant has less Fe in shoots, while *AtPCS1-OE* plants have more Fe in shoots than wild-type, suggested that these plants will differ in their sensitivity to Fe-limited conditions.

We therefore, grew wild-type, *cad1-3* and *AtPCS1-OE* plants hydroponically under standard and Fe-deficient conditions and found that leaves of the *cad1-3* mutant were the most sensitive to Fe-limitation (**Figure 20)**. Increased sensitivity of the mutant to Fe deficiency was manifested by a prominent chlorosis of young leaves (**Figure 20**), a classic manifestation of Fe deficiency in plants (Marschner, 1995). In contrast, leaves of *AtPCS1-OE* plants were more tolerant to Fe limitation than leaves of wild-type plants, which were chlorotic at the edges of leaf blades (**Figure 20**). These data are fully consistent with our analyses of Fe concentrations in tissues of different plant lines (**Figure 19**).

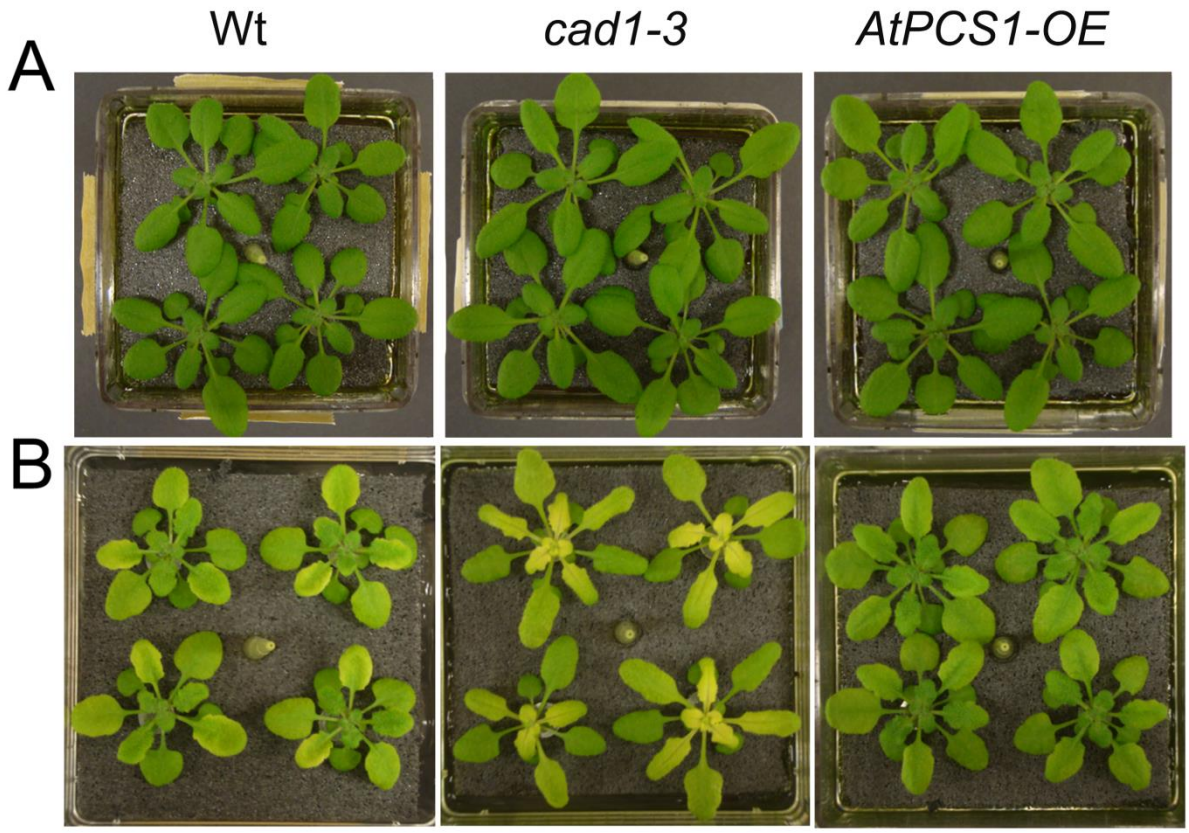

Figure 20: *A. thaliana* Wt, *cad1-3* and *AtPCS1-OE* plants were grown hydroponically for 4 weeks with 2.5 µM FeHBED **(A)**. In **B**, after 3 weeks of growth indicated plant lines were transferred to a fresh hydroponic solution without FeHBED were grown under these conditions for 1 week.

Our previous studies showed that the transcript level of genes encoding the Fe transport system *FRO2/IRT1* is downregulated in roots of *cad1-3* seedlings while is upregulated on roots of

AtPCS1-OE seedlings (**Figure 18**). To test whether similar phenomena is observed in mature plants and to correlate Fe accumulation and altered sensitivity to Fe deficiency of *cad1-3* and *AtPCS1-OE* *vs*. wild-type plants (**Figures 19-20**), the expression of *IRT1* and *FRO2* and also *OPT3*, was analysed in roots and shoots of mature plants. *OPT3*, encoding an oligopeptide transporter that is involved in the recirculation of Fe from the xylem to the phloem and Fe distribution from shoot to root and from old to young leaves and seeds (Zhai et al., 2014) (**Figure 21**).

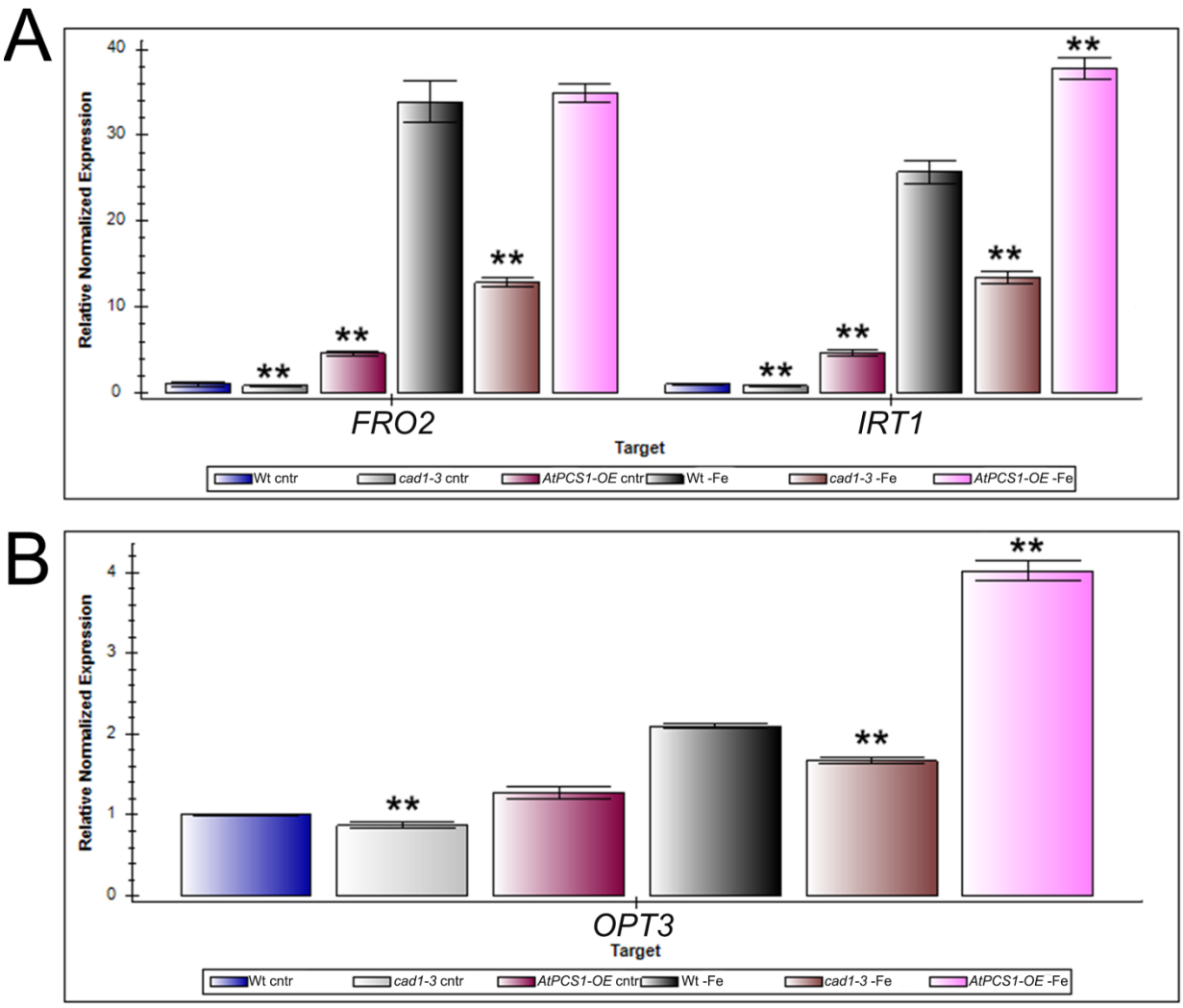

Figure 21: Transcript abundance of *FRO2*, *IRT1* **(A)** and *OPT3* **(B)** was analyzed in roots of four-week-old Wt, *cad1-3* and *AtPCS1-OE* plants. Plants were grown hydroponically. To achieve Fe deficiency condition, a set of three-week-old plants was transferred to a medium without Fe and was grown for one week before tissues were collected for RNA extraction and qRT-PCR analyses. Asterisks ** indicate statistically significant differences with a $p \leq 0.01$.

Results of qRT-PCR analyses reveled that expression of *IRT1*, *FRO2* and *OPT3* was upregulated by Fe deficiency conditions in roots of wild-type plants, which is consistent with

previous data (Vert et al., 2002; Zhai et al., 2014) and the fact that plants have triggered the physiological response to Fe deficiency.

Consistent with previous data (**Figure 18**), expression of *IRT1* and *FRO2* was downregulated in roots of mature *cad1-3* plants and upregulated in roots of mature *AtPCS1-OE* plants *vs.* wild-type, regardless whether plants were grown under control or Fe-limited conditions (**Figure 21A**). A similar phenomenon was observed in expression of *OPT3* (**Figure 21B**). These results show that regulation of not only Fe uptake but also Fe remobilization is altered in response to changes in *AtPCS1* expression. Furthermore, altered expression of genes encoding Fe uptake and remobilization systems is in agreement with altered Fe accumulation in leaves and altered sensitivity to Fe deficiency of different plant lines (**Figures 19-20**). Taken together, these results highlight a significant and a novel role of AtPCS1 in Fe homeostasis. The mechanistic basis of the role of AtPCS1 in Fe homeostasis is unknown.

GSH Homeostasis Regulates Iron Homeostasis

The substrate of AtPCS1 is GSH and the enzyme catalyzes a desglycylation reaction (Grill et al., 1989; Clemens et al., 1999; Ha et al., 1999; Vatamaniuk et al., 1999; Vatamaniuk et al., 2000; Beck et al., 2003; Blum et al., 2007). Previous data have shown that in the presence of only free GSH, AtPCS1 is in the acylated state and desglycinates GSH very effectively. As a result, the concentration of GSH decreases while the concentration of γ-Gly-Cys and Gly increases (Vatamaniuk et al., 2004). Based on the above, we hypothesize that under standard condition, AtPCS1 contributes to γ-Gly-Cys and Gly production and, in doing so, controls the concentration of GSH and a redox state of the cell. Consistent with this, we found that the *cad1-3* mutant accumulates more GSH (relative level) in leaves (**Figure 5**). We thus postulate that altered concentrations of GSH that are observed in the *cad1-3* mutant or in *AtPCS1-OE*, can be a contributing factor that regulates Fe homeostasis.

If the latter hypothesis is correct, then altering GSH concentration in plant cells either using exogenously supplied GSH or inhibitors of its synthesis, or GSH-biosynthetic mutants, would affect expression of *IRT1/FRO2* and cause other phenotypes that are characteristic for altered Fe homeostasis. To test this hypothesis, wild-type plants were grown with different concentrations of GSH and transcript abundance of *IRT1* and *FRO2* and root hair density was analysed.

We first analysed the effect of GSH on plant growth using length of a primary root of 10-day-old seedlings as a marker of toxicity. We found that increasing GSH concentration from 100 to 500 μM inhibited the growth of the primary root in dose-dependent manner (**Figure 22A**). This was not surprising, since GSH may also impose toxicity *per se* (May et al., 1998).

We then used these concentrations for testing the effect of GSH on transcript abundance of *IRT1* and *FRO2*. We found that with the increase of the GSH concentration, the expression of *IRT1* and *FRO2* was downregulated (**Figure 22B**). This finding was consistent with our prediction that downregulated expression of *IRT1* and *FRO2* in roots of the *cad1-3* mutant (**Figure 18**) might be due to increased concentrations of GSH, which, in turn, is due to the loss-of-function of AtPCS1.

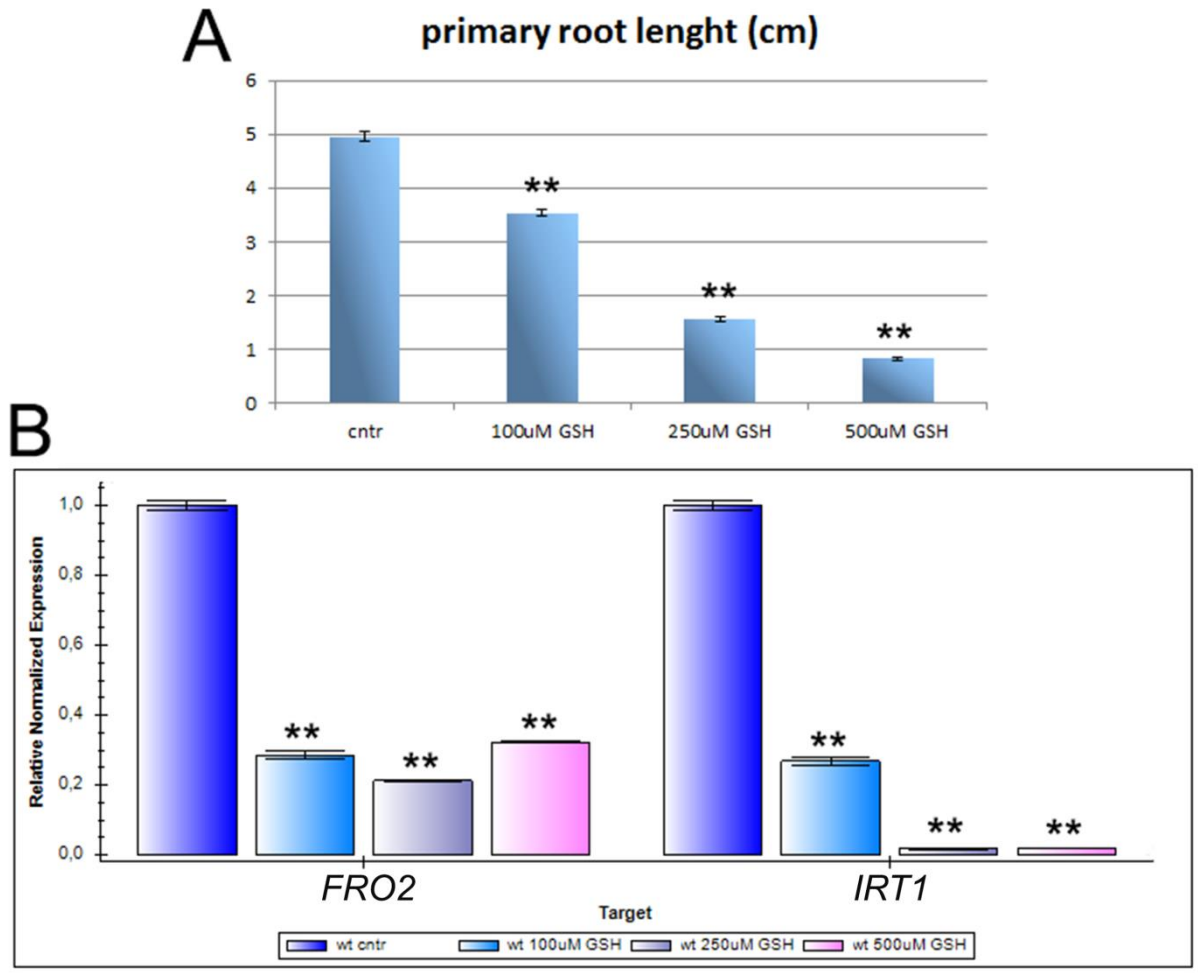

Figure 22: **(A)** Length of the primary root of Wt plants grown on solid ½ MS medium without (cntr) or with indicated concentrations of GSH. **(B)** Quantitative real-time (qRT)-PCR analysis of the expression of *IRT1* and *FRO2* in roots of 10-day-old Wt plants. Plants were grown on solid ½ MS medium without (cntr) or with indicated concentrations of GSH. Asterisks (**) indicate statistically significant differences ($p \leq 0.01$, n=3).

It was also found that supplementing plant growth medium with GSH increased root hair density (**Figure 23**), further indicating the effect of GSH on Fe homeostasis. Increased root hair density in plants that were grown on the medium supplemented with GSH (**Figure 23**) also resembled the phenotype observed in the *cad1-3* mutant grown under standard conditions (**Figure 16**). Taken together, our data support the role of AtPCS1 in Fe homeostasis, possibly *via* regulating the concentration of GSH in plant cells.

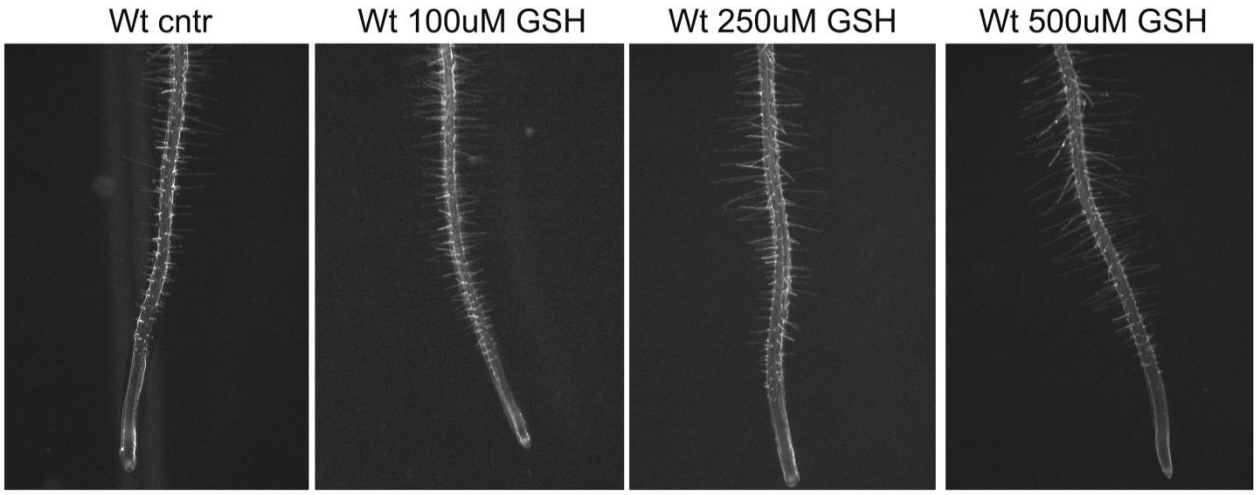

Figure 23: Root hair density of *A. thaliana* Wt plants grown for 10 days on medium with or without indicated concentrations of GSH.

To further test the role of GSH in Fe homeostasis, we used a specific inhibitor of GSH biosynthesis, L-buthionine sulfoximine (BSO) (Howden et al., 1995b). We expected that if GSH indeed is involved in the regulation of Fe homeostasis, than supplementing plant growth medium with BSO, will have an opposite to GSH effect on the expression of Fe uptake genes and root hair density. Specifically, we expected to find that BSO would increase expression of *IRT1* and *FRO2* in roots, and reduce root hair density of on the primary root *A. thaliana*.

To test these predictions, we first analysed the effect of different concentrations of BSO on the growth of wild-type plants, using the length of a primary root of 10-day-old seedlings as an indication of the effect. We found that the supplementation of ½ MS medium with BSO slightly inhibited growth of the primary root and this effect was dose dependent (**Figure 24A**). We then used these concentrations to analyse the effect of BSO on the expression of *IRT1* and *FRO2* and root hair density of wild-type *A. thaliana*. As we predicted, expression of *IRT1* and *FRO2* was upregulated in roots of plants grown with different concentrations of BSO, compared to plants grown under control conditions (**Figure 24B**). Moreover, root hair density was decreased on the primary roots of *A. thaliana* grown with different concentrations of BSO *vs.* plants grown under control conditions (**Figure 25**). The phenotype of wild-type plants treated with BSO fully reflects the phenotype of *AtPCS1-OE* plants grown under control condition, further supporting our hypothesis that AtPCS1 is involved in Fe homeostasis *via* AtPCS1-dependent regulation of the concentration of GSH in plant cells.

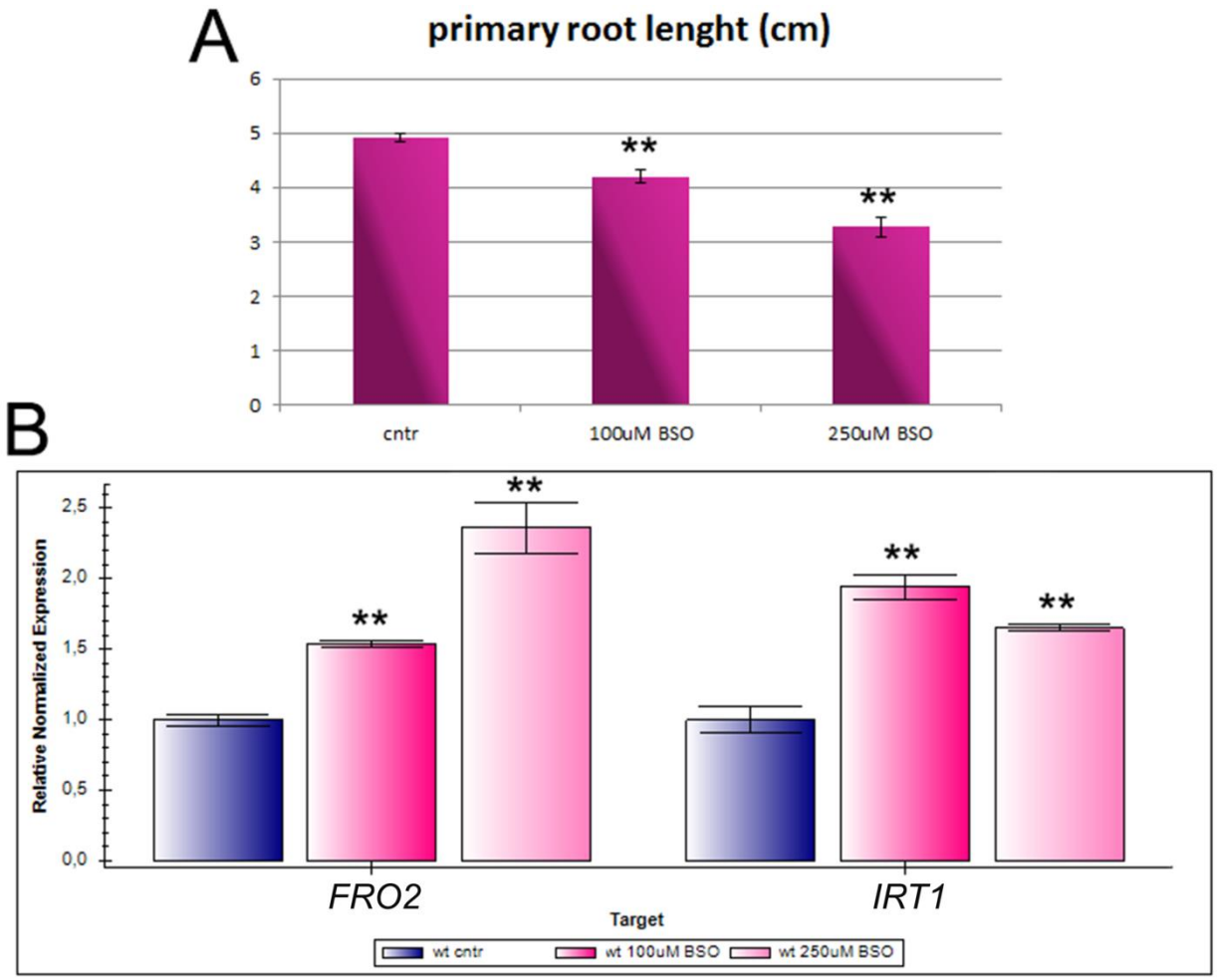

Figure 24: **(A)** Effect of BSO treatment on root elongation of Wt plants. Plants were grown in ½ MS medium without (cntr) and with indicated concentrations of BSO. The length of the primary roots was measured after 10 days of growth. Values correspond to means ± SE of 20 plants (n=3). Statistically significant differences are indicated with asterisks (**) with p≤ 0.01. **(B)** Quantitative real-time (qRT)-PCR analysis of the expression of *IRT1* and *FRO2* in roots of 10-day-old seedlings of *A. thaliana* grown either under control conditions or with different concentration of BSO. The asterisks ** indicate statistically significant differences with $p \leq 0.01$ (n=3).

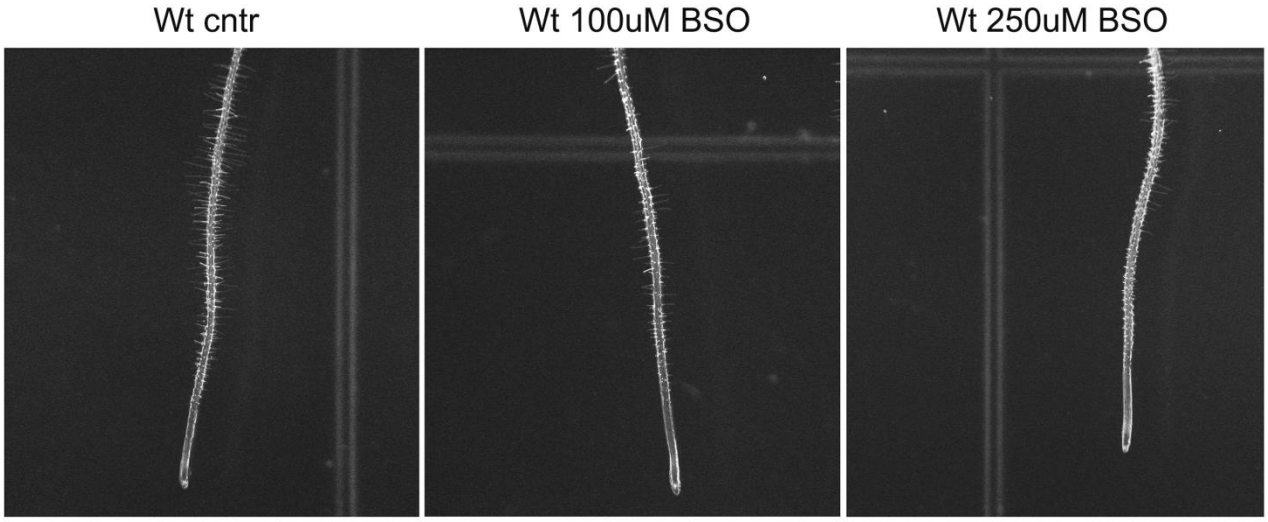

Figure 25: Root hair density of *A. thaliana* Wt plants grown under control condition (cntr) or with the indicated concentrations of L-buthionine sulfoximine (BSO).

To further validate our hypothesis that GSH concentration is important to regulate the expression of Fe transporters, we used the *cad2-1* mutant that has an alteration in a gene encoding the first enzyme of GSH biosynthesis, γ-glutamylcysteine synthetase (Cobbett et al., 1998). As a result of this alteration, the *cad2-1* mutant contains only 39% of the wild-type GSH level (Cobbett et al., 1998). As would be expected if GSH would be involved in Fe homeostasis, expression of *IRT1* and *FRO2* was upregulated in roots of the *cad2-1* mutant in comparison with wild-type plants, all grown under control conditions (**Figure 26**).

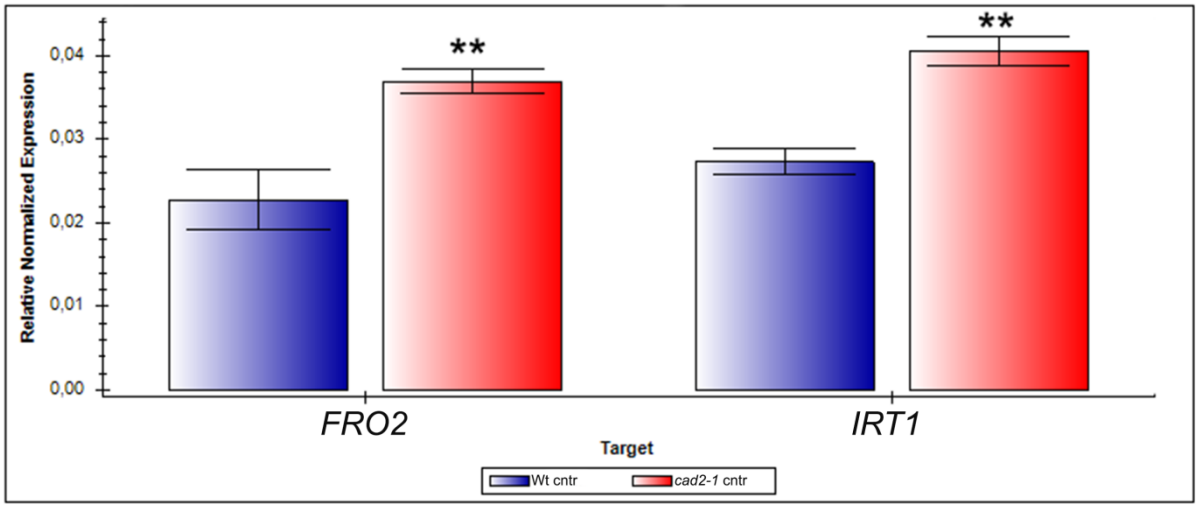

Figure 26: Transcript abundance of *FRO2* and *IRT1* in roots of Wt and *cad2-1* plants that were grown for 10 days under control condition. Asterisks (**) indicate statistically significant differences ($p \leq 0.01$).

To conclude, our results show for the first time the role of AtPCS1 in the regulation of Fe homeostasis that occurs indirectly *via* the effect of AtPCS1 on the concentration of GSH in plant cells.

Evolutionary History of Phytochelatins (and Phytochelatin Synthases)

At the same time, we studied the evolutionary history of PCS enzyme because in literature it is clear that higher plants are able to produce phytochelatins (PCs), but almost nothing is known until now about the response to excess and homeostatic metal(loid) concentrations in plants that first colonized the land environment (Petraglia et al., 2014; Degola et al., 2014). In detail, we checked the capability of bryophytes, charophytes (algal sisters of land plants) and lycophytes to

produce phytochelatins (PCs) after Cd (and other metal) treatments. In **Figure 27** it is represented a phylogenetic tree of basal land species and of those green plants that we investigated in this thesis.

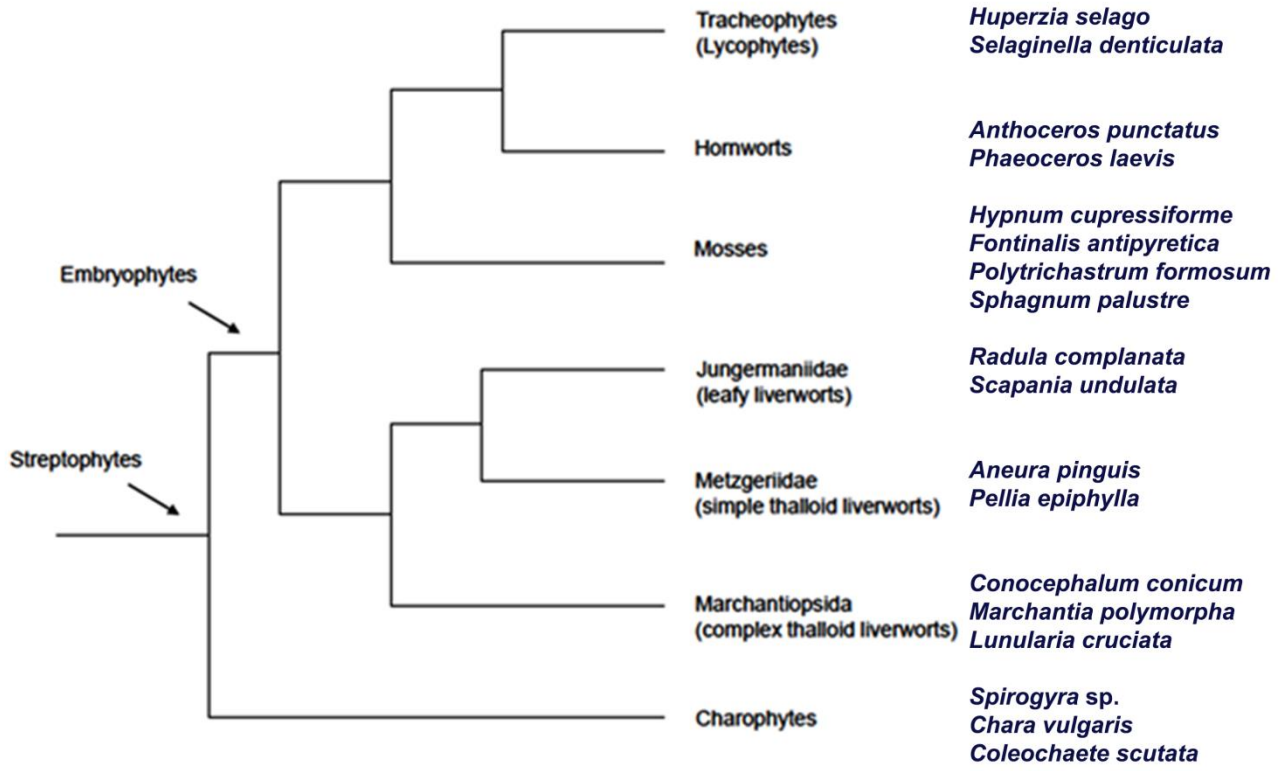

Figure 27: Simplified phylogeny of charophytic algae and land plants, related to the species investigated in this thesis. [Picture modified from Petraglia et al., 2014. The capability to synthesize phytochelatins and the presence of constitutive and functional phytochelatin synthases are ancestral (plesiomorphic) characters for basal land plants. Journal of Experimental Botany 65: 1153-1163].

All species indicated in **Figure 27** were treated with control medium and with 36 µM Cd for 48 hours and the extracts analyzed by HPLC and MS/MS to detect PC production. All charophytes investigated were shown to have the capability to produce PCs under Cd stress; in particular *C.vulgaris* and *C. scutata* until the oligomers PC_4, *Spirogyra* sp. PC_2 and PC_3 (**Table 5**). In the charophytes, the concentrations of GSH were not significantly affected by Cd treatment.

	GSH (control)	GSH (Cd-exposed)	PC_2 (Cd-exposed)	PC_3 (Cd-exposed)	PC_4 (Cd-exposed)	Total PCs (Cd-exposed)
Charophytes						
Spirogyra sp. (*n*=10+10)	105.5±9.7	144.7±16.2	2.7±0.9	1.9±0.7	ND	4.6±0.8
Chara vulgaris (*n*=10+10)	92.5±10.5	99.7±7.5	4.1±0.3	3.8±0.6	2.7±0.7	10.6±0.8
Coleochaete scutata (*n*=5+5)	222.3±12.1	212.2±7.7	9.5±0.4	16.8±1.2	14.1±0.7	40.4±0.8
Liverworts						
Conocephalum conicum (*n*=6+6)	1.4±0.2	6.8±2.4**	6.1±3.5	1.2±0.5	0.8±0.3	8.1±1.4
		16.6±4.3**[a]	2.9±0.3[a]	4.0±2.3[a]	2.9±0.7[a]	9.8±1.1[a]
		10.7±3.2**[b]	4.2±3.5[b]	2.6±1.4[b]	1.7±0.4[b]	8.5±1.8[b]
Marchantia polymorpha (*n*=4+4)	2.9±0.2	3.6±0.8	1.8±0.4	1.3±0.9	ND	3.1±0.6
Lunularia cruciata **(n=6 + 6)**	13.0 ±2.5	14.4 ±3.2	4.1 ±0.9	2.9± 0.8	4.2 ± 0.5	11.2± 0.7
Pellia epiphylla (*n*=3+3)	132.2±36.8	89.4±26.5	1.0±0.3	ND	ND	1.0±0.3
Radula complanata (*n*=3+3)	2.7±1.1	6.3±2.1	1.2±0.3	ND	ND	1.2±0.3
Aneura pinguis (*n*=4+4)	3.3±1.0	5.6±1.7	ND	ND	ND	ND
Scapania undulata (*n*=3+3)	20.5±3.5	17.8±2.2	ND	ND	ND	ND
Mosses						
Sphagnum palustre (*n*=6+6)	23.4±3.1	34.2±2.1*	4.5±0.3	5.8±0.2	3.0±0.7	13.3±0.8
Polytrichastrum formosum (*n*=4+4)	121.7±12.7	367.7±25.6**	ND	ND	ND	ND
Hypnum cupressiforme (*n*=4+4)	302.9±46.1	123.6±28.1	ND	ND	ND	ND
Fontinalis antipyretica (*n*=3+3)	25.7±7.0	148.0±19.1*	ND	ND	ND	ND
Hornworts						
Anthoceros punctatus (*n*=5+5)	2.8±0.7	1.9±0.8	ND	ND	ND	ND
Phaeoceros laevis (*n*=12+12)	4.5±0.9	1.8±0.2*	1.6±0.3	3.3±0.9	ND	4.9±0.6
Lycophytes						
Huperzia selago (*n*=5+5)	337.4±23.6	275.9±31.3	ND	ND	ND	ND
Selaginella denticulata (*n*=5+5)	67.7±10.6	126.4±15.9*	3.8±1.6	3.1±1.0	ND	6.9±1.3

Asterisks indicate significant differences in GSH concentrations between controls and Cd-exposed samples at *$P < 0.05$ or **$P < 0.01$, according to the Kruskal–Wallis non-parametric test; *n* for each experimental set (controls+Cd-exposed) is specified in parenthesis. ND, no PCs detected by HPLC and ESI-MS analyses.

Table 5: Content of glutathione (GSH) and phytochelatins (PCs) mesured in charophytes, bryophytes and lycophytes in control condition or exposed to 36 µM Cd for 72 h (in *Conocephalum conicum* also 36 µM Cd for 144h and 72 µM Cd for 72 h). GSH and PC concentrations (means ± SE) are expressed in nmol g^{-1} FW. [Picture modified from Petraglia et al., 2014. The capability to synthesize phytochelatins and the presence of constitutive and functional phytochelatin synthases are ancestral (plesiomorphic) characters for basal land plants. Journal of Experimental Botany 65: 1153-1163].

As regards bryophytes, amongst the liverworts belonging to the class Marchantiopsida (**Figure 27**), *C. conicum* was able to produce PCs until the oligomer PC_4, also at different concentrations of Cd and different exposure-times, with an increase in GSH level after Cd stress than in controls (**Table 5**). Differently, in *M. polymorpha* no differences in GSH levels between controls and Cd-exposed samples were found, and only the oligomers PC_2 and PC_3 were produced (**Table 5**). Likewise, in *L. cruciata* no difference in GSH content between control and treated samples was noticed, and PC production was found until PC_4 (**Table 5**).

In the liverworts belonging to the class Metzgeriidae (**Figure 27**), like *A. pinguis* and *P. epiphylla*, only the latter was able to produce PCs, only the PC_2 oligomer, and the concentration of GSH before and after Cd treatment was the same in both species (**Table 5**).

In *R. complanata* and *S. undulata*, belonging to Jungermanniidae class (**Figure 27**), PC_2 was induced in vivo by Cd only in the first specie, (**Table 5**) and also no difference in GSH content between control and Cd-exposed samples was evidenced.

Among the moss species investigated here, only in *S. palustre* the production of PC_2, PC_3, PC_4 was detected and the GSH level under Cd stress was higher than in controls (p=0.048). Also *P. formosum* and *F. antipyretica* showed large increases in GSH content under Cd treatment compared with controls (p=0.015 and p=0.042, respectively); whereas *H. cupressiforme* displayed an opposite trend (**Table 5**).

Going up to the phylogenetic tree (**Figure 27**), the response of two hornworts studied (*A. punctatus* and *P. laevis*) to Cd stress was different. In *A. punctatus*, no significant difference in GSH content was measured between control and Cd treatment and no PC synthesis was detected. In contrast, in *P. laevis* the GSH concentration under Cd stress was diminished (P=0.023) and the PC_2 and PC_3 synthesis was found (**Table 5**).

Finally, in the two lycophytes, *H. selago* and *S. denticulata*, only the latter was able to produce PCs. In particular, the GSH content under Cd stress increased compared with untreated samples (p=0.031) and synthesis of PC_2 and PC_3 was detected. In *H. selago*, high constitutive levels of GSH, without variation under Cd stress were detected, and no PC synthesis was measured in vivo (**Table 5**).

In **Figure 28** are reported representative *C. conicum*, *S. palustre* and *P. laevis* HPLC and ESI-MS chromatograms of samples in control condition and after Cd-exposition.

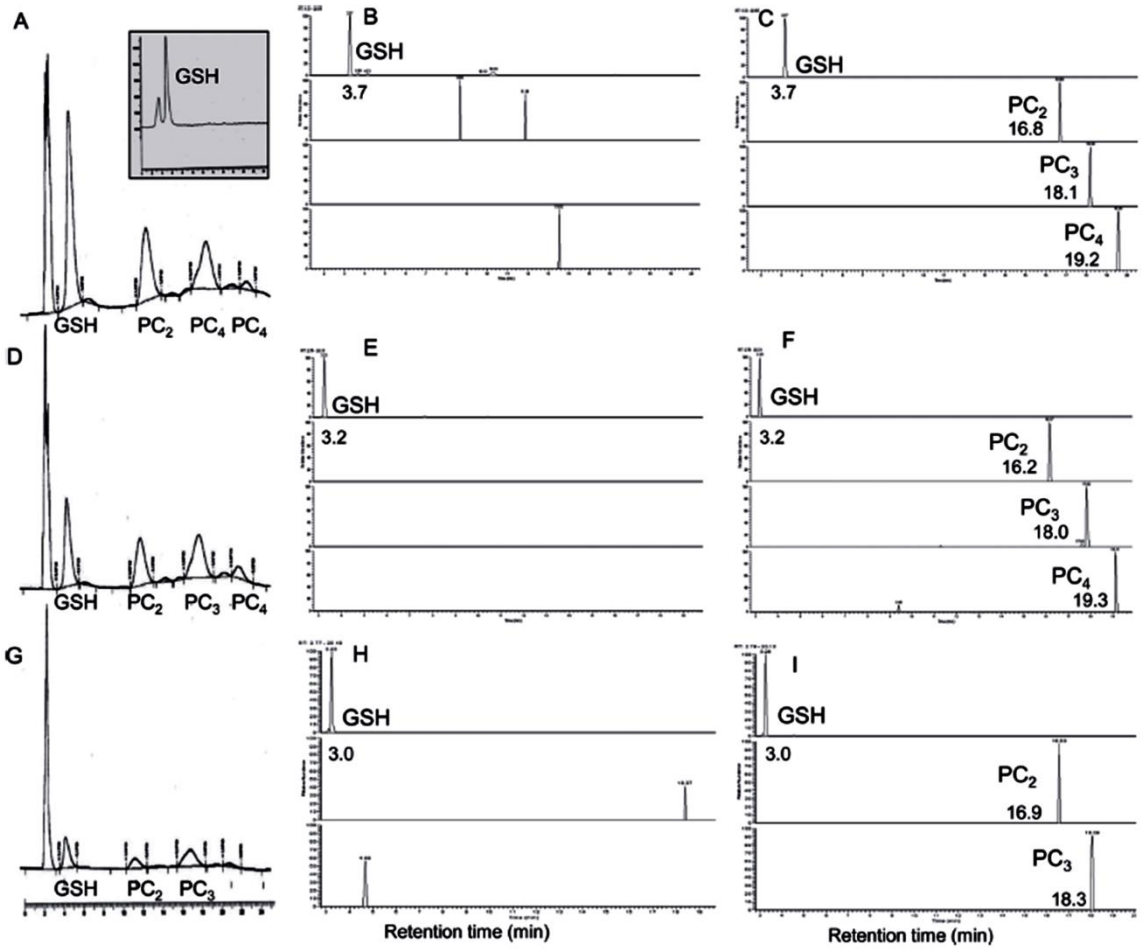

Figure 28: Representative Ellman-derivatized HPLC chromatograms of thiol-peptides from Cd-exposed **(A)** *Conocephalum conicum* (control in the insert), **(D)** *Sphagnum palustre* and **(G)** *Phaeoceros laevis*. Relative ESI-MS chromatograms of: *C. conicum* **(B)** GSH in controls and **(C)** GSH, PC_2, PC_3, PC_4 in Cd-exposed plants; *S. palustre* **(E)** GSH in controls and **(F)** GSH, PC_2, PC_3, PC_4 in Cd treated plants; *P. laevis* **(H)** GSH in controls and **(I)** GSH, PC_2, PC_3 in Cd-exposed plants. ESI-MS retention times are indicated below each thiol-peptide peak. [Picture from Petraglia et al., 2014. The capability to synthesize phytochelatins and the presence of constitutive and functional phytochelatin synthases are ancestral (plesiomorphic) characters for basal land plants. Journal of Experimental Botany 65: 1153-1163].

In **Figure 29** representative *Conocephalum conicum* MS/MS product-ion spectra and the relative fragmentation patterns for GSH, PC_2, PC_3 and PC_4 are reported.

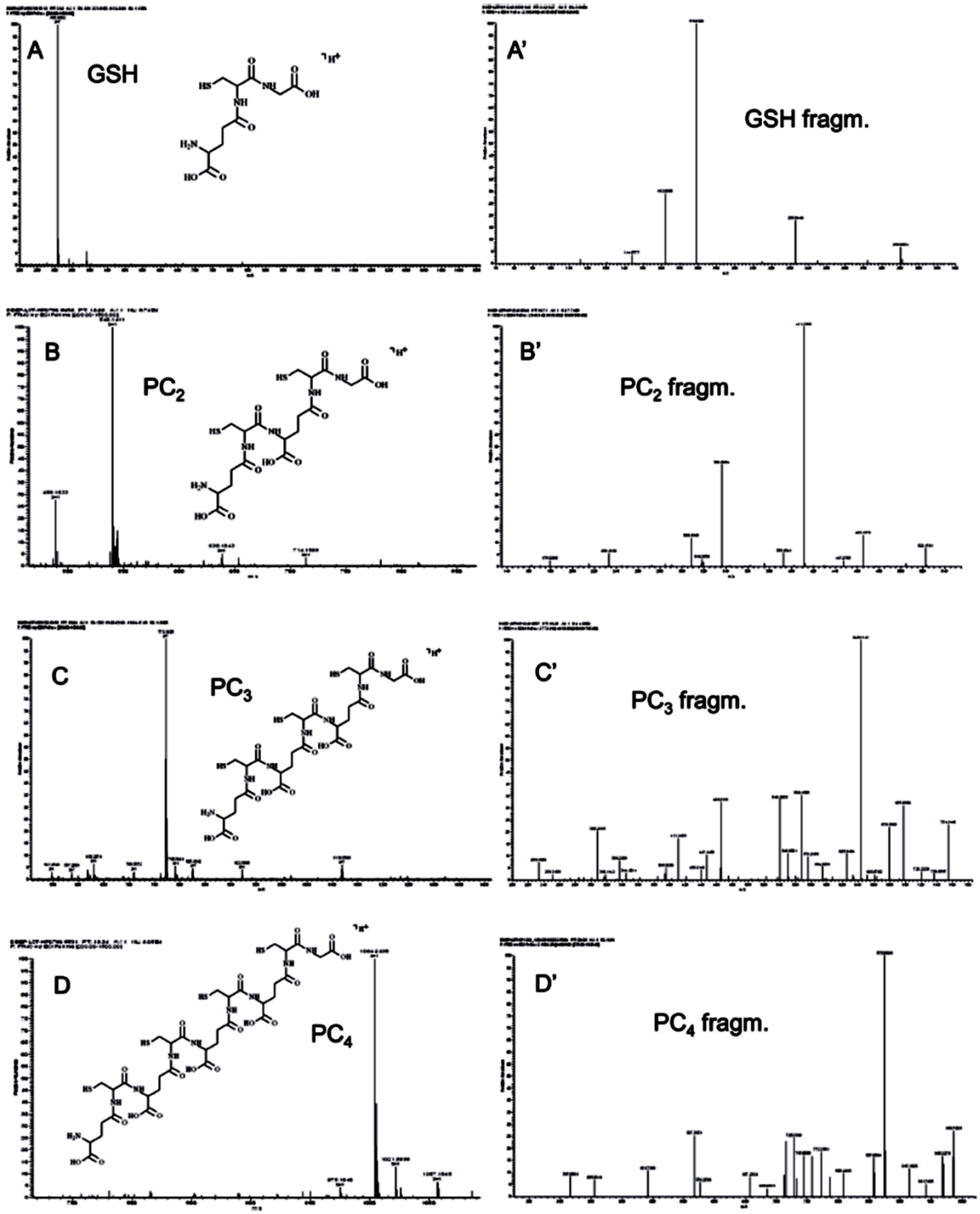

Figure 29: Representative *Conocephalum conicum* MS/MS product-ion spectra of thiol-peptides (**A** m/z 308=GSH; **B** m/z 540=PC_2; **C** m/z 772=PC_3; **D** m/z 1004=PC_4) deduced formulae, and relative fragmentation patterns at a normalized collision energy of 35 arbitrary units. The MS/MS thiol product-ion spectra from all other species were almost identical to that shown here. [Picture from Petraglia et al., 2014. The capability to synthesize phytochelatins and the presence of constitutive and functional phytochelatin synthases are ancestral (plesiomorphic) characters for basal land plants. Journal of Experimental Botany 65: 1153-1163].

Basal Land Species Possess Constitutive Phytochelatin Synthase

Western blot analyses were conducted to verify also the presence of a putative PCS band in some of the species investigated. As is shown in **Figure 30** PCS was detected in almost all species tested.

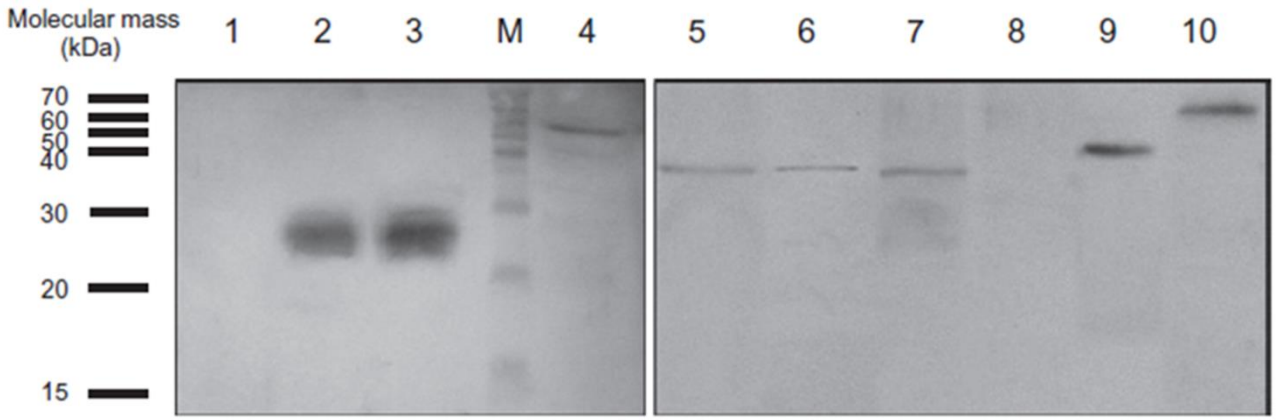

Figure 30: Western blot of PCS from bryophytes and one lycophyte species. A polyclonal antibody raised against *A. thaliana* PCS1 was employed. From left to right: (**1**) *Nostoc* sp. (Cyanobacteria); (**2**) sporophytes of *Phaeoceros laevis* (hornwort); (**3**) gametophytes of *Phaeoceros laevis* (hornwort); M, molecular mass marker (Pink Prestained Protein Ladder, range 15–75 kDa, Nippon Genetics Europe GmbH, Düren, Germany), merged with the autoradiographic membrane); (**4**) recombinant PCS1, *Arabidopsis thaliana* (AtPCS1, 50 ng, as an internal reference); (**5**) *Conocephalum conicum* (liverwort); (**6**) *Scapania undulata* (liverwort); (**7**) *Sphagnum palustre* (moss); (**8**) *Physcomitrella patens* (moss, negative control); (**9**) *Selaginella denticulata* roots (lycophyte); (**10**) *Arabidopsis thaliana* roots (positive control). [Picture from Petraglia et al., 2014. The capability to synthesize phytochelatins and the presence of constitutive and functional phytochelatin synthases are ancestral (plesiomorphic) characters for basal land plants. Journal of Experimental Botany 65: 1153-1163].

In the lanes 4 and 10 PCS1 of *A. thaliana* were shown, recombinant and from roots of plants, respectively; the bands show a molecular mass of ~ 56-58 kDa. All other PCSs identified from the basal land plants were lighter than the *AtPCS1*.

A band of ~ 28kDa was immunodetected in the sporophytes and gametophytes of *P. laevis*, lanes 2 and 3 respectively. Also the gametophytes of the liverworts *C. conicum* and *S. undulata*, and of the moss *S. palustre*, showed the presence of a putative PCS band of ~ 36 kDa (**Figure 30, lanes 5, 6, 7** respectively). The PCS of lycophyte *S. denticulata* was ~ 40 kDa (**Figure 30, lane 10**).
As expected, no PCS band was detected in *P. patens* (**Figure 30, lane 8**), and no putative PCS-like band was immunodetected in extracts from monocultures of *Nostoc* sp. (**Figure 30, lane 1**). This can exclude accidental contamination of the plants with cyanobacteria. Finally, also in charophytes no presence of non-specific bands was detected (data not shown).

PCS of Lunularia cruciata is Activated by Cadmium, Iron and Zinc

To investigate if the PCS of basal land plants is activated also by other metal(loid)s, and not only by Cd, we used the liverwort *Lunularia cruciata*, belonging to a very early clade of land plants, as well as one of the most primitive liverworts. As it is shown in **Table 5** and reported below too, *L. cruciata* was able to produce PCs after Cd treatment, but a little production of PC_2 was found also in control condition (**Table 6**).

Treatment	GSH	PC_2	PC_3	PC_4	Total PC_s
			(nmol SH g^{-1} fw)		
Cd 36 µM	14.4 ± 3.2	4.1 ± 0.9	2.9 ± 0.8	4.2 ± 0.5	11.2 ± 0.7
control	13.0 ± 2.5	1.9 ± 0.2	-	-	1.9 ± 0.2

Table 6: Content of GSH and PCs in *L. cruciata* in control and after treatment with 36 µM Cd for 72 h. [Picture from Degola et al., 2014. A Cd/Fe/Zn-responsive phytochelatin synthase is constitutively present in the ancient liverwort Lunularia cruciata (L.) Dumort. Plant Cell Physiology 55: 1884-1891].

To verify the reason of PC_2 production also in control condition, the content of metal(loid)s was measured in gametophytes of *L.cruciata* prior to any exogenous Cd treatment (**Table 7**).

Metal(loid) content (µg g^{-1} dw)							
Cd	Pb	Hg	Zn	Fe	Cu	Sb	As
n.d.	24.0 ± 1.9	n.d.	35.6 ± 3.5	71.8 ± 2.6	22.7 ± 0.6	n.d.	19.0 ± 0.9

Table 7: Metal(loid) content in *L. cruciata* gametophytes before Cd treatment (means +- SE; n = 3 for Cd, Pb, Hg, Sb and As; n = 6 for Fe, Cu and Zn; n.d. = not detected). [Picture from Degola et al., 2014. A Cd/Fe/Zn-responsive phytochelatin synthase is constitutively present in the ancient liverwort Lunularia cruciata (L.) Dumort. Plant Cell Physiology 55: 1884-1891].

The data showed the presence in *L. cruciata* gametophytes not only of essential heavy metals (Fe, Zn and Cu), but also of considerable levels of Pb and As (**Table 7**). May be this the fundamental cause of PC_2 production regardless of Cd exposure?

To test the capability of PC production, extracts of *L. cruciata* were incubated with different metal(loid)s for 90 min and the in vitro PCS activity was measured (**Table 8**).

Metal(oid)	PCS activity *L. cruciata* pmol PCs mg^{-1} protein min^{-1})	PCS activity *L. cruciata* 'fold' [metal(-loid)-exposed/ control]	PCS activity *L. cruciata* (response ratio)	PCS activity *A. thaliana* (pmol PCs mg^{-1} protein min^{-1})	PCS activity *A. thaliana* 'fold' [metal(-loid)-exposed/ control]	PCS activity *A. thaliana* (response ratio)	(PCS activity *L. cruciata*/*A. thaliana*) 100
Cd 100 µM	151.9 ± 11.3	5.9	1.59 ± 0.16*	2337.9 ± 409.2	5.8	1.74 ± 0.11*	6.5
Fe(II) 100 µM	31.4 ± 22.7	2.3	0.98 ± 0.14*	125.8 ± 49.8	4.7	1.47 ± 0.27*	24.9
Pb 100 µM	13.2 ± 1.8	n.i.	n.i.	64.8 ± 4.0	4.3	1.34 ± 0.28*	-
Hg 100 µM	22.5 ± 1.7	n.i.	n.i.	228.9 ± 58.8	10.0	2.29 ± 0.15*	-
As(III) 100 µM	27.9 ± 5.9	n.i.	n.i.	54.1 ± 18.2	2.0	0.66 ± 0.18*	-
Cu 100 µM	22.5 ± 2.9	n.i.	n.i.	66.1 ± 16.7	9.2	1.93 ± 0.23*	-
Cu 10 µM	6.1 ± 4.5	n.i.	n.i.	n.a.	-	-	-
Zn 100 µM	53.1 ± 6.2	1.6	0.37 ± 0.16*	3346.5 ± 217.0	8.3	2.11 ± 0.04*	1.6
Zn 10 µM	20.6 ± 0.7	n.i.	n.i.	n.a.	-	-	-
Sb(III) 100 µM	20.2 ± 5.4	n.i.	n.i.	4.6 ± 5.1	n.i.	n.i.	-
Sb(III) 10 µM	6.4 ± 1.7	n.i.	n.i.	n.a.	-	-	-

Activities are expressed in the columns as follows: (i) pmol of total PCs mg^{-1} protein min^{-1} (mean ± SE); (ii) 'fold': activity of the metal(loid)-incubated PCS *vs.* the respective control; and (iii) 'response ratio': ratio between the activity of the metal(loid)-affected PCS and the respective control (mean ± SE). For this last parameter a one-way ANOVA was performed, with * showing significance at $P < 0.05$. Where appropriate, the % PCS activity of *L. cruciata* relative to that of *A. thaliana* assayed under identical conditions is also given. ($n = 6$; n.a. = not assayed; n.i. = not induced).

Table 8: In vitro activities of PCSs from *L. cruciata* and *A. thaliana* (4 weeks old) incubated at 35 °C for 90 min in reaction buffer with different metal(loid)s. [Picture from Degola et al., 2014. A Cd/Fe/Zn-responsive phytochelatin synthase is constitutively present in the ancient liverwort Lunularia cruciata (L.) Dumort. Plant Cell Physiology 55: 1884-1891].

Unlike *AtPCS1*, used as a "reference" enzyme for the assay, the only metals that increased the *LcPCS* activity at the concentration of 100 µM, compared with controls, were Cd > Fe(II) > Zn; no induction was given by Cu, Pb, Hg, Sb(III) and As(III) (**Table 8**).

DISCUSSION

The Role of AtPCS1 in the Secondary Metabolism of A. thaliana

Metabolomic analysis highlights the effect of AtPCS1 enzyme on the secondary metabolism of *A. thaliana* plants grown not only after Cd treatment, but also in standard Gamborg's B5 medium (Gamborg et al., 1968) (control) (**Figures 3-4**). The distinct clusters of metabolites from wild-type, *cad1-3* and *AtPCS1-OE* plants along the first two principal components in OPLS-DA analysis (**Figures 3-4**) show the effect of AtPCS1 on the secondary metabolism. As expected, the substrate of PCS, glutathione (GSH), was one of the first molecules that was identified as differentially accumulated in wild-type, *cad1-3* and *AtPCS1-OE* plants. Two-fold higher GSH accumulation in *cad1-3 vs.* wild-type plants was also reported in Howden et al., 1995a, who used the glutathione reductase recycling assay. Our results from LC-ESI-MS analysis show a trend of increased accumulation of GSH in *cad1-3* leaves, with a value near the significance (p<0.06) and a clear low level of it in *AtPCS1-OE* plants *vs*. wild-type under both conditions (**Figure 5**). This is consistent with the role of PCS enzyme in desglycination of GSH also in presence of only free GSH; while the rate of the reaction increases more than 100-fold in the presence of Cd (Vatamaniuk et al., 2004) and that the concentration of GSH in cells and tissues is the product of an equilibrium between synthesis, degradation, use, and short and long-distance transport (Foyer et al., 2001).

In our data, the effect of AtPCS1 on GSH concentration is most prominent in leaves of *cad1-3* plants than in roots, both in control and after Cd exposure. GSH synthesis occurs in both chloroplastic and non-chloroplastic compartments and in photosynthetic and non-photosynthetic tissues (Foyer and Noctor, 2001), but it is primarily synthesized in the leaves (Noctor et al., 2002) and serves as a transport source of sulphur (S) that is delivered the via phloem to the sink tissues such as young tissues as well as roots (Takahashi et al., 2011). Our finding that AtPCS1-contributes to the regulation of GSH concentration in leaves, even in plants grown without Cd, suggests that AtPCS1 might be involved in S homeostasis and in the regulation of the sulphate uptake at the root level (Herschbach et al., 2000).

The abundance of GSH in *cad1-3* leaves, higher more than 2-fold *vs*. wild-type plants after Cd treatment, should depend on Cd-GS_2 accumulation in the cytosol that depletes the pool of free GSH which on itself is detrimental for plants under Cd and signals for more GSH production. On the contrary, in *AtPCS1-OE* plants, the low levels of GSH in all tissues and conditions tested can be correlated with the high expression of *AtPCS1,* and more substrate consumption is a consequence of increased abundance and activity of the enzyme.

The other metabolites that were differently accumulated in different plant lines, are produced by the glucosinolate pathway. In agreement with the previous report from Clay et al. (2009), we found an accumulation of 4-methoxy-indol-3-ylmethylglucosinolate (4-methoxy-I3G) in leaves of *cad1-3* plants grown under control condition (**Figure 6**). However, we did not find difference in the concentration of glucosinolates in leaves of *AtPCS1-OE* plants *vs*. wild-type (**Figure 6**).

Glucosinolate biosynthetic pathway is under feedback inhibition by glucosinolate accumulation and its hydrolytic products too (Clay et al., 2009). We hypothesize that the accumulation of 4-methoxy-I3G in leaves of *cad1-3* plants under control condition (**Figure 6**) inhibits the de novo synthesis of 8-methylthiooctylglucosinolates, which, in turn, accumulate less in roots of knockout mutants *vs*. wild-type plants (**Figure 7**).

Cd exposure increases the accumulation of 4-methoxy-I3G in *cad1-3* plants by a factor of about 1.5 and 4 in leaves and roots, respectively (**Figures 6-7**). Surprisingly, in *cad1-3* roots after Cd treatment we found also an accumulation of 4-methylsulfinylbutyl and 7-methylsulfinylheptyl glucosinolates that in control condition are more accumulated in *AtPCS1-OE* roots (**Figure 7**).

Recent studies demonstrate that the 4-methoxy-I3G, and its breakdown products contribute also to defense against pathogens, aphids and fungi (Halkier and Gershenzon, 2006; Kim and Jander, 2007; Bednarek et al., 2009).To test if the alteration of the glucosinolate pathway in *cad1-3* and *AtPCS1-OE* mutants affects plant responses to pathogens, we compared the sensitivity of wild-type, *cad1-3* and *AtPCS1-OE* plants to the hemibiotrophic bacterial pathogen, *Pseudomonas syringae* DC3000 (*PsDC3000*). Callose is one of most important mechanism of the defence responses to pathogen species and *cad1-3* mutants are not able to produces callose after Flg22 treatment (Clay et al., 2009); therefore, we predicted that the *cad1-3* mutant might be more sensitive to *PsDC3000* than the wild-type. As we expected, *cad1-3* plants were more susceptible than wild-type to *PsDC3000* (**Figure 8**); a similar trend for the same bacterium was shown in Clay et al. (2009) for *pen2-1* mutant that accumulate 4-methoxy-I3G and failed to deposit callose too. The *pad4* mutant was used as a control in our condition (**Figure 8**), that is more sensitive to pathogen as well (Xing and Chen, 2006). Surprisingly, *AtPCS1-OE* plants were also more sensitive to the pathogen *vs*. wild-type plants (**Figure 8**), while they accumulated the same level of 4-methoxy-I3G as wild-type (**Figures 6-7)** and were able to produce callose after treatment with Flg22, unlike *cad1-3* and *pen2-1* mutants (**Figure 9**). It is possible to hypothesize that increased sensitivity of *AtPCS1-OE* to *PsDC3000* is due to decreased level of GSH in their tissues (**Figure 5**). This hypothesis is based on the finding the *pad2-1* mutant contains about 20 % of the GSH present in

wild-type plants and is more susceptible to infection by bacteria, herbivore insects and fungal pathogens (Zipfel et al., 2004; Schlaeppi et al., 2008; Ferrari et al., 2003).

Therefore, the products of catabolism of 4-methoxy-I3G and homeostatic GSH level are components of the defence response to biotic stress in *A. thaliana.* We showed that this response mechanism involves AtPCS1.

The synthesis of callose is also activated under exposure to toxic heavy metals (Ueki et al., 2002 and 2005), but callose production after Cd treatment has not been experimentally validated in our mutants. **Figure 9** shows that Cd exposure induces callose deposition only in wild-type and *AtPCS1-OE* plants, even if the induction of the callose response was not as prominent as after Flg22 treatment (**Figure 9**); Cd treatment, however, did not stimulate callose deposition in *cad1-3* and *pen2-1* mutants. We hypothesize that the high accumulation of 4-methoxy-I3G in *cad1-3* plants (**Figures 6-7**) could be the reason, also after stress condition.

These results highlight that *AtPCS1* protects plants against the toxicity to heavy metals not only by producing PCs, but also by contributing to callose formation. Thus, AtPCS1 contributes to the restriction of heavy metal entry into the cells as well as to the PC-dependent vacuolar sequestration. Our data provide the first molecular evidence of the importance of callose deposition in protecting plants from Cd toxicity (**Figure 10**). This is evident by the increased sensitivity to Cd of the *pen2-1* mutant that is able to produce PCs, but is not able to synthesize callose (**Figure 10**). While the *pen2-1* mutant was more sensitive to Cd than wild-type plants, it was less sensitive to Cd than *cad1-3* plants (**Figure 10**), highlighting the importance of both, Cd-entry and PC-facilitated vacuolar sequestration of Cd for achieving full protection against Cd toxicity.

The metabolomic study also shows an upregulation of the phenylpropanoid pathway in *cad1-3* plants, grown under control or under Cd treatment. In detail, an accumulation of sinapic acid hexoside was found in leaves of *cad1-3* plants under control condition (**Figure 11**). Sinapic acid is involved in lignin synthesis (Lim et al., 2001). Consistent with our findings, Cd treatment upregulates the transcript levels of genes encoding proteins involved in monolignols synthesis in both roots and leaves (Herbette et al., 2006), suggesting an increase in lignin biosynthesis. In our experiments the exposure to 36 µM Cd for only 24 h did not change the concentration of hydroxycinnamic acids in wild-type plants; in contrast, we found increased accumulation of sinapic acid hexoside in leaves, and ferulic acid derivate in roots of *cad1-3* plants *vs*. wild-type (**Figure 11**). Since *cad1-3* plants are not able to produce PCs and callose too, the increase in lignin biosynthesis might represent one of the mechanisms important for counteracting Cd toxicity. On the contrary, we hypothesized that the high production of PCs in *AtPCS1-OE* plants is sufficient to detoxify the cells from Cd exposition with the low accumulation of sinapic acid after treatment.

Since these latter metabolites are implicated in lignin biosynthesis, we hypothesized differences in cell wall properties among wild-type, *cad1-3* and *AtPCS1-OE* plants. This speculation was tested using the so-called "stretch experiment". This assay highlighted differences in stretchability among stems of 2-month-old plant line (**Figure 12**). At the same time a preliminary analysis of lignin concentration did not show significant differences in lignin staining between plant lines (**Figure 13**), even though the stained area in *cad1-3* and *AtPCS1-OE* was thicker and the color was more intense as compared to wild-type (**Figure 13**). More experiments will be done to analyze the individual levels of monolignols.

Finally, we also found increased levels of metabolites from the phenylpropanoid pathway, *i.e.* the concentration of kaempferol and quercetin was higher in leaves and roots, respectively, in *cad1-3 vs.* wild-type plants (**Figure 14**). It has been shown that these flavonols regulate auxin retention and transport *in vivo* (Brown et al., 2001; Buer and Muday, 2004; Jacobs and Rubery, 1988; Murphy et al., 2000; Peer et al., 2001). Therefore, our future investigation will be directed towards analyses of the role of AtPCS1 in auxin distribution in *A. thaliana*.

In conclusion, the metabolomic study provides a powerful tool for the identification of the effects of AtPCS1 enzyme on the secondary metabolism of *A. thaliana*, by revealing its role in glucosinolate and phenylpropanoid pathways.

AtPCS1 and Iron Homeostasis

AtPCS1 is well known for its important role in metal(loid) detoxification (Grill et al., 1989; Clemens et al., 1999; Ha et al., 1999; Vatamaniuk et al., 1999; 2000; 2004; Romanyuk et al., 2006). Interestingly, *AtPCS1* is constitutively expressed in roots and shoots of *A. thaliana* and is not upregulated in presence of heavy metal excess (Vatamaniuk et al., 2000; Cobbett, 2000). In contrast, expression level of *AtPCS1* significantly increases in roots of *A. thaliana*, grown under Fe deficiency (Colangelo and Guerinot, 2004). Consistent with Colangelo and Guerinot (2004), we found that expression of *AtPCS1* increased more than 2-fold in roots of plants grown under low Fe-supply *vs.* control conditions (**Figure 15**). These findings prompted us to test the role of *AtPCS1* in Fe homeostasis.

One of the morphological responses to low Fe supply is an increase of root hair density. This response increases the absorptive surface layer of the root and thus, plays an important role in the uptake of nutrients from the environment (Lopez-Bucio et al., 2003). We found that root hair density was significantly higher in *cad1-3* mutant and was significantly lower in *AtPCS1-OE* plant compared to the wild-type, all grown under control conditions (**Figure 16**). These differences were also evident under Fe limitation treatment (**Figure 17**). These data suggest an alteration of Fe

homeostasis in mutant plants. Specifically, increased root hair density of the *cad1-3* mutant suggested that it tissues might experience Fe deficiency, while decreased root hair density of *AtPCS1-OE* suggest that it tissues might accumulate or sense more Fe than roots of wild-type plants. This hypothesis was further confirmed by finding a downregulation of the expression of genes encoding Fe transporter, *IRT1* and ferric reductase, *FRO2*, in *cad1-3* plants and their upregulation in *AtPCS1-OE* plants *vs.* wild-type, all grown under control condition (**Figure 18**).

These results demonstrated for the first time that *AtPCS1* is involved controlling the expression of Fe transporters, and thus, possibly, in regulating Fe homeostasis. Analyses of Fe concentration in tissues of different plant lines showed that Fe concentration in *cad1-3* leaves was only 15 % of that of the wild-type (**Figure 19A**). Interestingly, we did not find difference in Fe concentration among roots of *cad1-3* and wild-type lines (**Figure 19B**). This fact was surprising, given the decreased expression of the *IRT1/FRO2* Fe uptake system (**Figure 18**) and increased root hair density (**Figure 16**) in knockout mutant plants.

To reconcile these data, we propose that the *cad1-3* mutant might be defective in Fe uptake due to decreased expression of *IRT1/FRO2* (**Figure 18**). To compensate for this defect, the *cad1-3* mutant retains Fe in the root in unavailable form (*e.g.* in the vacuole), which, in turn, leads to decreased root-to-shoot Fe partitioning and decreased Fe content in the shoot (**Figure 19A**). In contrast, the Fe concentration in leaves and roots of *AtPCS1-OE* plants was 60-fold and 15-fold higher respectively, when compared with the corresponding tissues in wild-type plants (**Figure 19**).

Symptoms of Fe deficiency are more prominent in younger tissues (Marschner, 1995). Therefore, we expected that if *AtPCS1* functions in the Fe homeostasis, then young leaves of the *cad1-3* plants would be more sensitive to Fe deficiency. By contrast, young leaves of *AtPCS1-OE* would be more tolerant to Fe deficiency than young leaves of the wild-type. Consistent with this hypothesis, we observed that young leaves of the *cad1-3* mutant were significantly more chlorotic compared with the wild-type grown under the same conditions (**Figure 20B**). As we predicted, young leaves of *AtPCS1-OE* plants were more tolerant to Fe limitation than leaves of wild-type plants, which were chlorotic on the edges of leaf blades (**Figure 20B**). This phenotype was consistent with the expression pattern of *IRT1* and *FRO2;* also *OPT3*, which encodes a Fe transporter involved in Fe partitioning from source to sink tissues (Zhai et al., 2014), was altered in *cad1-3* and *AtPCS1-OE* plants (**Figure 21**). Indeed, expression of *IRT1*, *FRO2* and *OPT3* was downregulated in *cad1-3* plants and upregulated in *AtPCS1-OE* plants (**Figure 21**). In contrast to *AtPCS1-OE* plants (**Figure 20**), the *cad1-3* mutant exhibited Fe starvation phenotypes even when grown under Fe sufficient conditions (**Figure 16**) and, also Fe levels were limited (**Figure 19**). The low or high concentration of Fe in *cad1-3* and *AtPCS1-OE* plants respectively, is a consequence of

the deregulated metal transport in mutant roots *via IRT1*, *FRO2* and tissues partitioning, *via OPT3* (Welch et al., 1993; Cohen et al., 1998; Vert et al., 2002; Zhai et al., 2014). Based on these results, we concluded that *AtPCS1* functions also in Fe homeostasis.

The Mechanistic Basis of the Role of AtPCS1 in Fe Homeostasis

To gain insights into the role of AtPCS1 in Fe homeostasis, we turned into the basic mechanisms of AtPCS1-mediated catalysis. The substrate of AtPCS1 is GSH and a Me-GS($_n$) complex, were Me is a transition element such as Cd, Zn, Cu, and (n) reflects the valency of the transition element (Vatamaniuk et al., 2000). Previous data have shown that in the presence of Me-GS($_n$) and GSH, AtPCS1 is in the acylated state and desglycinates GSH very effectively. As a result, the concentration of GSH decreases while the concentration of γ-Gly-Cys and Gly increases (Vatamaniuk et al., 2004). Depending on the concentration of Me-GS($_n$) and GSH, the reaction could proceed towards formation of PCs, or can be terminated at the level of γ-Gly-Cys and Gly production. Consistent with this is a clear demonstration of a preference of AtPCS1 for the desglycylation reaction from GS-conjugate than for a transpeptidation of GSH to PCs (Beck et al., 2003; Vatamaniuk et al., 2004).

On the basis of these data, we hypothesized that AtPCS1 regulates the Fe transporters expressions, by regulating the concentration of GSH and changes in GSH levels (and therefore the redox state of cells) has an effect on Fe homeostasis.

To test this hypothesis, wild-type plants were grown in the presence of different GSH concentrations. As expected, supplementation of the growth medium with GSH downregulated the expression of *IRT1* and *FRO2* (**Figure 22**). Furthermore, GSH treatment increased root hair density (**Figure 23**). This phenotype resembles the phenotype of the *cad1-3* mutant grown under control condition (**Figure 16**). These data show the effect of GSH on Fe homeostasis and suggest that AtPCS1 acts on Fe homeostasis *via* regulating GSH concentration.

In parallel, wild-type plants were grown also in the presence of different concentrations of L-buthionine sulfoximine (BSO), an inhibitor of GSH synthesis (Howden et al., 1995a). According to our hypothesis, the low level of intracellular GSH upregulated the expression of Fe uptake genes (**Figure 24**). BSO also reduced root hair density (**Figure 25**). These phenotypes resembled the phenotype observed in *AtPCS1-OE* plants grown under control conditions (**Figure 16**) and further supported our hypothesis that AtPCS1 acts on Fe homeostasis *via* regulating GSH concentration.

We then used the *cad2-1* mutant of *A. thaliana*, containing only 39% of the wild-type GSH level because of an alteration in a gene encoding the first enzyme in GSH biosynthesis, γ-glutamylcysteine synthetase (Cobbett et al., 1998). We found that expression of *IRT1* and *FRO2* is

upregulated in roots of the *cad2-1* mutant in comparison with wild-type plants grown under standard conditions (**Figure 26**). These data further support our hypothesis that GSH is involved in regulating Fe homeostasis and that AtPCS1 acts through regulating the concentration of GSH in the cell. Specifically, we propose that loss of AtPCS1 function results in GSH accumulation in leaves with a consequent downregulation of Fe transporters, thus resulting in Fe starvation condition; on the contrary, overexpression of *AtPCS1* results in low GSH accumulation with a consequent upregulation of Fe transporters and Fe hyperaccumulation in leaves and roots.

Evolutionary Hystory of PCS Enzyme

The data obtained from the study of PCS evolution highlight the presence of constitutive and functional PCS enzymes also in the first plants that colonized the land environment presumably in the Ordovician-Silurian-Devionian Periods. PC in vivo production (**Table 5**) and western-immunoreactive PCS bands (**Figure 30**) were found in: (1) a number of liverworts; (2) the moss *S. palustre*; (3) gametophytes and sporophytes of the hornwort *P. laevis*; and (4) the lycophyte *S. denticulata*. Moreover, PC synthesis was found in all charophytes (sisters of land plants) tested, in agreement with Volland et al. (2013) that found a PC production in the charophytic alga *M. denticulata*.

Hence, a functional PCS enzyme is present in charophytes, in all the lineages of bryophytes, as well as in early tracheophytes. As it is shown in **Figure 30**, the length of the PCS enzyme is different among the tested species, and it is shorter in land plants compared to *AtPCS1*. It is hypothesized that such dimensional variations might be mainly ascribed to the length of the C-terminal domain (as detailed by Rea, 2012) that plays a role in conferring a better thermal stability, as well as in protecting against metal-induced oxidative damage possibly occurring in the N-terminal domain (Matsumoto et al., 2009).

In particular, the PCS immunodetected from gametophytes and sporophytes of *P. laevis*, has an apparent molecular mass of ~28 KDa, theoretically the same size of cyanobacterial PCS-like enzyme (Harada et al., 2004; Tsuji et al., 2004; Vivares et al., 2005). This is really interesting from an evolutionary standpoint because it might be interpreted as an ancestral horizontal transfer of the PCS, perhaps from an archaic cyanobacterium to an early hornwort, with the subsequent further full acquisition of PC production, since *Nostoc* synthesizes only traces of PC_2 (Tsuji et al., 2004) or not produce PCs (Harada et al., 2004; Vivares et al., 2005).

A longer PCS (with a better thermal stability and an improved response to metal ions and to oxidative agents) might potentially have been promoted in the course of evolution, up to the achievement of the full length dimension of the angiosperm PCSs.

These results demonstrate that the capability for PC production under metal stress and the presence of a constitutive and functional PCS enzyme actually represent ancestral (plesiomorphic) characters. Also, the capability of PC production under metal stress was, in some cases, probably independently lost during evolution, as supported by the absence of a PCS and PCs in the investigated mosses, with the exception of *S. palustre*. At the same time, the apparent discrepancy between the lack of in vivo detectable PC production in *S. undulata* (**Table 5**) and the demonstrated presence of PCS enzyme by western blot (**Figure 30**) might possibly be due to morphological/ultrastructural characteristics (*i.e.* cell wall thickness, mucilage canals, *etc.*) that could reduce or prevent Cd from reaching the cytosolic PCS in amounts sufficient for inducing an in vivo detectable synthesis of PCs.

PCS of the liverwort L. cruciata

To study if PCS of basal land plants is activated also by other metal(loid)s, other than Cd, we used the liverwort *L. cruciata* that have been recognized to belong to a very early clade of land plants. Surprisingly, in **Table 6** is reported a constant presence of PC_2 production, also in control condition. This may indicate that the PC_2 oligomer could be synthesized at a basal level in order to manage trace metal micronutrient (*e.g.* Fe, Zn and Cu) homeostasis/excess or the presence of non-essential metals in *L. cruciata* samples. To test this, the content of metal(loid)s was measured in gametophytes of *L. cruciata* prior to exogenous Cd treatment (**Table 7**). The data showed the presence of essential heavy metals (Fe, Zn and Cu), and also considerable levels of Pb and As (**Table 7**).

In order to ascertain the possible direct relationship between metal(loid) homeostasis/excess and LcPCS activity, the enzymatic assay in vitro showed no induction of LcPCS by Cu, Pb, Hg, Sb(III) and As(III), but only by Cd, Fe(II) and Zn (**Table 8**). Thus, the presence of PC_2 in control samples of *L. cruciata* (**Table 6**) could well be ascribed to the homeostatic presence of Fe(II) and Zn in the gametophyte tissues. AtPCS1 activity was used as a "reference" enzyme for the assay, that is activated by all the metal(loid)s employed, except Sb(III) (**Table 8**).

In general, the LcPCS, as well as the PCSs of other basal plants studied previously (Petraglia et al., 2014), appear to be less active compared with the AtPCS1. This could be due to C-terminal domain that probably is shorter in early land plants (**Figure 30**) than AtPCS1, that might improve the N-terminal core catalysis resulting in an overall increment of the enzyme's responsiveness to metals, high temperature and oxidative stress (Vatamaniuk et al., 2000; Ruotolo et al., 2004; Romanyuk et al., 2006; Matsumoto et al., 2009).

According to the results obtained with *A. thaliana* as far as the involvement of AtPCS1 in Fe homeostasis is concerned, we also found an important confirmation of this role/function in *L. cruciata* PCS.

CONCLUSIONS

To conclude, the experimental work performed in this doctoral thesis highlights novel aspects of *AtPCS1* roles/functions in *A. thaliana.* First, the metabolomic study has identified the role of *AtPCS1* in glucosinolate and phenylpropanoid pathways and has shown the relationship between *AtPCS1*, heavy metal and pathogen resistance, through cell wall (callose- and lignin-driven) remodeling. Second, it has been shown that *AtPCS1* is involved in the regulation of Fe homeostasis and that this is in turn achieved *via* the regulation of the concentrations of GSH.

Future work will address the role of *AtPCS1* in auxin partitioning and lignin biosynthesis and further details the involvement of *AtPCS1* in the regulation of Fe homeostasis.

Also, we demonstrated that the ability to produce PCs and the presence of constitutive and functional PCS enzyme is a common trait occurring also in the first plants that colonized the land environment. In particular, the liverwort *L. cruciata* possesses a PCS showing a (adaptive?) function aimed at regulating the Fe/Zn homeostasis, together with a role aimed at detoxifying Cd.

Future work will address the sequencing of PCS gene of these first land plants.

REFERENCES

Arteca R.N., Arteca J.M. (2000). A novel method for growing *Arabidopsis thaliana* plants hydroponically. Physiologia Plantarum 108: 188-193.

Beck A., Lendzian K., Oven M., Christmann A., Grill E. (2003). Phytochelatin synthase catalyzes key step in turnover of glutathione conjugates. Phytochemistry 62: 423-431.

Becker B., Marin B. (2009). Streptophyte algae and the origin of embryophytes. Annals of Botany 103: 999-1004.

Bednarek P., Bednarek M.P., Svatoš A., Schneider B., Doubský J., Mansurova M., Humphry M., Consonni C., Panstruga R., Sanchez-Vallet A., Molina A., Schulze-Lefert P. (2009). A glucosinolate metabolism pathway in living plant cells mediates broad-spectrum antifungal defense. Science 323: 95-101.

Blum R., Beak A., Korte A., Stengel A., Letzel T., Lendzian K., Grill E. (2007). Function of phytochelatin synthase in catabolism of glutathione-conjugates. The Plant Journal 49: 740-749.

Bonawitz N.D., Chapple C. (2010). The genetics of lignin biosynthesis: connecting genotype to phenotype. The Annual Review of Genetics 44: 337-363.

Bradford M.M. (1976). A rapid and sensitive method for the quantitation of microgram quantities of protein utilizing the principle of protein-dye binding. Analytical Biochemistry 72: 248-254.

Brown D.E., Rashotte A.M., Murphy A.S., Normanly J.,Tague B.W., Peer W.A., Taiz L., Muday G.K. (2001). Flavonoids act as negative regulators of auxin transport in vivo in *Arabidopsis*. Plant Physiology 126: 524-535.

Brunetti P., Zanella L., Proia A., De Paolis A., Falasca G., Altamura M.M., Sanità di Toppi L., Costantino P., Cardarelli M. (2011). Cadmium tolerance and phytochelatin content of *Arabidopsis* seedlings over-expressing the phytochelatin synthase gene *AtPCS1*. Journal of Experimental Botany 62: 5509-5519.

Bruns I., Sutter K., Menge S., Neumann D., Krauss G.J. (2001). Cadmium lets increase the glutathione pool in bryophytes. Journal of Plant Physiology 158: 79-89.

Buer C.S., Munday G.K. (2004). The transparent testa4 mutation prevents flavonoid synthesis and alters auxin transport and the response of *Arabidopsis* roots to gravity and light. The Plant Cell 16: 1191-1205.

Carginale V., Sorbo S., Capasso C., Trinchella F., Cafiero G., Basile A. (2004). Accumulation, localisation, and toxic effects of cadmium in the liverwort *Lunularia cruciata*. Protoplasma 223: 53-61.

Chiaudani G., Vighi M. (1997). Applicazione di un saggio algale standard per lo studio di fenomeni di tossicità. Nuovi Annali d'Igiene e Microbiologia 28: 145-163.

Clay N.K., Adio A.M., Denoux C., Jander G., Ausubel F.M. (2009). Glucosinolate metabolites required for an *Arabidopsis* innate immune response. Science 323: 95-101.

Clemens S., Kim E.J., Neumann D., Schroeder J.I. (1999). Tolerance to toxic metals by a gene family of phytochelatin synthases from plants and yeast. The Embo Journal 18: 3325-3333.

Clemens S., Schroeder J.I., Degenkolb T. (2001). Caenorhabditis elegans expresses a functional phytochelatin synthase. European Journal of Biochemistry 268: 3640-3643.

Cobbett C.S, Goldsbrough P. (2002). Phytochelatins and metallothioneins: roles in heavy metal detoxification and homeostasis. Annual Review of Plant Biology 53: 159-182.

Cobbett C.S. (1999). A family of phytochelatin synthase genes from plant, fungal and animal species. Trends in Plant Science 4: 335-337.

Cobbett C.S. (2000). Phytochelatin biosynthesis and function in heavy-metal detoxification. Current Opinion in Plant Biology 3: 211-216.

Cobbett C.S., May M.J., Howden R., Rolls B. (1998). The glutathione-deficient, cadmium-sensitive mutant, *cad2-1*, of *Arabidopsis thaliana* is deficient in gamma-glutamylcysteine synthetase. The Plant Journal 16: 73-78.

Cohen C.K., Fox T.C., Garvin D.F., Kochian L.V. (1998). The role of iron-deficiency stress responses in stimulating heavy-metal transport in plants. Plant Physiology 116: 1063-1072.

Colangelo E.P., Guerinot M.L. (2004). The essential basic helix-loop-helix protein FIT1 is required for the iron deficiency response. The Plant Cell 16: 3400-3412.

Coleman R.A., Underwood A.J., Benedetti-Cecchi L., Aberg P., Arenas F., Arrontes J., Castro J., Hartnoll R.G., Jenkins S.R., Paula J., Della Santina P., Hawkins S.J. (2006). A continental scale evaluation of the role of limpet grazing on rocky shores. Oecologia 147: 556-564.

de Knecht J.A., van Dillen M., Koevoets P.L.M., Schat H., Verkleij J.A.C., Ernst W.H.O. (1994). Phytochelatins in cadmium-sensitive and cadmium tolerant *Silene vulgaris*. Plant Physiology 104: 255-261.

Degola F., De Benedictis M., Petraglia A., Massimi A., Fattorini L., Sorbo S., Basile A., Sanità di Toppi L. (2014). A Cd/Fe/Zn-responsive phytochelatin synthase is constitutively present in the ancient liverwort *Lunularia cruciata* (L.) Dumort. Plant Cell Physiology 55: 1884-1891.

Eide D., Broderius M., Fett J., Guerinot M.L. (1996). A novel iron-regulated metal transporter from plants identified by functional expression in yeast. Proceedings of the National Academy of Sciences, USA 93: 5624-5628.

Fahey J.W., Zalcmann A.T., Talalay P. (2001). The chemical diversity and distribution of glucosinolates and isothiocyanates among plants. Phytochemistry 56: 5-51.

Ferrari S., Plotnikova J.M., De Lorenzo G., Ausubel F.M. (2003). *Arabidopsis* local resistance to *Botrytis cinerea* involves salicylic acid and camalexin and requires *EDS4* and *PAD2*, but not *SID2*, *EDS5* or *PAD4*. The Plant Journal 35: 193-205.

Foyer C.H., Noctor G. (2001). The molecular biology and metabolism of glutathione. In: Grill D., Tausz M., De Kok L., eds. Significance of glutathione in plant adaptation to the environment. Kluwer Academic Publishers: 27-57.

Foyer C.H., Theodoulou F.L., Delrot S. (2001). The functions of intercellular and intracellular glutathione transport systems. Trends in Plant Science 6: 486-492.

Gamborg O.L., Miller R.A., Ojima K. (1968). Nutrient requirement of suspensions cultures of soybean root cells. Experimental Cell Research 50: 151-158.

Gayomba S.R., Jung H.I., Yan J., Danku J., Rutzke M.A., Bernal M., Krämer U., Kochian L.V., Salt D.E., Vatamaniuk O.K. (2013). The CTR/COPT-dependent copper uptake and SPL7-dependent copper deficiency responses are required for basal cadmium tolerance in *A. thaliana*. Metallomics 5: 1262-1275.

Geisler M., Blakeslee J.J., Bouchard R., Lee O.R., Vincenzetti V., Bandyopadhyay A., Titapiwatanakun B., Peer W.A., Bailly A., Richards E.L., Ejendal K.F.K., Smith A.P., Baroux C., Grossniklaus U., Muller A., Hrycyna C.A., Dudler R., Murphy A.S., Martinoia E. (2005). Cellular efflux of auxin catalyzed by the *Arabidopsis* MDR/PGP transporter AtPGP1. The Plant Journal 44: 179-194.

Gekeler W., Grill E., Winnacker E.L., Zenk MH. (1989). Survey of the plant kingdom for the ability to bind heavy metals through phytochelatins. Zeitschrift für Naturforschung 44c: 361-369.

Glawischnig E. (2007). Camalexin. Phytochemistry 68: 401-406.

Glawischnig E., Hansen B.G., Olsen C.E., Halkier B.A. (2004). Camalexin is synthesized from indole-3-acetaldoxime, a key branching point between primary and secondary metabolism in *Arabidopsis*. Proceedings of the National Academy of Science, USA 101: 8245-8250.

Glazebrook J., Zook M., Mert F., Kagan I., Rogers E.E., Crute I.R., Holub E.B., Hammerschmidt R., Ausubel F.M. (1997). Phytoalexin-deficient mutants of *Arabidopsis* reveal that *PAD4* encodes a regulatory factor and that four *PAD* genes contribute to downy mildew resistance. Genetics 146: 381-392.

Grill E., Loffler S., Winnacker E.L., Zenk M.H. (1989). Phytochelatins, the heavy-metal-binding peptides of plants, are synthesized from glutathione by a specific γ-glutamylcysteine dipeptidyl transpeptidase (phytochelatin synthase). Proceedings of the National Academy of Sciences, USA 86: 6838-6842.

Grill E., Winnacker E.L., Zenk M.H. (1985). Phytochelatins: the principal heavy-metal complexing peptides of higher plants. Science 230: 674-676.

Guerinot ML. (2000). The ZIP family of metal transporters. Biochimica et Biophysica Acta 1465: 190-198.

Ha S.B., Smith A.P., Howden R., Dietrich W.M., Bugg S., O'Connell M.J., Goldsbrough P.B., Cobbett C.S. (1999). Phytochelatin synthase genes from *Arabidopsis* and the yeast *Schizosaccharomyces pombe*. The Plant Cell 11: 1153-1163.

Hacham Y., Koussevitzky S., Kirma M., Amir R. (2014). Glutathione application affects the transcript profile of genes in *Arabidopsis* seedling. Journal of Plant Physiology 171: 1444-1451.

Halkier B.A., Gershenzon J. (2006). Biology and biochemistry of glucosinolates. The Annual Review of Plant Biology 57: 303-333.

Hammerschmidt R. (1999). Phytoalexins: What have we learned after 60 years? Annual Review of Phytopathology 37: 285-306.

Hansen B.G., Halkier B.A. (2005). New insight into the biosynthesis and regulation of indole compounds in *Arabidopsis thaliana*. Planta 221: 603-606.

Harada E., von Roepenack-Lahaye E., Clemens S. (2004). A cyanobacterial protein with similarity to phytochelatin synthases catalyzes the conversion of glutathione to γ-glutamylcysteine and lacks phytochelatin synthase activity. Phytochemistry 65: 3179-3185.

Hemm M.R., Ruegger M.O., Chapple C. (2003). The *Arabidopsis ref2* mutant is defective in the gene encoding *CYP83A1* and shows both phenylpropanoid and glucosinolate phenotypes. The Plant Cell 15: 179-194.

Herbette S., Taconnat L., Hugouvieux V., Piette L., Magniette M.L.M., Cuine S., Auroy P., Richaud P., Forestier C., Bourguignon J., Renou J.P., Vavasseur A., Leonhardt N. (2006). Genome-wide transcriptome profiling of the early cadmium response of *Arabidopsis* roots and shoots. Biochimie 88: 1751-1765.

Herschbach C., Zalm E., Schneider A., Jouanin L., De Kok L.J., Rennenberg H. (2000). Regulation of sulfur nutrition in wild-type and transgenic poplar over-expressing γ-glutamylcysteine synthetase in the cytosol as affected by atmospheric H_2S. Plant Physiology 124: 461-473.

Hindt M.N., Guerinot M.L. (2012). Getting a sense for signals: regulation of the plant iron deficiency response. Biochimica et Biophysica Acta 1823: 1521-1530.

Howden R., Andersen C.R., Goldsbrough P.B., Cobbett C.S. (1995b). A cadmium-sensitive, glutathione-deficient mutant of *Arabidopsis thaliana*. Plant Physiology 107: 1067-1073.

Howden R., Goldsbrough P.B., Andersen C.R., Cobbett C.S. (1995a). Cadmium-sensitive, *cad1* mutants of *Arabidopsis thaliana* are phytochelatin deficient. Plant Physiology 107: 1059-1066.

Hussain D., Haydon M.J., Wang Y., Wong E., Sherson S.M., Young J., Camakaris J., Harper J.F., Cobbett C.S. (2004). P-type ATPase heavy metal transporters with roles in essential zinc homeostasis in *Arabidopsis*. The Plant Cell 16: 1327-1339.

Jackson P.J., Robinson N.J., Whitton B.A. (1991). Low molecular mass metal complexes in the freshwater moss *Rhynchostegium riparioides* exposed to elevated concentrations of zinc, copper,

cadmium and lead in the laboratory and field. Environmental and Experimental Botany 31: 359-366.

Jacobs M., Rubery P.H. (1988). Naturally occurring auxin transport regulators. Science 241: 346-349.

Jung H.I., Gayomba S.R., Rutzke M.A., Craft E., Kochian L.V., Vatamaniuk O.K. (2012). COPT6 is a plasma membrane transporter that functions in copper homeostasis in *Arabidopsis* and is a novel target of SQUAMOSA promoter-binding protein-like 7. The Journal of Biological Chemistry 287: 33252-33267.

Kenrick P., Crane P.R. (1997). The origin and early evolution of plants on land. Nature 389: 33-39.

Kim J.H., Jander G. (2007). Myzus persicae (green peach aphid) feeding on *Arabidopsis* induces the formation of a deterrent indole glucosinolate. The Plant Journal 49: 1008-1019.

Kim J.H., Lee B.W., Schroeder F.C., Jander G. (2008). Identification of indole glucosinolate breakdown products with antifeedant effects on Myzus persicae (green peach aphid). The Plant Journal 54: 1015-1026.

Koes R.E., Quattrocchio F., Mol J.N.M. (1993). The flavonoid biosynthetic pathway in plants: function and evolution. BioEssays 16: 123-132.

Kondo N., Imai K., Isobe M., Goto T., Murasugi A., Wada-Nakagawa C. (1984). Cadystin A and B, major unit peptides comprising cadmium binding peptides induced in a fission yeast-separation, revision of structures and synthesis. Tetrahedron Letters 25: 3869-3872.

Kopriva S., Wiedemann G., Reski R. (2007). Sulfate assimilation in basal land plants-what does genomic sequencing tell us? Plant Biology 9: 556-564.

Koren'Kov V., Park S., Cheng N.H., Sreevidya C., Lachmansingh J., Morris J., Hirschi K., Wagner G.J. (2007). Enhanced Cd^{2+}-selective root-tonoplast-transport in tabaccos expressing *Arabidopsis* cation exchangers. Planta 225: 403-411.

Lahner B., Gong J., Mahmoudian M., Smith E.L., Abid K.B., Rogers E.E., Guerinot M.L., Harper J.F., Ward J.M., McIntyre L., Schroeder J.I., Salt D.E. (2003). Genomic scale profiling of nutrient and trace elements in *Arabidopsis thaliana*. Nature Biotechnology 21: 1215-1221.

Lee S., Moon J.S., Ko T.S., Petros D., Goldsbrough P.B., Korban S.S. (2003). Overexpression of *Arabidopsis* phytochelatin synthase paradoxically leads to hypersensitivity to cadmium stress. Plant Physiology 131: 656-663.

Lewis D.R., Ramirez M.V., Miller N.D., Vallabhaneni P., Ray W.K., Helm R.F., Winkel B.S., Muday G.K. (2011). Auxin and ethylene induce flavonol accumulation through distinct transcriptional networks. Plant Physiology 156: 144-164.

Li Y., Dhankher O.M., Carreira L., Lee D., Chen A., Schroeder J.I., Balish R.S., Meagher R.B. (2004). Overexpression of phytochelatin synthase in *Arabidopsis* leads to enhanced arsenic tolerance and cadmium hypersensitivity. Plant and Cell Physiology 45: 1787-1797.

Ligrone R., Duckett J.G., Renzaglia K.S. (2012). Major transitions in the evolution of early land plants: a bryological perspective. Annals of Botany 109: 851-871.

Lim E.K., Li Y., Parr A., Jackson R., Ashford D.A., Bowles D.J. (2001). Identification of glucosyltransferase genes involved in sinapate metabolism and lignin synthesis in *Arabidopsis*. The Journal of Biological Chemistry 276: 4344-4349.

Lipka V., Dittgen J., Bednarek P., Bhat R., Wiermer M., Stein M., Landtag J., Brandt W., Rosahl S., Scheel D., Llorente F., Molina A., Parker J., Somerville S., Schulze-Lefert P. (2005). Pre- and postinvasion defenses both contribute to nonhost resistance in *Arabidopsis*. Science 310: 1180-1183.

Lopez-Bucio J., Cruz-Ramirez A., Herrera-Estrella L. (2003). The role of nutrient availability in regulating root architecture. Current Opinion in Plant Biology 6: 280-287.

Marrs K.A. (1996). The functions and regulation of glutathione S-transferase in plants. Annual Review in Plant Physiology and Plant Molecular Biology 47: 127-157.

Marschner H. (1995). Mineral nutrition of higher plants. London; San Diego: Academic Press.

Matsumoto S., Vestergaard M., Konishi T., Nishikori S., Shiraki K., Tsuji N., Hirata K., Takagi M. (2009). Role of C-terminal cys-rich region of phytochelatin synthase in tolerance to cadmium ion toxicity. Journal of Plant Biochemistry and Biotechnology 18: 1-6.

May M.J., Vernoux T., Leaver C., Montagu M.V., Inzè D. (1998). Glutathione homeostasis in plants: implications for environmental sensing and plant development. Journal of Experimental Botany 49: 649-667.

McCourt R.M., Delwiche C.F., Karol K.G. (2004). Charophyte algae and land plant origins. Trends in Ecology and Evolution 19: 661-666.

Meister A. (1995). Glutathione metabolism. Methods in Enzymology 251: 3-7.

Mendoza-Cozatl D.G., Jobe T.O., Hauser F., Schroeder J.I. (2011). Long-distance transport, vacuolar sequestration, tolerance, and transcriptional responses induced by cadmium and arsenic. Current Opinion in Plant Biology 14: 554-562.

Murphy A., Peer W.A., Taiz L. (2000). Regulation of auxin transport by aminopeptidases and endogenous flavonoids. Planta 211: 315-324.

Mutoh N., Hayashi Y. (1988). Isolation of mutants of *Schizosaccharomyces pombe* unable to synthesize cadystin, small cadmium-binding peptides. Biochemical and Biophysical Research Communications 151: 32-39.

Noctor G., Gomez L., Vanacker H., Foyer C.H. (2002). Interactions between biosynthesis, compartmentation and transport in the control of glutathione homeostasis and signalling. Journal of Experimental Botany 53: 1283-1304.

Nurnberger T., Lipka V. (2005). Non-host resistance in plants: new insights into an old phenomenon. Molecular Plant Pathology 6: 335-345.

Palmer C.M., Guerinot M.L. (2009). Facing the challenges of Cu, Fe and Zn homeostasis in plants. Nature Chemical Biology 5: 333-340.

Peer W.A., Brown D.E., Tague B.W., Munday G.K., Taiz L., Murphy A.S. (2001). Flavonoid accumulation patterns of transparent testa mutants of *Arabidopsis*. Plant Physiology 126: 536-548.

Peer W.A., Murphy A.S. (2007). Flavonoids and auxin transport: modulators or regulators? Trends in Plant Science 12: 556-563.

Petraglia A., De Benedictis M., Degola F., Pastore G., Calcagno M., Ruotolo R., Mengoni A., Sanità di Toppi L. (2014). The capability to synthesize phytochelatins and the presence of constitutive and functional phytochelatin synthases are ancestral (plesiomorphic) characters for basal land plants. Journal of Experimental Botany 65: 1153-1163.

Pires N.D., Dolan L. (2012). Morphological evolution in land plants: new designs with old genes. Philosophical Transactions of the Royal Society B: Biological Sciences 367: 508-518.

Qiu Y.L. (2008). Phylogeny and evolution of charophytic algae and land plants. Journal of Systematics and Evolution 46: 287-306.

Qiu Y.L., Li L., Wang B., Chen Z., Knoop V., Groth-Malonek M., Dombrovska O., Lee J., Kent L., Rest J., Estabrook G.F., Hendry T.A., Taylor D.W., Testa C.M., Ambros M., Crandall-Stotler B., Duff R.J., Stech M., Frey W., Quandt D., Davis C.C. (2006). The deepest divergences in land plants inferred from phylogenomic evidence. Proceedings of the National Academy of Sciences, USA 103: 15511-15516.

Rauser W.E. (1990). Phytochelatins. Annual Review of Biochemistry 59: 61-86.

Rea P.A. (2012). Phytochelatin synthase: of a protease a peptide polymerase made. Physiologia Plantarum 145: 154-164.

Rea P.A., Vatamaniuk O.K., Rigden D.J. (2004). Weeds, worms, and more. Papain's long-lost cousin, phytochelatin synthase. Plant Physiology 136: 2463-2474.

Rensing S.A., Lang D., Zimmer A.D., et al. (2008). The Physcomitrella genome reveals evolutionary insights into the conquest of land by plants. Science 319: 64-69.

Rice C.M., Ashcroft W.A., Batten D.J., Boyce A.J., Caulfield J.B.D., Fallick A.E., Hole M.J., Jones E., Pearson M.J., Rogers G., Saxton J.M., Stuart F.M., Trewin N.H., Turner G. (1995). A Devonian auriferous hot spring system, Rhynie, Scotland. Journal of the Geological Society London 152: 229-250.

Robinson N.J., Procter C.M., Connolly E.L., Guerinot M.L. (1999). A ferric-chelate reductase for iron uptake from soils. Nature 397: 694-697.

Romanyuk N.D., Rigden D.J., Vatamaniuk O.K., Lang A., Cahoon R.E., Jez J.M., Rea P.A. (2006). Mutagenic definition of a papain-like catalytic triad, sufficiency of the N-terminal domain for single-site core catalytic enzyme acylation, and C-terminal domain for augmentative metal activation of a eukaryotic phytochelatin synthase. Plant Physiology 141: 858-869.

Ruotolo R., Peracchi A., Bolchi A., Infusini G., Amoresano A., Ottonello S. (2004). Domain organization of phytochelatin synthase functional properties of truncated enzyme species identified by limited proteolysis. The Journal of Biological Chemistry 279: 14686-14693.

Schlaeppi K., Bodenhausen N., Buchala A., Mauch F., Reymond P. (2008). The glutathione-deficient mutant *pad2-1* accumulates lower amounts of glucosinolates and is more susceptible to the insect herbivore *Spodoptera littoralis*. The Plant Journal 55: 774-786.

Schmidt W. (1999). Mechanisms and regulation of reduction-based iron uptake in plants. The New Phytologist 141: 1-26.

Schmidt W., Tittel J., Schikora A. (2000). Role of hormones in the induction of iron deficiency responses in *Arabidopsis* roots. Plant Physiology 122: 1109-1118.

Stadtman E.R. (1990). Metal ion-catalyzed oxidation of proteins: biochemical mechanism and biological consequences. Free Radicals in Biology and Medicine 9: 315-325.

Su T., Xu J., Li Y., Lei L., Zhao L., Yang H., Feng J., Liu G., Ren D. (2011). Glutathione-indole-3-acetonitrile is required for camalexin biosynthesis in *Arabidopsis thaliana*. The Plant Cell 23: 364-380.

Takahashi H., Kopriva S., Giordano M., Saito K., Hell R. (2011). Sulfur assimilation in photosynthetic organisms: molecular functions and regulations of transporters and assimilatory enzymes. The Annual Review of Plant Biology 62: 157-184.

Thordal-Christensen H. (2003). Fresh insights into processes of nonhost resistance. Current Opinion in Plant Biology 6: 351-357.

Treutter D. (2006). Significance of flavonoids in plant resistance: a review. Environmental Chemistry Letters 4: 147-157.

Tsuji N., Nishikori S., Iwabe O., Matsumoto S., Shiraki K., Miyasaka H., Takagi M., Miyamoto K., Hirata K. (2005). Comparative analysis of the two-step reaction catalyzed by prokaryotic and eukaryotic phytochelatin synthase by an ion-pair liquid chromatography assay. Planta 222: 181-191.

Tsuji N., Nishikori S., Iwabe O., Shiraki K., Miyasaka H.,Takagi M., Hirata K., Miyamoto K. (2004). Characterization of phytochelatin synthase-like protein encoded by alr0975 from a prokaryote, *Nostoc* sp. PCC 7120. Biochemical and Biophysical Research Communications 315: 751-755.

Ueki S., Citovsky V. (2005). Identification of an interactor of cadmium ion-induced glycine-rich protein involved in regulation of callose levels in plant vasculature. Proceedings of the National Academy of Sciences, USA 102: 12089-12094.

Ueky S., Citovsky V. (2002). The systemic movement of a tobamovirus is inhibited by a cadmium-ion-induced glycine-rich protein. Nature Cell Biology 4: 478-486.

Vanderpoorten A., Goffinet B. (2009). Introduction to bryophytes. Cambridge: Cambridge University Press.

Vanholme R., Demedts B., Morreel K., Ralph J., Boerjan W. (2010). Lignin biosynthesis and structure. Plant Physiology 153: 895-905.

Vatamaniuk O.K., Bucher E.A., Ward J.T., Rea P.A. (2001). A new pathway for heavy metal detoxification in animals. The Journal of Biological Chemistry 276: 20817-20820.

Vatamaniuk O.K., Mari S., Lang A., Chalasani S., Demkiv L.O., Rea P.A. (2004). Phytochelatin synthase, a dipeptidyltransferase that undergoes multisite acylation with γ-Glutamylcysteine during catalysis. The Journal of Biological Chemistry 279: 22449-22460.

Vatamaniuk O.K., Mari S., Lu Y.P., Rea P.A. (1999). *AtPCS1*, a phytochelatin synthase from *Arabidopsis*: Isolation and in vitro reconstitution. Proceedings of the National Academy of Sciences, USA 96: 7110-7115.

Vatamaniuk O.K., Mari S., Lu Y.P., Rea P.A. (2000). Mechanism of heavy metal ion activation of phytochelatin (PC) synthase. The Journal of Biological Chemistry 275: 31451-31459.

Verbruggen N., Hermans C., Schat H. (2009). Mechanisms to cope with arsenic or cadmium excess in plants. Current Opinion in Plant Biology 12: 364-372.

Vert G., Grotz N., Dédaldéchamp F., Gaymard F., Guerinot M.L., Briat J.F., Curie C. (2002). IRT1, an *Arabidopsis* transporter essential for iron uptake from the soil and for plant growth. The Plant Cell 14: 1223-1233.

Villarreal J.C., Cargill D.C., Hagborg A., Söderström L., Renzaglia K.S. (2010). A synthesis of hornwort diversity: patterns, causes and future work. Phytotaxa 9: 150-166.

Vivares D., Arnoux P., Pignol D. (2005). A papain-like enzyme at work: native and acyl-enzyme intermediate structures in phytochelatin synthesis. Proceedings of the National Academy of Sciences, USA 102: 18848-18853.

Volland S., Schaumlöffel D., Dobritzsch D., Krauss G.J., Lütz-Meindl U. (2013). Identification of phytochelatins in the cadmium-stressed conjugating green alga *Micrasterias denticulata*. Chemosphere 91: 448-454.

Welch R.M., Norvell W.A. (1993). Growth and nutrient uptake by barley (*Hordeum vulgare* L. cv Herta): studies using an N-(2-Hydroxyethyl)ethylenedinitrilotriacetic acid-buffered nutrient solution technique. Plant Physiology 101: 627-631.

Weng J.K., Akiyama T., Bonawitz N.D., Li X., Ralph J., Chapple C. (2010). Convergent evolution of syringyl lignin biosynthesis via distinct pathways in the lycophyte *Selaginella* and flowering plants. The Plant Cell 22: 1033-1045.

Wittstock U., Burow M. (2010). Glucosinolate breakdown in *Arabidopsis*: mechanism, regulation and biological significance. The Arabidopsis Book e0134. 10.1199/tab.0134.

Wittstock U., Halkier B.A. (2002). Glucosinolate research in the *Arabidopsis* era. Trends in Plant Science 7: 263-270.

Wodniok S., Brinkmann H., Glöckner G., Heidel A.J., Philippe H., Melkonian M., Becker B. (2011). Origin of land plants: do conjugating green algae hold the key? BMC Evolutionary Biology 11: 104-113.

Wojas S., Clemens S., Hennig J., Sklodowska A., Kopera E., Schat H., Bal W., Antosiewicz D.M. (2008). Overexpression of phytochelatin synthase in tobacco: distinctive effects of *AtPCS1* and *CePCS* genes on plant response to cadmium. Journal of Experimental Botany 59: 2205-2219.

Xing D., Chen Z. (2006). Effects of mutations and constitutive overexpression of *EDS1* and *PAD4* on plant resistance to different types of microbial pathogens. Plant Science 171: 251-262.

Yin R., Han K., Heller W., Albert A., Dobrev P., Zazimalova E., Schaffner A. (2013). Kaempferol 3-O-rhamnoside-7-O-rhamnoside is an endogenous flavonol inhibitor of polar auxin transport in *Arabidopsis* shoots. New Phytologist 201: 466-475.

Zenk M.H. (1996). Heavy metal detoxification in higher plants--a review. Gene 179: 21-30.

Zhai Z., Gayomba S.R., Jung H., Vimalakumari N.K., Piñeros M., Craft E., Rutzke M.A., Danku J., Lahner B., Punshon T., Guerinot M.L., Salt D.E., Kochian L.V., Vatamaniuk O.K. (2014). OPT3 is a phloem-specific iron transporter that is essential for systemic iron signaling and redistribution of iron and cadmium in *Arabidopsis*. Plant Cell doi/10.1105/tpc.114.123737.

Zipfel C., Robatzek S., Navarro L., Oakeley E.J., Jones J.D.G., Felix G., Boller T. (2004). Bacterial disease resistance in *Arabidopsis* through flagellin perception. Letters to Nature 428: 764-767.

ACKNOWLEDGEMENTS

This PhD research was carried out at three different Universities and I am grateful to all my supervisors for their help during my project.

Prof. Luigi Sanità di Toppi, University of Parma, department of Life Sciences. Thanks for your support during the research about the evolutionary history of PCS enzyme and for your work and time during these years. Thanks to you for making me start my doctoral research and giving me the possibility to work for my PhD project. I am grateful also to Dr. Alessandro Petraglia, from the University of Parma, for his contribution to this research.

Prof. Olena K. Vatamaniuk, Cornell University, Ithaca (NY, USA), department of Crop and Soil Science. Your help and your patience in guiding me through the discovery of PCS functions have been decisive to obtain the results concerning the Arabidopsis section of the project. I am deeply grateful to you that always given a substantial contribution to the success of my thesis. Olena thanks for your enthusiasm during our meeting about the laboratory results and for making me feel at home during my stay in USA.

Prof. Flavia Guzzo, University of Verona, department of Biotechnology. I am thankful to you that allowed me spending some months in your laboratory to learn the world of the metabolomics analysis. Flavia thanks for your time and your work.

Thanks to all my labmates: Jiapei, Sheena, Lu, Sungjin, Nanditha, Ha-il, Mauro, Pamela e Francesca. It was very nice stay in laboratory with you guys!

I full acknowledgement Oxford University Press for the kind permission of reproducing the text and the figures/tables of the following papers:

- Petraglia A., De Benedictis M.*, Degola F., Pastore G., Calcagno M., Ruotolo R., Mengoni A., Sanità di Toppi L. (2014). The capability to synthesize phytochelatins and the presence of constitutive and functional phytochelatin synthases are ancestral (plesiomorphic) characters for basal land plants. Journal of Experimental Botany 65: 1153-1163.
- Degola F., De Benedictis M.*, Petraglia A., Massimi A., Fattorini L., Sorbo S., Basile A., Sanità di Toppi L. (2014). A Cd/Fe/Zn-responsive phytochelatin synthase is constitutively present in the ancient liverwort *Lunularia cruciata* (L.) Dumort. Plant Cell Physiology 55: 1884-1891.

(* co-first name)